Experiments on random lasers

Experiments on random lasers

ACADEMISCH PROEFSCHRIFT

ter verkrijging van de graad van doctor
aan de Universiteit van Amsterdam,
op gezag van de Rector Magnificus
prof. dr. J. J. M. Franse
ten overstaan van een door het college voor promoties
ingestelde commissie in het openbaar te verdedigen
in de Aula der Universiteit
op dinsdag 4 december 2001 te 14:00 uur

door

Gijs van Soest

geboren te Assen

Promotiecommissie:

Promotor	Prof. Dr. A. Lagendijk
Overige leden	Prof. Dr. D. Lenstra Prof. Dr. H. B. van Linden van den Heuvell Prof. Dr. C. M. Soukoulis Dr. R. Sprik Prof. Dr. J. P. Woerdman

Faculteit der Natuurwetenschappen, Wiskunde en Informatica

The work described in this thesis is part of the research program of the "Stichting Fundamenteel Onderzoek der Materie (FOM)", which is financially supported by the "Nederlandse Organisatie voor Wetenschappelijk Onderzoek (NWO)".

It was carried out at the
Van der Waals-Zeeman Instituut, Valckenierstraat 65,
1018 XE Amsterdam, The Netherlands,
where a limited number of copies of this thesis is available.

Ontwerp: Miranda Ensink, Gijs van Soest.
Druk: Ponsen & Looijen BV, Wageningen.

ISBN: 90-6464-648-1

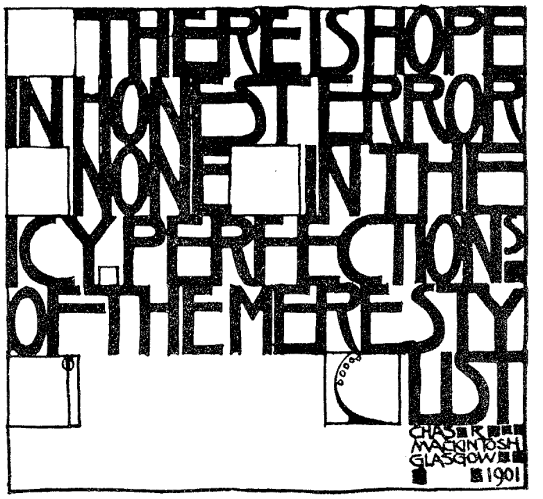
THERE IS HOPE
IN HONEST ERROR
NONE IN THE
ICY PERFECTIONS
OF THE MERE STYLIST
CHAS R
MACKINTOSH
GLASGOW
1901

C. Contents

1 Introduction: light diffusion and lasers **11**

1.1 Waves in complex media 11
1.1.1 Light interacting with matter 12
1.1.2 Single particle scattering 14
1.2 Light transport 16
1.2.1 Multiple scattering and diffusion 18
1.2.2 Random walks 21
1.2.3 Anderson localization and photonic band gaps 22
1.3 The laser 22
1.3.1 Rate equations 24
1.3.2 Amplified spontaneous emission 28
1.3.3 Laser dyes 28
1.4 Random lasers 30
1.4.1 Issues in random laser physics 30
1.4.2 Is it a laser? 32

2 Amplifying volume in scattering media **33**

2.1 Phenomenology 34
2.1.1 Laser threshold 34
2.1.2 Reabsorption 35
2.2 Qualitative explanation of the random laser threshold 37
2.3 Amplifying volume in scattering media 38
2.3.1 Experimental method 38
2.3.2 Weakly scattering medium 40
2.4 Random walk simulation 41
2.5 Discussion 44

3 Dynamics of the threshold crossing **47**
3.1 The photon bomb 48
3.2 Transport equations 49
3.3 β-factor in a random laser 50
3.3.1 Spontaneous emission seeding in cavity and random lasers . 50
3.3.2 Quantitative construction of β in a random laser 51
3.3.3 Discussion 53
3.4 Closer investigation of the transport equations 54
3.4.1 Analogy with conventional lasers 55
3.4.2 Intrinsic dynamics 57
3.5 Transport properties of random lasers 60
3.5.1 Spatial behavior 62
3.5.2 Temporal features 64
3.5.3 Laser threshold and the explosion 65
3.5.4 Comparison with earlier work 67

4 Interference in random lasers **71**
4.1 Experimental considerations 71
4.2 Speckle in random lasers 73
4.2.1 Sample and setup 74
4.2.2 Intensity statistics 76
4.2.3 Speckle spot size 78
4.2.4 Possible experiments? 80
4.3 Enhanced backscattering in random lasers 81
4.3.1 Experimental details 82
4.3.2 Results from experiment 83
4.3.3 Comparison with theory of chapter 3 85
4.3.4 Discussion 88
4.4 Conclusions 89

5 Narrow peaks in fluorescence from scattering systems **91**
5.1 Critical review 92
5.1.1 Observations and interpretations from the literature 92
5.1.2 Localization and random ring cavities 94
5.1.3 Thin film “random” laser 96
5.2 Experimental results 98
5.2.1 ZnO powders 98
5.2.2 Scattering dye solutions 103
5.3 Discussion and conclusions 105
5.3.1 ZnO powders 106

5.3.2 Dye suspensions 108
5.3.3 Conclusions 109

A Properties of Sulforhodamine B and Coumarin 6 **111**

B Pump units and terminology **113**

References **115**

Summary **123**

Samenvatting **127**

Dankwoord **133**

1. Introduction: light diffusion and lasers

This thesis is about random lasers: systems in which light is both multiply scattered and amplified. It draws on many aspects of the interaction between light and matter. This chapter is a primer that introduces these aspects in such a way that the necessary elements from laser physics and light in complex dielectric media can be brought together in one picture of random lasers. Only the material that is actually used for theory and experiments is presented in a quantitative manner.

1.1 Waves in complex media

The propagation of waves in scattering media is a subject with many facets. Meteorology, astronomy, seismology and remote sensing are but a few of the many disciplines that make use of the concept of wave transport in complex media. Although techniques and terminology differ, the central idea is the same across al these disciplines: while the (classical) wave travels, it interacts with "particles" in the medium. This interaction can be either scattering or absorption or both. We only consider elastic scattering: no energy is transferred to or from the wave field. Then, scattering is an interaction that changes the direction of propagation of the wave field, while absorption changes the amplitude of the wave, see figure 1.1. If absorption is understood in the usual sense, the change is downward: the amplitude diminishes. However, for the current work, we allow for a negative absorption which makes the amplitude increase, to describe gain. In this section, by absorption we mean absorption in this general sense.

The word "complex" is used here to signify composite, made up of related parts. It derives from the Latin "complectere", meaning "to embrace". The constituent parts of the medium are inextricably mixed, and the properties of wave transport in such a medium are largely determined by its composite nature. The wave–matter

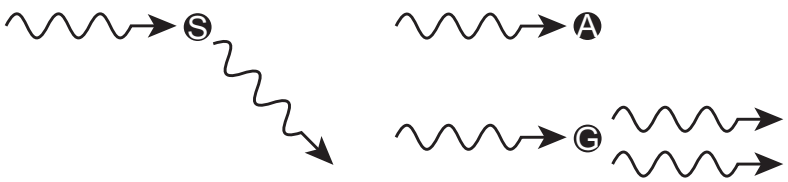

Figure 1.1 A sketch of the processes of scattering *(left; S)* and absorption *(right)* where we allow for positive *(A)* and negative *(G)* absorption coefficients. The latter situation corresponds to amplification.

interaction cannot be understood by decomposing the medium in its components and treating those separately.

1.1.1 Light interacting with matter

A medium interacting with a wave field as outlined above need not be very complex, from the wave's perspective. The "particles" may be the atoms that constitute the medium. In the case of light, the atoms are microscopic dipoles that scatter the electromagnetic field, but because of their small size and spacing compared to the wavelength, they do so in unison. The scattered fields sum up to a field that has all the characteristics (frequency content, wave vector spread, etc.) of the incident wave, except that it has a a lower velocity c, compared to the vacuum speed of light c_0. The interaction is described by the refractive index $\eta = \frac{c_0}{c}$, and the medium is considered homogeneous [1, 2].

Difficulties arise with inhomogeneity, if the scattering properties of the medium are nonuniform on distances of order λ or larger. Substantial phase differences, relative to 2π, can build up in the scattered field, which then looks very different from the incident field. The interference pattern formed in this way is called speckle, a name suggested by the grainy look of the intensity distribution of scattered laser light.

Scattering can give rise to very complicated field distributions, especially if there are many scatterers that are randomly positioned. This calls for a statistical approach: particular realizations of the field are not only difficult to obtain, they are also not very relevant since a change in direction of the incident field or a change in conformation of the scatterers can change the field completely. Techniques like dynamic light scattering make use of statistical properties of the speckle to extract information about the scattering medium. The diffusion approximation to transport described in section 1.2.1 is an example of an ensemble averaged approach.

The effect of absorption is in principle much less complicated. It only modifies the amplitude of the field, but does not change its direction of propagation. Energy

Figure 1.2 Comparison of (coherent) scattering and (incoherent) fluorescence in an energy diagram. Light may scatter off a two-level atom by resonance fluorescence (1). If there is more internal structure to the atom also Rayleigh scattering (2) is possible. Light may also be absorbed and re-emitted in fluorescence (3), in which the energy is stored in an atomic excitation (★) for some time.

is removed from the field by the medium, and dissipated. How this happens is not our concern if we try to describe the wave transport, although for experiments it is of course important to know what happens on a molecular scale. This is discussed in detail in section 1.3.3.

The amount of scattering per particle is usually quantified in the scattering cross section σ_s, the ratio of the power removed by scattering to incident intensity, with units of area. The absorption cross section σ_a is analogously defined. The extinction is the total power removed from the incident beam, and its cross section is $\sigma_{ext} = \sigma_s + \sigma_a$. The differential scattering cross section $\frac{d\sigma_s}{d\Omega} d\Omega$ specifies how much energy is radiated into a specific solid angle.

Microscopic picture As a side-track, we outline how the processes of (in)elastic scattering and absorption may be microscopically unified into one picture, see ref. 3. The interactions between light and a two-level atom can be classified as resonance fluorescence or ordinary fluorescence. The processes are shown schematically in figure 1.2.

Resonance fluorescence is a coherent process, in which the atomic dipole oscillator is driven by the incident light field and so takes part of the energy from the field to radiate it in a spherical wave: indeed, the atom is scattering the light. It is resonant because the photon energy $\hbar\omega_\ell$ has to match the energy $\hbar\omega_0$ of the atomic transition within the line broadening $2\Delta\omega$. The frequency of the scattered field is identical to that of the incident field, ω_ℓ.

For a multilevel atom the same formalism can be extended to Rayleigh scattering, which is elastic but not necessarily resonant. The scattering cross section σ_s does depend on the frequency difference with the respective atomic levels $(\omega_\ell - \omega_i)$ with maxima at $\omega_\ell = \omega_i$. σ_s is the sum of the electric dipole interactions of the light with all energy levels of the atom, and so it can be nonzero far away from the atomic resonances. It is important to realize that the higher levels of the atom are not

populated in an intermediate state, although all atomic states contribute to the cross section.

Ordinary fluorescence is an incoherent process in which the photon energy is first absorbed by the atom, stored for some time τ and then re-emitted. There is no relation between the phases of incident and radiated fields and the frequency of the latter may be anywhere within the broadened atomic transition line $\omega_0 \pm \Delta\omega$. The emitted field is not part of the scattered field as originating from elastic processes.

1.1.2 Single particle scattering

The particles that are the scatterers may interact with light in different ways, depending on their size. For light scattering, three qualitatively distinct ranges are important: Rayleigh scattering, Mie scattering, and geometric optics. We mentioned already that atoms can scatter light (Rayleigh scattering; the first range). The scattering by an ensemble of atoms can be written as the product of the single atom scattering cross section and a structure factor that arises from the summed scattered fields of individual atoms [4]. For an ensemble much larger than λ consisting of many closely spaced ($\ll \lambda$) atoms the structure factor is zero except in the forward direction, the spherical waves emanating from each atom cancel in all other directions. This is a homogeneous medium as described on page 12, and we can apply geometric optics (the third range). In Mie scattering (the second range), particles with a size of about a wavelength can produce strong resonances in the structure factor due to interference in the scattered field.

Scattering is characterized by two important numbers: the size parameter x of the particle and the refractive index contrast m.

$$x = ka \equiv \frac{2\pi\eta a}{\lambda}\ ; \qquad m \equiv \frac{\eta_1}{\eta}\ ; \tag{1.1}$$

where a is the "radius" of the particle (see the paragraphs on Mie scattering below for refining considerations about the shape of the particle), and η and η_1 are the refractive indices of medium and scatterer, respectively.

Rayleigh scattering Scattering of light by particles much smaller than the wavelength (x, $mx \ll 1$), such as atoms, molecules, and very fine dust, is called Rayleigh scattering. Its hallmark is the proportionality of the scattering cross section to $1/\lambda^4$, of which several derivations can be found in the literature (different formulations are given in refs. 3, 5–7). We paraphrase the elegant consideration by Lord Rayleigh himself [8]:

- A dimensionless ratio between scattered and incident field may depend on these quantities: volume V of the particle, position $\mathbf{r}$, wave velocity c, dielectric

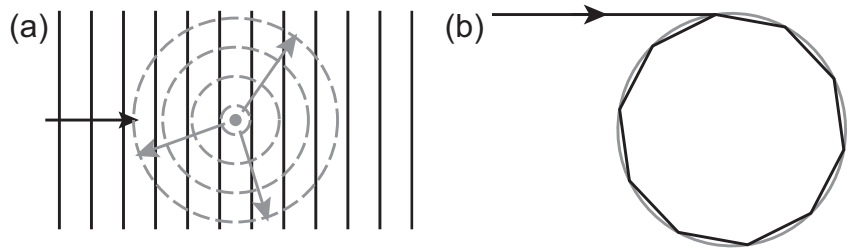

Figure 1.3 Sketches of scattering *(a)* in the Rayleigh limit, and *(b)* in the geometric optics limit. In *(a)* the scatterer takes out a part of the incident plane wave and radiates it as a spherical scattered wave. In *(b)* the scatterer is large enough ($x \gg 1$) to allow drawing the light as a ray inside. As an example a whispering gallery mode of a disk or sphere, excited by the incident wave, is shown.

constants of sphere ε_1 and surroundings ε_0, and wavelength λ with appropriate units. c is the only one with a unit containing time and thus can not play a role, the dielectric constants have units involving capacitance and thus can only appear as $\varepsilon_1/\varepsilon_0$, which leaves the ratio $V/(r\lambda^2)$ as the only candidate (compatible with the known $1/r$ decay of the amplitude). Squaring this to get the ratio between scattered and incident energy reveals a proportionality to $1/\lambda^4$. ■

The dielectric constant of the scatterer appears (for $\varepsilon_0 = 1$) as the factor $V\frac{\varepsilon_1-1}{\varepsilon_1+2}$, the static polarizability of a small dielectric sphere.

As is well known, scattering of light in the atmosphere is accurately described by Rayleigh scattering. The strong dependence on the wavelength causes blue light to be scattered about 6 times more efficiently than red light, accounting for the blue sky and the red sun at sunset.

Mie scattering If x is of order 1 the problem of scattering can only be solved by a formal solution of Maxwell's equations with appropriate boundary conditions. There is no short route towards physical insight [9], other than the handwaving argument given by Feynman [10], summarized below:

■ The N microscopic dipoles that make up a scatterer radiate in phase if they are within half a wavelength of each other, which produces a scattered field that is N times the field of one dipole due to constructive interference. Thus the scattered energy from this collection of N dipoles is $(N \cdot 1)^2 = N^2$ times the field of 1, compared to a scattered energy of $N \cdot (1)^2 = N$ if the phases are independent. This indicates that scattering in this regime can be very strong, with sharp resonances as a function of x and m. In these resonances, σ_s can become as large as λ^2 (several times the geometric cross section of the scatterer), and there is considerable angular structure in the differential cross section. ■

The problem can only be exactly solved for certain simple shapes such as a sphere or a cylinder. Scattering by a sphere of arbitrary size is called Mie scattering, after one of the early physicists who worked on the problem. An extensive treatment of the problem is given in ref. 11. The scatterers used in our experiments do fall in the range of $x \approx 1$, but they are irregularly shaped, all different and polydisperse, instead of being spheres of equal size. The detailed results of Mie theory are therefore of limited use. We content ourselves with noticing that our particles are strongly scattering and that every particle has a different cross section, the details of which will not affect the experimental results.

Geometric optics For scatterers much larger than the wavelength, geometric (ray) optics can be used for the propagation of the intensity, if necessary with appropriate corrections for the wave character of light. The light can be pictured as a ray inside the material. This need not at all be trivial or dull, as is witnessed by natural marvels like the rainbow [12] or devices like microsphere lasers [13] (lasing on a whispering gallery mode, see figure 1.3b), both of which can be described to a certain extent by geometric optics.

1.2 Light transport

To incorporate all of the diversity outlined above into a comprehensive transport theory for light traveling through matter, consisting of many particles interacting with the light in various ways, is certainly a formidable task. Also, such a theory will be unpractical for describing actual experiments because of its involved nature; it may be correct, but also very cumbersome.

In order to be able to describe transport, a distinction in several regimes is made depending on how strongly the interaction with the medium changes the wave field. We then work with an approximate version of transport theory that suits the regime of the physical system under study. Two quantities determine the magnitude of the effect on the light: the strength of the interaction X (X is "s" for scattering or "a" for absorption) of one particle with the field, and the number of particles. The former is quantified as the cross section σ_X, the latter as the particle density n.

$$\kappa_X = n\sigma_X \quad \text{or its inverse} \quad \ell_X = \frac{1}{n\sigma_X} \tag{1.2}$$

quantify how strongly the material influences the wave field by the interaction X. κ_X is called the coefficient of the interaction. It has the dimensions of inverse length. Every slice dz of the medium that is traversed takes out a proportional fraction of the

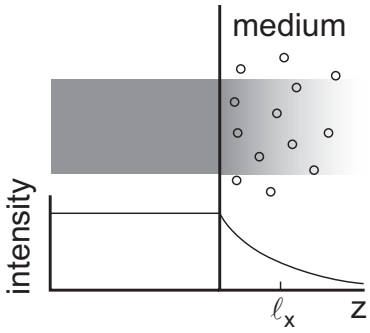

Figure 1.4 Diminishing intensity of the incident beam due to scattering or absorption. ℓ_X is the characteristic length.

intensity I: $\mathrm{d}I = -\kappa_X I \,\mathrm{d}z$, and so we arrive at Beer's law:

$$I(z) = I_0 e^{-\kappa_X z}, \tag{1.3}$$

provided that the particles are independent, so that (1.2) holds.

$\ell_X = 1/\kappa_X$ sets a length scale: the traveled distance at which the intensity in the beam is reduced to I_0/e by scattering or absorption; see figure 1.4. ℓ_X is also called the mean free path, the average distance between two scattering or absorption events. Two examples with realistic numbers:

- A dye solution with a concentration $n = 10^{-4}$ M and an molecular absorption cross section $\sigma_\mathrm{a} = 1.6 \cdot 10^{-16}$ cm^2 has an absorption length $\ell_\mathrm{a} = 1$ mm.
- A colloidal suspension with a concentration $n = 2 \cdot 10^{12}$ cm^{-3} and a scattering cross section $\sigma_\mathrm{s} = 5 \cdot 10^{-10}$ cm^2 has a scattering mean free path $\ell_\mathrm{s} = 10\,\mu$m.

If these parameters apply to one medium that both scatters and absorbs, the scattering is much more important because it reduces the intensity in the incident beam much faster than absorption does: the interaction having the largest coefficient determines the regime of the transport. As mentioned on page 13 the combined effect is called extinction. Its magnitude is measured by $\kappa_\mathrm{ext} = \kappa_\mathrm{a} + \kappa_\mathrm{s}$, so $\ell_\mathrm{ext}^{-1} = \ell_\mathrm{a}^{-1} + \ell_\mathrm{s}^{-1}$.

There are two other relevant length scales: the size of the system L and the wavelength λ. We assume for the current discussion that $\lambda \ll \ell_X \ll L$. A medium with $L \ll \ell_X$ is optically thin: the interaction with the light is small, the intensity is reduced by a fraction of the order $\frac{\ell_X}{L}$, and the system can be considered essentially transparent.

Our prime interest is in systems where $\ell_\mathrm{s} \ll L$: this regime is called multiple scattering. In this regime (1.3) no longer holds, because multiple scattering can reintroduce the scattered light in the direction of the incident beam. However, ℓ_s will be larger than λ. Multiple scattering makes a medium look turbid or opaque,

and white if it is nonabsorbing and if all wavelengths are scattered equally. The propagation direction of the light is continuously changed, causing incident light to be partly scattered back towards its source. In a transparent medium light travels in straight lines, so we can see through it. An absorbing medium removes certain wavelengths from the incident spectrum, but the propagation direction of the light is not affected (apart from refraction), so it is transparent, only not for all colours.

If $\ell_X < \lambda$, the situation is totally different. The interaction takes effect within one wavelength and affects the transport very strongly. Such a strong absorption ($\ell_a < \lambda$), for instance, is coupled to a high conductivity as in a metal which makes it reflecting [14]. There is, therefore, hardly any energy carried by the wave inside the material, and the small amount that is, is dissipated. If the material is very strongly scattering, with $\ell_s < \lambda$, interference needs to be taken into account even after ensemble averaging because the energy transport by the wave field is affected. To appreciate the physics of very strong multiple scattering, we first need to introduce diffusion of light. We return briefly to the modification of wave transport due to interference in very strongly scattering media in section 1.2.3.

1.2.1 Multiple scattering and diffusion

In this section we will work out the situation where $\lambda \ll \ell_s \ll L$, we use refs. 15 and 16 as a basis. $\lambda \ll \ell_s \ll L$ means that (in an averaged description) we can disregard the wave character of the light, and that the light encounters many scattering events in the medium. We further assume a random distribution of scatterers, we will touch briefly upon ordered media in section 1.2.3.

The transport can be considered as light particles with a certain distribution in space on a more-or-less random walk with a step length equal to the scattering mean free path. The degree of randomness in the walk depends on how strongly each scattering event changes the direction of the walk, and so on the differential scattering cross section. Mie scattering, for example, is primarily in the forward direction; it takes a few scatterings to randomize the direction of the light.

The walk can be made really random be adopting a different step length: the transport mean free path ℓ, the length after which the light has lost its initial direction completely. Unlike ℓ_s, it accounts for the direction light is scattered into.

$$\ell = \frac{\ell_s}{1 - \langle \cos\theta \rangle}, \tag{1.4}$$

where $\langle \cos\theta \rangle$ is the average cosine of the scattering angle, which can be found from the differential cross section. Rayleigh scattering is an example of $\langle \cos\theta \rangle = 0$ or $\ell = \ell_s$, while Mie scattering may have $\langle \cos\theta \rangle \approx 0.5$, so $\ell = 2\ell_s$. For diffusion of

the intensity, ℓ is the important length scale. We are interested in the regime where $\ell \ll L$, so the light transport is truly diffusive.

Since the propagation on length scales ℓ is random, there is a net flow of light only if there is nonuniform density, otherwise all microscopic propagation cancels. In order to find a description of the transport in this situation, we turn to the continuity equation, expressing conservation of energy in transport:

$$\frac{\partial W}{\partial t} + \boldsymbol{\nabla} \cdot \mathbf{J} = S\,, \tag{1.5}$$

We work with "particle" densities by normalizing the field energy density and current density to the photon energy. Then W is the energy density in m^{-3}, $\mathbf{J}$ is the current density in $\mathrm{m}^{-2}\mathrm{s}^{-1}$, and S is the source of diffusing light. The current density is the net flow of light into a small volume surrounding the point we consider, per area per time. Since the flow is driven by the density variations, the simplest possible dependence is given by Fick's law:

$$\mathbf{J} = -D\boldsymbol{\nabla} W\,. \tag{1.6}$$

D is the diffusion constant in $\mathrm{m}^2\mathrm{s}^{-1}$. It determines the magnitude of macroscopic light transport, and the link with the microscopic propagation velocity c [17] and the transport mean free path ℓ is:

$$D = \tfrac{1}{3} c\ell\,. \tag{1.7}$$

Combining (1.5) and (1.6), we arrive at the diffusion equation:

$$\frac{\partial W}{\partial t} = D\nabla^2 W + S\,. \tag{1.8}$$

This equation is valid for conservative systems, i.e. in absence of any absorption. It shows immediately that the density itself is a dynamic quantity: in a stationary situation, we are left with $\boldsymbol{\nabla} \cdot \mathbf{J} = S$, and only the constant current can be obtained. This is used in total transmission measurements [18], for example. The source is often a directional beam that is gradually, after one ℓ of travel into the medium, originating the diffusing density. It can be realistically modeled by an exponentially decaying term, similar to (1.3).

Absorption can be taken into account as a special kind of sink (a negative source), one that is proportional to the local intensity:

$$\frac{\partial W}{\partial t} = D\nabla^2 W - \kappa_\mathrm{a} c W + S\,. \tag{1.9}$$

Gain is incorporated by a similar term with a negative κ_a.

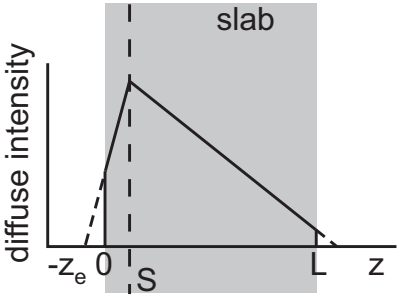

Figure 1.5 Diffuse intensity in a nonabsorbing, finite slab of thickness L, with a source "plane" $S = S_0\delta(z-\ell)$ to model a plane wave incident at $z = 0$ [19]. The flux is given by (1.6), in particular the total transmission (the flux through the rear interface) is proportional to $\frac{\ell+z_e}{L+2z_e}$.

Boundary conditions The diffusion equation is a second order partial differential equation and accordingly it needs boundary conditions before it can be solved. Physically, no diffuse intensity can enter the medium through the interface, which mathematically translates into the mixed boundary condition [15]:

$$\begin{aligned} W - z_e\frac{\partial W}{\partial z} &= 0 \qquad z = 0\,; \\ W + z_e\frac{\partial W}{\partial z} &= 0 \qquad z = L\,; \end{aligned} \tag{1.10}$$

for a slab that is finite only in the z-direction. The extrapolation length z_e is a length of order ℓ. The diffuse density extrapolates to zero a distance z_e outside the interface. z_e depends on the coefficient of internal reflection [20, 21], but this dependence is weak for our samples with an internal reflection correction of a few percent. See figure 1.5.

Diffusive absorption length The average distance between begin and end points of a trajectory traveled in time t is $\sqrt{Dt}$. The length of such a trajectory is ct. In a medium with multiple scattering and absorption, this allows a determination of the average distance of diffuse propagation after which the intensity has decayed to $1/e$ by absorption [22]: when $t = t_a \equiv \ell_a/c$ the path length is ℓ_a and the average distance between begin and end points is

$$L_a = \sqrt{\frac{\ell\ell_a}{3}}\,. \tag{1.11}$$

This length is called the diffusive absorption length. It gives the penetration depth of light in an absorbing, multiply scattering medium.

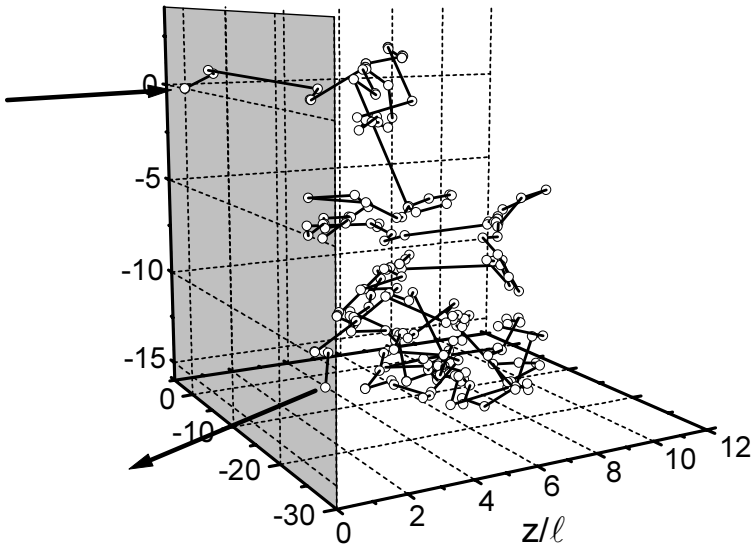

Figure 1.6 Example of a random walk: the path starts (enters) at the upper arrow $(x,y,z) = (0,0,0)$ and ends (exits) at the lower arrow, where $z = 0$ again. The shaded plane is the interface of the medium. All axes are in units of ℓ. The step length is an exponential variate with average ℓ.

1.2.2 Random walks

The diffusion description of transport stems from particle transport in fluids, e.g. molecular diffusion in a gas. In that framework the idea of a random walk is natural, because we can imagine the microscopic transport as a molecule flying for some distance, experiencing a collision and heading off in a different direction. A diffusing wave is not a particle, but still, the analogy with a random walk is a very good one if we look at the energy density. We can simulate transport as a random walk performed by light particles, with a density being the energy density divided by the photon energy. The particle distribution in space $P(\mathbf{r})$ as well as the probability $P(\mathbf{r}_1, \mathbf{r}_2)$ to go from one position $\mathbf{r}_1$ to another $\mathbf{r}_2$ correspond well with analytical results.

Practically, a random walk simulation is done as follows: for a step a direction is chosen with a uniform distribution, and a length with an exponential distribution (characteristic length ℓ). These give the new position of the particle after the step. This procedure is repeated, until a certain condition is fulfilled (stepped out of the medium, gets absorbed, etc.). The path is then added to the statistics.

In this thesis, we will use both the analytical diffusion theory and the stochastic random walks. Diffusion theory is continuous and results can easily be calculated for large systems and long times (see chapter 3). However, it can be numerically difficult

to apply in situations with variation in more than one spatial dimension (e.g., a finite beam width). In such a situation we use a Monte Carlo random walk simulation (see section 2.4). The problem is studied stochastically by launching many walks and keeping track of where they go to get a statistical answer to the question we pose. It can be conveniently implemented in any geometry, but since every step has to be calculated and stored separately, it is unwieldy for getting dynamic results for long times, and accordingly, for large systems.

1.2.3 Anderson localization and photonic band gaps

If the scattering is so strong that $k\ell_s < 1$, where $k = \frac{2\pi}{\lambda}$, destructive interference between scattered waves inhibits the propagation of waves over length scales larger than the localization length: $D \to 0$. This phenomenon is called Anderson localization, after its discoverer [23]. Localization of classical waves [24] is briskly pursued experimentally [25–27], by matching the scale of the inhomogeneity to the wavelength, and by increasing the refractive index contrast.

In ordered inhomogeneous dielectrics, a similar effect may occur. The multiply scattered waves form an electromagnetic Bloch wave due to the periodicity. The iridescence of opals is Bragg reflection of light in an ordered dielectric with a variation in the refractive index on the order of the wavelength of light: opals are an example of photonic crystals. A stronger interaction (larger dielectric contrast) broadens the Bragg reflections, and if they cover all angles for a certain frequency, light propagation at that frequency is inhibited in the crystal [28]. This phenomenon is called a photonic bandgap, and it is intensely sought after [29].

1.3 The laser

In order to understand what happens in a random laser, a good understanding of conventional lasers, especially of the laser threshold is needed. The basic concepts are presented here in such a way that they can easily be adapted for use with the random case. Laser is an acronym for light amplification by stimulated emission of radiation. There are basically two functional parts in a laser: a light amplifier and a feedback mechanism. In conventional lasers (random lasers will be introduced in section 1.4) the feedback mechanism is an optical cavity, consisting of high quality mirrors. Gain media come in many varieties; dyes are described in more detail in section 1.3.3. A schematic is shown in figure 1.7.

The cavity is in its simplest form a Fabry-Perot resonator of length L, the longitudinal modes of which are standing waves, which undergo a phase shift of an integer times 2π in one round trip through the cavity. Light in a cavity mode experiences

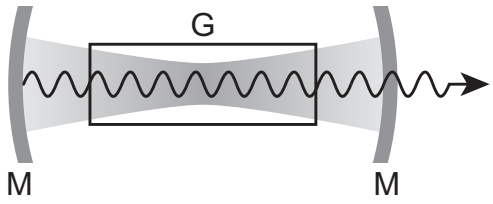

Figure 1.7 Schematic of a laser: *G* is the gain medium; *M* are the mirrors forming the cavity. A cavity mode is also shown: light in this mode can resonate in the cavity and is amplified. It forms a unidirectional laser beam, transmitted through one of the mirrors.

resonant feedback: it is reflected back on itself after one round trip through the cavity. One of the mirrors is not completely reflecting, allowing the output beam to be transmitted. This transmission is a loss factor of the cavity mode. The cavity modes have a well-defined direction along (or close to, depending on the exact geometry) the cavity axis, and a well-defined frequency (broadened by the loss rate).

The amplifier consists of a medium with several atomic or molecular (electronic) energy levels: see figure 1.8. Since all experiments in this thesis are done with a laser dye as the gain medium, we will speak about molecules as the active particles. Energy is stored in the medium by populating a metastable level above the ground state; this energy supply is called pumping. We separate the decay from the excited state into three categories: spontaneous, stimulated, and non-radiative [30]. Non-radiative decay only generates heat and can for our purposes be considered as just a loss of radiative efficiency.

Stimulated emission is the process that is put to use in amplification: the radiation field interacts resonantly with the excited oscillator that is the molecular dipole, enhancing the field while preserving phase and wave vector [31]. In a quantum physical picture, the interaction of the excited molecule with an electromagnetic field induces an molecular decay yielding an additional photon that has exactly the same properties as the incident field. An incident photon is "copied", and the effect is an amplification of the radiation field. The process depends on molecules available in the excited state, and for a net gain to occur we need more molecules in the excited state than in the ground state of the transition. This is called population inversion.

The classical analogue of spontaneous emission is the radiation damping of the molecular oscillator, with a decay time τ. Light originating from such a transition is emitted in all directions and is broadened in frequency due to the finite lifetime: a spontaneously decaying molecule may emit a photon into any direction with any energy within the molecular linewidth (it is the fluorescence at discussed at the end of section 1.1.1).

The laser threshold Spontaneous emission acts as the noise of the laser amplifier that can start the laser oscillation: spontaneously emitted radiation that happens to

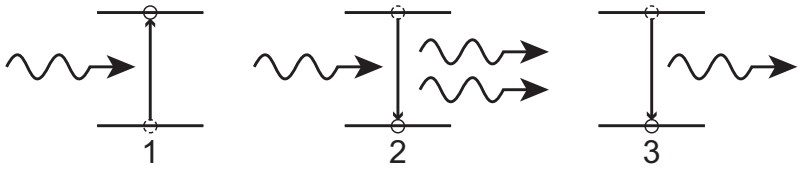

Figure 1.8 The processes of (1) absorption, (2) stimulated and (3) spontaneous emission in a photon–particle picture.

be in a cavity mode can be amplified by stimulated emission if the available gain at that frequency is sufficient to compensate mode losses. This condition is called the laser threshold: at low pump rate the population of the excited state is low and a standing wave can not build up because intensity is lost from the mode (by mirror transmission) faster than it is generated in the amplification process. There is not much stimulated emission, spontaneous emission dominates. Since this goes in all directions, there is no output beam.

At high pump rate a population inversion large enough to compensate cavity losses can be maintained and the laser oscillates in a single mode. The field in the lasing mode is so strong that most molecules do not get the time to decay spontaneously before they are induced to decay by the field. Nearly all the light is in the lasing mode, producing a coherent output beam. The pump rate at which one behavior crosses over into the other is called the threshold pump rate, r_{th} in figure 1.9.

1.3.1 Rate equations

The processes introduced above can be described quantitatively by a coupled set of kinetic rate equations, (1.12) for the number of photons q in the cavity mode, and (1.13) for the population N_1 of the upper laser level of the gain medium. Since our subsequent discussion will not rely on the quantum properties of the field, we will conclude by rewriting the results of the analysis in classical terms. We follow refs. 32 and 33:

$$\frac{\mathrm{d}q}{\mathrm{d}t} = -\gamma_{\mathrm{c}} q + qBN_1 + \beta\Gamma N_1 \,; \tag{1.12}$$

$$\frac{\mathrm{d}N_1}{\mathrm{d}t} = r - qBN_1 - \Gamma N_1 \,. \tag{1.13}$$

These equations are valid for a single mode which corresponds to a monochromatic radiation field at frequency ω_ℓ, with an energy spectrum $\rho(\omega) = q\hbar\omega\delta(\omega - \omega_\ell)$. We assume that only populations of the lower level of the pumping transition N_0 and the upper level of the laser transition N_1 are significant, so $N = N_0 + N_1$ is the total

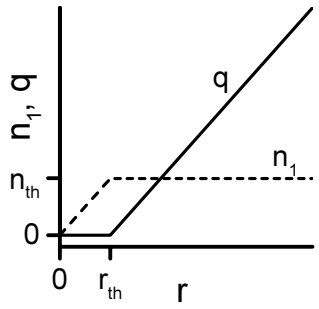

Figure 1.9 Steady state dependence of the photon number (q) and inversion (N_1) on the pump rate r, as a result of (1.12) and (1.13). $r_{\rm th}$ is the threshold pump rate, N_{th} is the value of the inversion far above threshold.

number of molecules in the gain medium interacting with the field. The cavity decay rate due to losses such as mirror transmission, scattering and absorption is given by $\gamma_{\rm c}$. $\Gamma = 1/\tau$ is the spontaneous decay rate, r is the pump rate (comprising, for the moment, N_0), and β is the spontaneous emission factor, the fraction of spontaneous emission that contributes to lasing.

B is a (constant) parameter governing the stimulated emission rate; it is equal to the amount of the spontaneous emission rate per frequency interval into the lasing mode (of all modes), $B = \Gamma/p$, where p is the (usually very large) number of cavity modes within the gain bandwidth of the medium. This suggests for the spontaneous emission factor $\beta = 1/p$, a number that is usually much smaller than 1. Then (1.12) becomes

$$\frac{{\rm d}q}{{\rm d}t} = -q\gamma_{\rm c} + N_1 B(q+1)\,, \tag{1.14}$$

where the last term expresses that the photon number in the mode can never really vanish due to spontaneous emission.

An analysis of the rate equations (1.12) and (1.13) in steady state brings out the essential features of a laser, as shown in figure 1.9. We separate the analysis in a pump regime well above threshold and well below threshold. What we mean by "well above/below" will be explained duely.

If we isolate q from (1.12) and N_1 from (1.13), we can gauge the behavior below threshold by realizing that for small pump rates $qB \ll \Gamma$, or equivalently $q \ll p$. The result is an inversion that grows linear with the pump rate, and a photon number that is small until the inversion comes close to the threshold inversion:

$$N_1 = \frac{r}{\Gamma}\,; \qquad\qquad q = \frac{N_1}{N_{\rm th} - N_1} \qquad \text{with } N_{\rm th} \equiv \gamma_{\rm c}/B\,. \tag{1.15}$$

Here we have defined the threshold inversion $N_{\rm th}$, the ratio between the loss rate and the generation rate per excited particle in the gain medium. Extrapolating N_1 to $N_{\rm th}$ gives the pump rate needed to reach the threshold: $r_{\rm th} = \Gamma\gamma_{\rm c}/B$. Note that before N_1

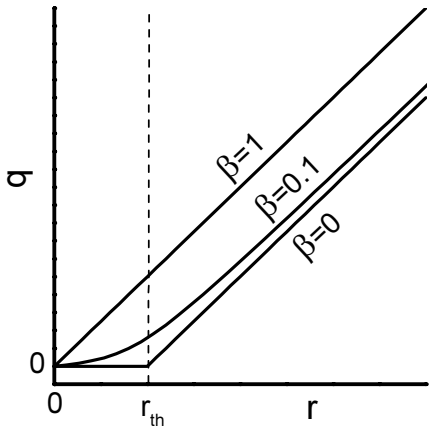

Figure 1.10 β determines the sharpness of the laser threshold. The photon number q as determined from (1.12) and (1.13) is plotted as a function of pump rate r (cf. figure 1.9). The threshold is indicated by $r_{\rm th}$. The abrupt bend for $\beta = 0$ turns into a smoother transition for larger β, limited by the "thresholdless" $q \propto r$ for $\beta = 1$.

actually reaches $N_{\rm th}$ the photon number q becomes very large, and saturation will start to affect the inversion as soon as $q \sim p$.

Since above threshold the photon number $q \gg 1$, the spontaneous "+1" noise photon in (1.14) can be neglected. We then find a steady state inversion independent of the pump rate, clamped at $N_{\rm th}$. From (1.13) we see the photon number increasing linearly with r:

$$N_1 = \frac{\gamma_{\rm c}}{B}\,; \qquad\qquad q = p\left(\frac{r}{r_{\rm th}} - 1\right). \tag{1.16}$$

The constant $N_{\rm th}$ results from an equilibrium between excitation by the pump and de-excitation by induced decay, a process called gain saturation.

There is a range of pump rates $r \approx r_{\rm th}$ with a width of order $r_{\rm th}/\sqrt{p}$, where $q \sim \sqrt{p}$. Here (1.15) crosses over into (1.16), and neither can be applied exactly. In most lasers this range where the generation and loss rates are comparable is very narrow.

The β-factor The fraction of spontaneous radiation that contributes to lasing is called β. In the science of cavity lasers this parameter is of great interest because of the promise of a "thresholdless laser" with $\beta = 1$, in which all spontaneous emission is radiated into the lasing mode [34, 35].

The "sharpness" of the laser threshold is governed by the value of β, as can be seen in figure 1.10. Solving the laser rate equations (1.12) and (1.13) with $\beta = 0$ yields a sharp bend in the photon number q as a function of pump rate which is really a discontinuity in the derivative. Below threshold $q = 0$ and above $q \propto r - r_{\rm th}$. In the other limit, $\beta = 1$, $q \propto r$. For $0 < \beta < 1$ there is a threshold, which becomes less sharp as β gets larger. The range of pump rates where q deviates appreciably

from the $\beta = 0$ line is the threshold crossing region that is not described by (1.15) and (1.16). For $\beta = 1$ this holds for all pump rates. ■

In this description of a laser, no use was made of the resonant property of the feedback, or the coherence of the field. Nor was the existence of other modes taken into account. These refinements are important in a careful analysis of a cavity laser system but not for a random laser. The current discussion is limited to the demonstration of the principle. The extreme multimode nature of a random laser will be taken into account in β, see section 3.3.

For the discussions presented in this thesis, primarily those in chapter 3, we are interested in the energy *density* of the laser field. The energy density u is related to the (expectation value of the) photon number q by $u = \hbar\omega_\ell \langle q \rangle / V$, with V the mode volume [36]. We assume $\langle q \rangle \gg 1$, so that u can be taken continuous, and normalize u to the photon energy to obtain $W = u/(\hbar\omega_\ell)$, an energy density in units m^{-3}. The population density for level x is obtained in a similar way: $n_x = N_x/V$.

The pump rate $r = Rn_0$ and the value of B need to be connected to experimental parameters. For r this relation depends on the pumping mechanism, and we choose to leave it unspecified until chapter 3. B is replaced by B', the stimulated emission rate at unit energy density. It is related to the frequency dependent stimulated emission cross section, and has to be normalized to the density of modes instead of p now that we work with the energy density [37].

$$B' = \frac{\pi^2 c^3}{\omega_\ell^2} \Gamma g(\omega_0, \omega_\ell) = \sigma_e(\omega_\ell) c \,, \tag{1.17}$$

with $g(\omega_0, \omega)$ the function describing the emission lineshape centered at ω_0. Then (1.12) and (1.13) turn into

$$\frac{dW}{dt} = -\gamma_c W + \sigma_e c n_1 W + \beta \Gamma n_1 \,; \tag{1.18}$$

$$\frac{dn_1}{dt} = n_0 R - \sigma_e c n_1 W - \Gamma n_1 \,. \tag{1.19}$$

The energy and inversion densities below and above threshold, (1.15) and (1.16), are scaled accordingly.

One remark about the energy density is in order: below threshold the characteristics of the (intrinsically quantum) spontaneous emission noise dominate those of the (classical) coherent cavity field. This implies that a continuum description cannot be used to adequately describe the below threshold regime, unless, strictly speaking, $\beta = 0$. We use W below threshold as a macroscopic, more or less phenomenological quantity, considering only its magnitude and do not discuss its fluctuations or coherence properties, which are the domain of true quantum descriptions.

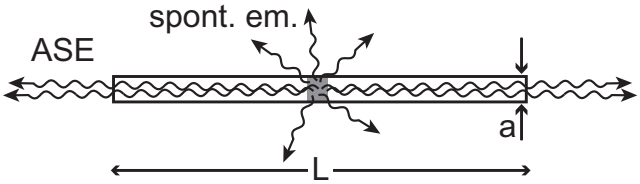

Figure 1.11 "Mirrorless lasing" in an amplifier of length L and width a. Spontaneous emission along the length is amplified, producing a narrow ASE beam.

1.3.2 Amplified spontaneous emission

In absence of a cavity, spontaneous emission is also amplified by a single pass through the gain medium. If the amplification factor is large, as may occur in high gain systems or long amplifiers, this amplified spontaneous emission (ASE) may share some properties with laser light [38], such as a "laser" threshold, a directional beam and (limited) coherence, even though there is no feedback, let alone resonant feedback. Another term for this phenomenon is mirrorless lasing, and its properties are discussed quantitatively in ref. 39.

The shape of an amplifying medium can impose a preferred direction on the radiation it emits. As figure 1.11 shows, spontaneous emission along the long axis of an amplifier experiences a larger amplification than that in other directions, producing a beam of ASE with a divergence depending on the length (aspect ratio L/a) of the amplifier. The spectrum is also narrower than the spontaneous emission spectrum because the gain curve $\sigma_e(\lambda)$ has a maximum, around which the amplification is strongest. This is the process of gain narrowing.

The ASE threshold behavior arises from saturation: if the intensity of the traveling wave in the amplifier becomes large enough to extract all the stored energy (the saturation intensity $I_{sat} = \frac{\hbar\omega}{\sigma_e\tau}$ [40]), the output intensity grows linearly with pump power, like in an ordinary laser. Below I_{sat} (shorter amplifier or lower gain) spontaneous emission into the other directions carries off part of the energy and the output intensity grows more slowly. This threshold is "softer" than a laser threshold produced by feedback in a cavity, but for long and thin amplifiers, the difference can be hard to tell. X-ray lasers, consisting of an elongated high gain plasma, are based on ASE [41], because of the lack of good mirrors in that wavelength range.

1.3.3 Laser dyes

A gain medium that is used in many practical systems is a dye solution. It consists of organic fluorescent molecules in water or an organic solvent. A dye can exhibit very high gain and can be pumped efficiently, due to the large emission and absorption

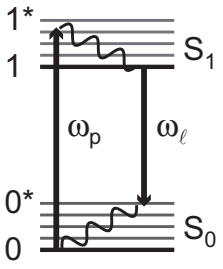

Figure 1.12 Energy scheme of a laser dye molecule. Both and ground state S_0 and the first excited S_1 are composed of a multiplet of vibrational states. Pump light (of frequency ω_p) is absorbed, putting the molecule in a high vibrational level of S_1. This quickly relaxes (with a time constant of order 0.1 ps) to a vibrational level at the bottom of S_1. This has a lifetime of a few ns, after which it decays to a high level in S_0, followed by again a quick vibrational relaxation.

cross sections ($10^{-20} - 10^{-19}$ m^2) and large fluorescence quantum efficiency (0.7 – 0.8) [30, 42]. For these reasons, we chose to use dyes as the gain medium in our experiments. The large gain bandwidth allows a broad tuning range for dye lasers.

Dyes have another advantage: they form a so-called four-level system. A schematic of the energy levels in a typical dye is given in figure 1.12. Population inversion, needed for lasing, can not be produced in a two-level system by resonant optical absorption, because saturation limits the inversion to 50%. In a four-level system, the upper lasing level 1 is populated via a higher-energy state 1^* that decays quickly into state 1, which is relatively long-lived. The lower state 0^* is also unstable and decays fast to the ground state 0. By this scheme the lower laser level is almost unpopulated, facilitating population inversion and minimizing absorption at the laser wavelength. Nearly all molecules are either in level 0 or in level 1, and the other levels can be left out of the rate equations. The laser transition is effectively decoupled from the pumping transition, sidestepping the 50% inversion limit.

For our experiments we mostly used a solution of Sulforhodamine B in methanol, with a concentration of $\sim 10^{-3}$ M. It can, like all rhodamines, be pumped with a pulsed frequency-doubled Nd:YAG laser at 532 nm, and has one of the highest stimulated emission cross sections available [43]. The maximum of σ_e is in the yellow, near 580 nm. An additional advantage of Sulforhodamine B over related dyes is that it is zwitterionic, rather than an ionic salt. A large amount of charge added to a colloidal suspension screens the electrostatic repulsion between the particles and thus can promote aggregation and sedimentation. Screening by a zwitterionic solution is less strong and accordingly the suspension is more stable. Detailed information on dye parameters is in appendix A. The typical wide absorption and fluorescence spectra of Sulforhodamine B, produced by the vibrational broadening of the $S_0 \leftrightarrow S_1$ transitions, are shown in figure 1.13.

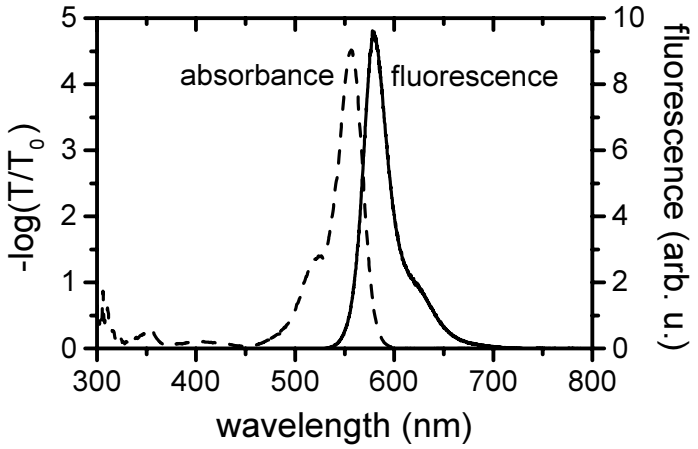

Figure 1.13 Absorption and emission spectra of Sulforhodamine B (4 μM solution in spectroscopic grade methanol). Absorbance was measured with an Ocean Optics S2000 fiber optic grating spectrometer by transmission of an Ocean Optics PX-2 flash lamp. The fluorescence emission spectrum was obtained with a Princeton Instruments Intensified CCD camera coupled to an Oriel MS 257 f/4 spectrometer, with CW excitation (Ar^+ laser, $\lambda = 514.5$ nm).

1.4 Random lasers

Light diffusion and laser physics meet in the random laser: a multiply scattering medium that amplifies light. In our case it usually consists of a suspension of scatterers in a Sulforhodamine B/methanol solution. The scatterers are a TiO_2 (rutile) colloid, with a refractive index $\eta_1 = 2.7$ [44]. This suspension is optically pumped with pulsed green light. Another possibility to make a random laser is e.g. to grind a laser crystal into a powder [45].

Since light is strongly scattered, a random laser looks turbid, like paint. Furthermore, the dye absorbs green light making the suspension appear pink. Upon optical pumping, the light from the material propagates diffusely inside, and is emitted into all solid angles. Instead of leaving the solution immediately along a straight path, the light spends a long time inside the medium because of the diffusive transport, thus getting the chance of being amplified strongly if there is sufficient gain. A schematic of the process is given in figure 1.14. Multiple scattering acts as a feedback mechanism.

1.4.1 Issues in random laser physics

One can view random lasers from the perspective of a "peculiar laser", or from the perspective of multiple scattering with an extra feature: gain. We do both, and in

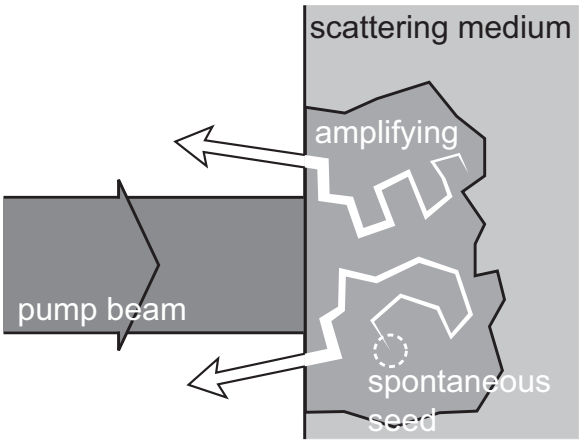

Figure 1.14 Schematic representation of a random laser. Pump light is absorbed in a scattering medium that can be optically excited. Part of the system becomes amplifying. The emission originates from a spontaneous seed that is amplified while it travels through the medium. Multiple scattering increases the path length and provides feedback if the light leaves the gain region into the rest of the system.

this thesis we want to present one consistent picture uniting those two approaches. A random laser resembles a normal laser in some aspects, as is reviewed in section 2.1. In chapter 2 we present experiments that investigate the role of transport length scales in lasing [46, 47].

How amplification influences light transport is a question stemming from the other view on random lasers. Gain in a diffusive medium mainly amplifies long light paths, just like absorption attenuates them. These long paths are responsible for many of the salient features of light in random media, such as enhanced backscattering (see chapter 4) and ultimately localization. Straightforwardly trying to solve the diffusion equation with a gain term as in (1.9) results in an intensity divergence, as was shown in an early paper by Letokhov [48], due to the possibility of infinitely long paths in the medium. The mechanism by which this problem is avoided, and its connection with the laser threshold, is the subject of chapter 3 [49].

In a diffusive laser the spatial selectivity of a cavity, which is essential in concentrating the stored energy in a few modes, does not exist. The only selection mechanism is the wavelength dependence of the gain, as discussed in section 1.3.2. Said otherwise, the electromagnetic modes of the system are broad (because of the large losses) and strongly overlapping; they do not form a good basis to study the properties of the light [50, 51]. Recently, unusual spectral features were observed in the fluorescent emission of semiconductor powder films and dye suspensions [52, 53]. As an explanation, the researchers proposed that very strong scattering could decouple the modes of the system, not unlike what happens in Anderson localization. This was called “random lasing with resonant feedback”, due to the supposed formation of random cavities. We present a critical review, including our own experiments and interpretations regarding this phenomenon, in chapter 5.

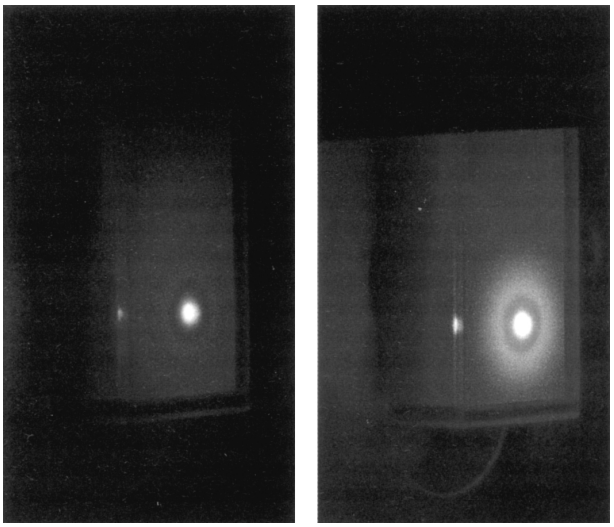

Figure 1.15 Photographs of a random laser in a glass cuvette below *(left)* and above *(right)* threshold. The bright white spot is laser emission, gray areas are scattered pump light. Above threshold the emission is much brighter.

1.4.2 Is it a laser?

Often when discussing (diffusive) random lasers, the question is asked: "But isn't that just ASE?" If the emission is going into all radiation modes of the system one can not speak of a genuine laser [54]. The lasing effect in a random laser is produced by long paths as in ASE, which can show a laser-like threshold, as was discussed in section 1.3.2. It is certainly not oscillating in a single mode [55]. On the other hand, a random laser does have a clear feedback mechanism: multiple scattering. It is non-resonant, even disordered, and works qualitatively different than feedback by a resonant cavity, but it turns out (chapter 3) that it does have a loss-like term associated with it in its intensity rate equation, cf. (1.12). Which is unlike ASE.

We deem the question "Is it a laser?" a matter of semantics, and let the physics of random lasers speak for itself.

2. Amplifying volume in scattering media

We investigate the influence of the excitation spot diameter on the laser threshold of a scattering amplifying medium. Fluorescence spectra are recorded from a suspension of dielectric scatterers in a laser dye. The threshold pump fluence is found to increase by a factor 70 if the excitation beam diameter becomes comparable to the mean free path ℓ. This increase is explained using a simple model describing diffusion out of the amplifying volume, and confirmed by a Monte Carlo simulation.

The output characteristics of a random laser show a threshold as a function of the excitation power, or pump rate. This in itself is a remarkable observation, and one of the central themes of this work is to investigate why this nonlinear dependence exists and what determines its properties. As was discussed in the previous chapter, the threshold in an ordinary laser is the pump rate where the supplied amount of energy to the system is large enough to establish a gain that overcomes the loss in the lasing mode. In a random laser, light propagates diffusively and a clear lasing mode can not be identified. Still, the threshold is there to be explained, and a clue is that it does not exist in systems without multiple scattering, as will be shown later in this chapter. Apparently, diffusive transport plays a role in the threshold and that means that the characteristic length scale for transport should have an influence.

As a short introduction to known results and for later reference, a concise survey of observations surrounding the random laser threshold is given in section 2.1, followed by a qualitative discussion of the physical mechanisms giving rise to these phenomena in 2.2. After this introduction, we will discuss the experiments and simulations that demonstrate the importance of the transport length for light amplification in a random medium. A remark about units: in the following discussion, and in the other chapters describing experiments, the pump energy supply will be quantified in units of energy/area representing a fluence, typically of the order $\mu\mathrm{J}/\mathrm{mm}^2$. The

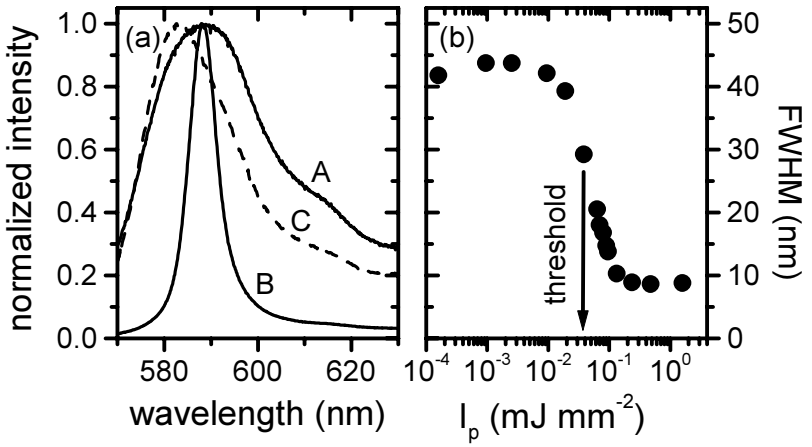

Figure 2.1 *(a)* Fluorescence of the TiO_2-dye suspension at 4 μJ (A) and 0.1 mJ (B) pump pulse energy, compared to the fluorescence of the neat dye solution (C). $\ell = 100$ μm, pump spot diameter 2 mm. *(b)* The threshold is identified as the pump fluence where the width of the spectrum "collapses".

radiated fluorescence will be called emitted intensity. Inside the medium, this is not necessarily an intensity, but we do stationary measurements which have a readout that is proportional to the intensity. See also appendix B.

2.1 Phenomenology

2.1.1 Laser threshold

The random laser threshold was first observed [56] in the intensity and spectral width of the emission. The fluorescence spectra of a typical random laser, consisting of a suspension of TiO_2 [44] scatterers in Sulforhodamine B laser dye, are shown in figure 2.1(a). The system is excited by a pump pulse from a frequency doubled Nd:YAG of duration 6 ns. Curve A is the fluorescence spectrum obtained from the sample when pumped with an excitation pulse energy of 4 μJ. It resembles the emission of the neat dye solution, shown as spectrum C for reference. The difference between A and C is caused by reabsorption of the emitted light by unexcited dye molecules [57], as will be shown in more detail in section 2.1.2. Curve B is the fluorescence spectrum of the same suspension, pumped with a pulse energy of 0.1 mJ.

Attention is immediately drawn to the much smaller width of the emission spectrum at high pump fluence. This indicates that the emission contains large fraction of stimulated emission that is strongest in the spectral region where the net gain is highest. The threshold is shown in figure 2.1(b) where the full width at half maxi-

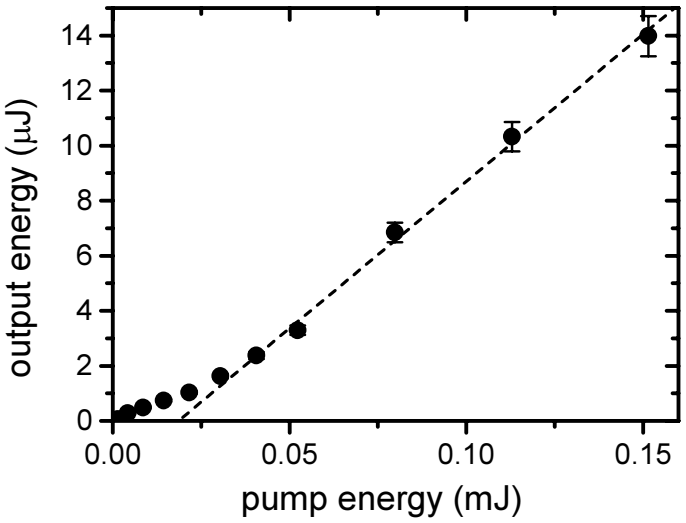

Figure 2.2 Intensity at the peak of the emission spectrum vs. pump pulse energy. The threshold is lower than in figure 2.1 because ℓ is shorter in this measurement.

mum (FHWM) of these spectra is plotted as a function of pump fluence: the width drops suddenly at a well defined fluence, which we call the laser threshold.

The laser threshold shows as a kink in the intensity at the peak of the emission spectrum as a function of pump fluence. For low pump intensities, the fluorescence is low and increases only slowly, while above threshold, the emitted intensity increases linearly with pump fluence and is generally much higher. An example of this measurement is shown in figure 2.2.

Another observation is the marked shortening of the output pulse upon crossing the threshold [58]. Below threshold, the fluorescence consists of spontaneous emission only, resulting in an output pulse duration limited by the natural lifetime of the dye, a few nanoseconds. Stimulated emission, on the other hand, is generated instantaneously so that the emission above threshold, resulting mainly from stimulated processes, is much faster and its picosecond duration is also related to the transport time in the scattering medium and the pump rate. This will be presented in more detail in chapter 3.

2.1.2 Reabsorption

The redshift that is observed in the emission spectrum of the scattering sample compared to the emission of the neat dye (see figure 2.1) is caused by absorption of the blue part of the fluorescence by ground state dye molecules. The blue part of the spectrum is absorbed, and re-emitted in a frequency distribution that is the spon-

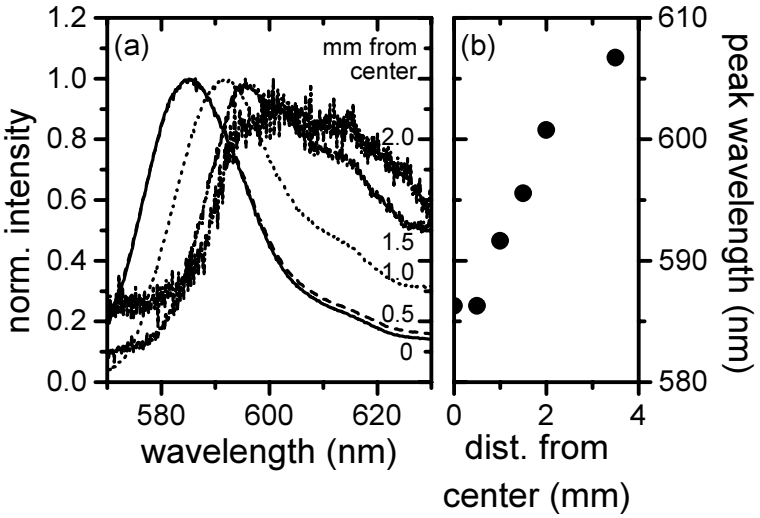

Figure 2.3 Redshift in a random laser caused by reabsorption. The lines in *(a)* are the fluorescence emission spectra obtained from regions successively farther from the center of the center of the pump spot, meaning that a longer path has been traversed. The Sulforhodamine B concentration is 1 mM, the transport mean free path is $\ell = 100\ \mu$m, and the pump pulse energy is 0.5 μJ in a focused spot of 0.1 mm diameter, far below threshold. The noise increases because the intensity goes down by a factor 100 from 0 to 2 mm and spectra have been normalized to their maxima. In *(b)*: position of the maximum intensity as a function of distance from the center.

taneous emission spectrum, which on average is redder than the reabsorbed light. These combined phenomena constitute a redshift.

The traveled path length Λ in a scattering sample can be much longer than in the neat solution, enhancing not only the amplification factor $\exp(\kappa_g \Lambda)$, but also the absorption factor $\exp(-\kappa_a \Lambda)$, where $\kappa_{g,a}$ are the gain and absorption coefficients. κ_a is appreciable only in the bluest part of the emission spectrum, as was already mentioned in section 1.3.3.

By imaging different parts of the fluorescent spot on the entrance slit of the spectrometer we can roughly select the average path length in the medium: if d is the distance from the (small) pump spot, $\langle \Lambda \rangle = 3d^2/\ell$. In figure 2.3 this procedure is used to investigate the effect of reabsorption. We use a pump fluence well below threshold to avoid saturation of the dye. The visible spot of fluorescence has a diameter of several millimeters on the slit (width $\times$ height = 0.25×1.0 mm^2) in the entrance plate of the spectrometer. The optical magnification factor is 1. Figure 2.3 clearly shows that, on moving away from the center, more and more intensity is removed from the blue part of the spectrum, broadening and redshifting the peak.

2.2 Qualitative explanation of the random laser threshold

In this section these observations will be used to compose a qualitative picture of the threshold. The spectral narrowing is intimately connected to the threshold as measured in the emitted peak intensity; actually they are one phenomenon [59].

As was discussed in section 1.3, the threshold of a laser depends on the balance between gain and loss of light in the system. The total amount of amplification depends on the product $\kappa_g\Lambda$, counting only the path length traveled in the amplifying medium. In a random laser the feedback mechanism is multiple scattering. Incomplete feedback is a loss factor. Accordingly, the loss and the distribution of traveled path lengths originate from the same mechanism: diffusion of light. If we now assume that the transport parameters do not depend strongly on the wavelength of the light (most random lasers consist of polydisperse, nonspherical scatterers, washing out the fine wavelength structure in the scattering properties of the material) then all spectral features of the emission must be due to the wavelength dependence of the gain. For demonstration purposes we use the small signal gain limit to describe the intensity in a certain path: $\exp[\kappa_g(\lambda)\Lambda]$. Light with wavelengths near the maximum of the gain is amplified more, receiving a larger spectral weight. This is the gain narrowing mentioned in section 1.3.2.

Evidently, this mechanism does not cause more light to be emitted by the system above threshold, it is just spectrally redistributed. The wavelength variation of the gain of the amplifying medium is the only selection mechanism in a random laser that distinguishes "laser" light from spontaneous emission. This means that the sharp bend at the laser threshold in the curve of emitted intensity vs. pump power is only observed in the frequency range near the maximum, and should not be present in the spectrally integrated intensity.

In a conventional laser, the threshold can be observed in the total output intensity of the laser mode, because there is an additional selection mechanism for lasing that is often much more restrictive than the spectral dependence of the gain: the mode profile of the cavity. Only light radiated in the "right" solid angle, i.e. subtended by the lasing mode, contributes, and the dominance of stimulated transitions above the laser threshold causes the abrupt change in behavior. If the radiation from a conventional laser would be collected in all directions, the threshold kink would disappear, because all the radiation, stimulated (laser) and spontaneous (non-laser), light is detected, analogous to a measurement of spectrally integrated emission from a random laser. We will revisit this analogy in the discussion of the β-factor of a random laser in 3.3.

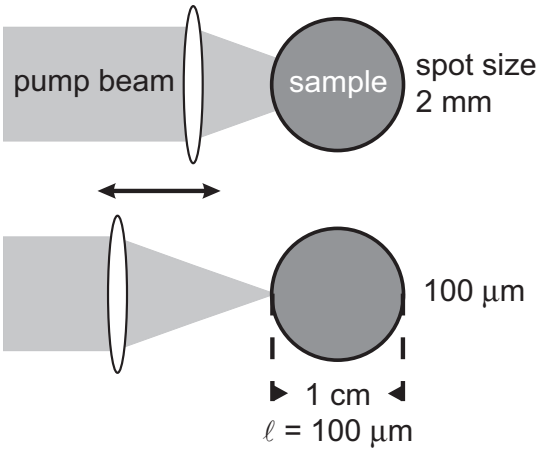

Figure 2.4 Schematic of the experimental situation. The lens is moved to change the size of the pump spot.

2.3 Amplifying volume in scattering media

In this section, we present experiments which demonstrate that the threshold of the system depends on the size of the pumped volume. The spatial distribution of gain is governed by the spreading of pump light in the system. The path length involved in the amplification process is the length of diffusive paths through the gain volume. The gain volume is cylindrical; the diameter is set by the diameter of the excitation spot. The thickness d is related to the diffuse absorption length $L_a = \sqrt{\ell \ell_a/3}$. In the absence of saturation, $d = L_a$, otherwise (as in this study) $d > L_a$. Due to multiple scattering, the loss as well as the amplified path lengths, and hence the lasing threshold, depend on the gain volume [60].

2.3.1 Experimental method

We record fluorescence spectra from a TiO_2-dye [44] suspension as a function of excitation spot diameter and pump pulse energy. The scatterers are suspended in 1.0 mM Sulforhodamine B dye dissolved in methanol. The TiO_2 volume fraction is 10^{-3}, resulting in a transport mean free path $\ell = 100 \pm 20$ μm. ℓ is obtained from coherent backscattering, measured without the pump beam. The inelastic length of the dye solution is $\ell_a = 110$ μm. The thickness of the sample cell is $L = 1$ cm. During the experiments the suspension is stirred continuously to avoid sedimentation and dye degradation.

The pump source is a Spectra Physics DCR-2A frequency-doubled Q-switched Nd:YAG laser, giving 9 mJ pulses with a pulse duration of $\tau_p = 6$ ns at a repetition rate of 20 Hz, with a wavelength of 532 nm. The pulses are attenuated using a pair of Glan prisms, of which one can be rotated to vary the pump pulse energy between 0

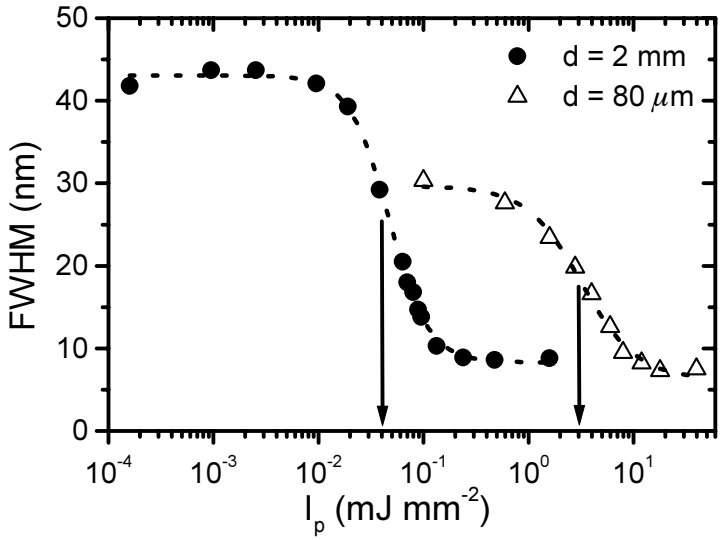

Figure 2.5 Linewidth vs. pump fluence for 2 mm (●) and 80 μm (△) pump diameters. The lines are fits to the data. The threshold, indicated by the arrow, depends on spot size.

and 9 mJ. The pump beam is incident on the sample through a lens ($f = 6$ cm), which is on a translation stage. By moving the lens along the pump beam the diameter (beam waist at $1/e^2$) of the spot on the sample cell is varied between 80 μm (in the focus) and 2 mm. The excitation and detection directions are at an angle of $\approx 20^\circ$. The fluorescence is focused on the entrance slit of a Spex 1672 Czerny-Turner type $f = 250$ mm spectrometer, used in single stage configuration. The spectrum is recorded with a Princeton Instruments 1412 diode array (1024 pixels $\times$ 14 bits).

In figure 2.5 the full width at half maximum (FWHM) of the spectra is plotted as a function of the pump fluence. From these data we define the laser threshold as the inflection point of a sigmoidal fit through the data points. This procedure is repeated for a number of different excitation spot sizes. On decreasing the pump beam diameter, the threshold intensity shifts to values that are 70 times higher than those measured with the largest spot sizes. There is a difference in FWHM below threshold for the two curves shown in figure 2.5, due to a difference in spectral shape which is caused by reabsorption. The change of FWHM within one series can however be reliably used to determine the threshold. The diameter of the pump beam strongly influences the threshold intensity, as is evident from figure 2.6. A consequence of this result is that an experiment on random lasers will yield different results depending on whether a focused pump beam or a plane wave excitation is used. Note that we vary the beam size independently of ℓ. In earlier work [56, 58] ℓ was varied and (occasionally) $\ell > L$, so necessarily also $\ell >$ pump beam size. A

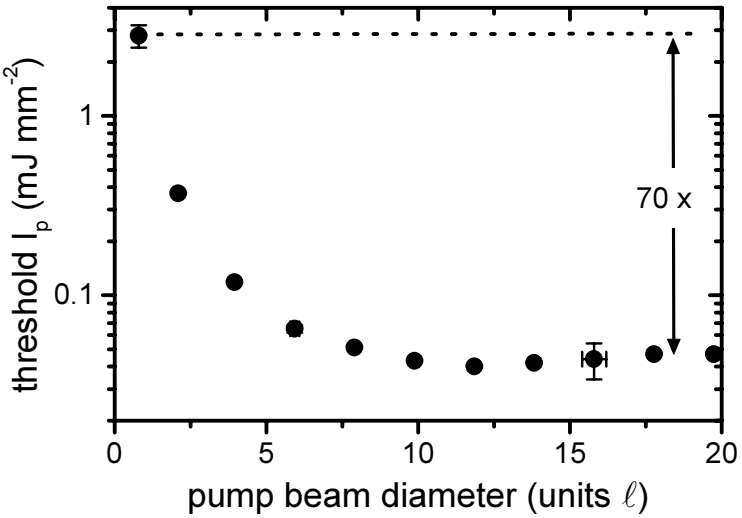

Figure 2.6 The threshold excitation intensity vs. pump beam diameter in units $\ell = 100\ \mu$m. At small pump spots, the threshold pump fluence increases by a factor 70 with respect to the threshold large pump diameter.

change in properties of the system must then be attributed to the strongly differing transport in the diffusive ($\ell \ll L$) and single-scattering regimes. For comparison, the weakly scattering regime will be discussed in 2.3.2.

The increase of the threshold for small excitation regions is explained in the following way (figure 2.7). Light is emitted in the pumped region of the sample, from where it starts to diffuse. If the pumped area is large, the amplifying volume is large. Light that is emitted in the pumped volume can travel a long path inside the part of the system that has gain: it is amplified strongly. If a path reaches the passive (unexcited) part of the system, there is a large probability that it will return to the amplifying region because of the large pumped area. For a small excitation beam diameter, the light paths will very probably leave the amplifying region after a short time, with a small chance to return. This means that a larger gain is needed to compensate losses, i.e. the threshold is higher.

2.3.2 Weakly scattering medium

We asserted earlier that a change in the threshold pump intensity due to a change in excitation spot size would be an effect of multiple scattering. In order to verify this claim, we repeated the experiment on a neat dye solution and on a suspension with $\ell \approx 2$ cm ($> L$).

In a dye solution that is only weakly scattering or even not scattering at all, a

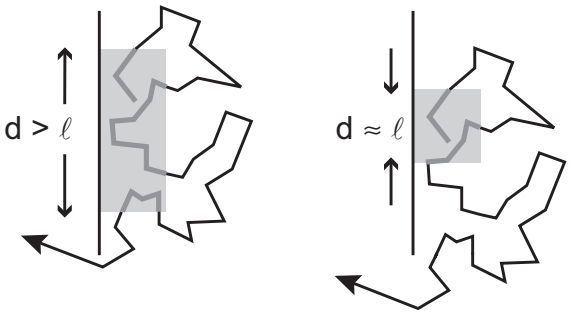

Figure 2.7 A schematic representation of the mechanism responsible for the higher threshold observed with a small beam: the same path is amplified more strongly in a large amplifying volume *(left)* than in a small one *(right)*. The amplifying volume is the shaded area, the vertical line is the sample interface.

bright beam of amplified spontaneous emission (ASE) can arise because the light is hardly scattered while traveling through the amplifying part of the dye. Spontaneously emitted light can travel unobstructed, and the spatial dimensions of the gain volume may impose a preferred direction, as discussed in section 1.3.2. ASE appears as a relatively narrow (≈ 2 nm) spectral feature in the emission spectrum, and has a clear directionality along the largest extension of the gain region.

In the case of weak scattering, light may be removed from the ASE beam by scattering, which may look similar to the spectral narrowing as observed in figure 2.1. The observations in the famous, but debated, article in Nature by Lawandy and coworkers [56] are explained at least partly by this post-amplification scattering [61].

We found that there is no clear threshold in either situation, unless the ASE is collected. The FWHM of the fluorescence spectrum does depend on the excitation intensity, but not on the excitation spot size. Neither does the ASE threshold for these transparent systems depend on spot size. This confirms that the relation between pump beam size and threshold is due to multiple scattering.

2.4 Random walk simulation

In order to check this explanation quantitatively, we performed a Monte Carlo simulation of random walks in the geometry [62] depicted in figure 2.8. The left panel shows a schematic of the system as we model it. The vertical line is the sample interface, pump light is incident from the left (not shown). The shaded box is the pumped volume. The wiggly line is a light path, which is amplified if it is the gain volume (thick lines). To avoid confusion, note that in the following paragraphs the edge of the system is called the *interface*, and the edge of the amplifying volume is called the *boundary*. Both are important in the simulation, but their roles are different.

Assuming a sharply bounded box of homogeneous gain coefficient is admittedly a fairly crude approximation of the actual gain profile, and we find a much more accurate distribution in chapters 3 and 4. However, the method used there is difficult

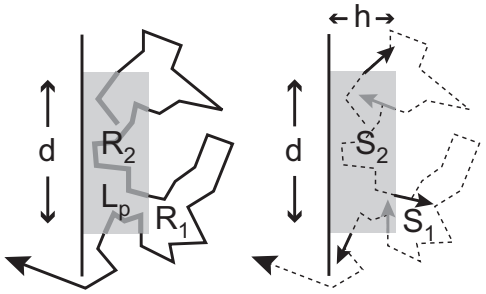

Figure 2.8 *Left:* A model geometry of the system: the box is the amplifying volume, the wiggly line represents a path. *Right:* Implementation of this path used in the simulation. The return probabilities R_1 and R_2 are calculated for S_1 (outside the gain volume) and S_2 (inside). For S_2 we also evaluate the pathlength L_p in the gain volume.

to apply in systems where the excitation is not a plane wave, the limit we are studying here. The assumption of a sharp boundary will doubtlessly affect the numerical accuracy of the results of the simulation, but the convincing performance of this model in ref. 62 encourages trust in the qualitative features of the outcome.

For the simulation, parts of the trajectory inside and outside the gain volume are considered separately. We simulate one set S_1 traveling out of the gain volume, and another S_2 traveling inward (figure 2.8, right). All paths, both in S_1 and in S_2, start at random points, uniformly distributed on the boundary of the amplifying box. The simulation runs until the path returns to the boundary, and then it is counted as returned, or until it leaves the medium through the interface. Returning paths stay close to the boundary on average. So, paths in S_1 can also end by exceeding a (large) maximum number of steps. With this division into two categories we try to construct a quantitative analogy to cavity loss, i.e. mirror reflectivity.

It is always "good" for the amount of amplification per path to return to the boundary of the excited volume. For a path in S_1 this is obvious: returning to the pumped volume will cause it to be amplified further. For a path in S_2, the only other possibility is to leave the sample through the interface which means it is lost. A return to the boundary of the amplifying box means remaining inside the medium, though it leaves the amplifying part. Hence, the probability to return to the amplifying/passive boundary may be compared to the reflectivity of a cavity mirror in an ordinary laser. We calculate the return probabilities R_1 (for S_1) and R_2 (for S_2).

For paths in S_2, we also keep track of the traveled path length L_p. The threshold gain κ_{th} is the amplification per unit path length needed to compensate "cavity" losses. It is calculated from

$$\exp\left(\kappa_{th} L_p\right) R_1 R_2 = 1 \; . \tag{2.1}$$

Our simulation is performed for a series of different radii of the gain volume between 0.5ℓ and 100ℓ, resulting in an R_1, R_2 and L_p for each radius. The depth is kept fixed at $h = 3\ell$, a number estimated from the amount of pump photons per

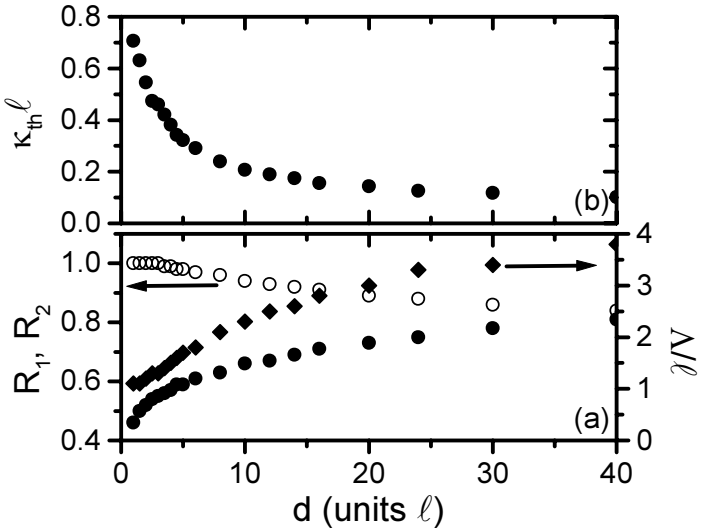

Figure 2.9 Simulation results. *(a)* R_1 (●) and R_2 (○) are the return probabilities of light outside and inside the box respectively; while L_p (◆) is the path length in the box. *(b)* The threshold gain coefficient κ_{th} obtained from these data.

pulse injected into the sample and the resulting saturation. For large beam radii the gain volume has the shape of a pancake, which is sensible. For small beam radii the volume is a rod-shaped, while in reality some lateral spreading of order ℓ will occur. In this limit, different shapes (e.g. a cone or a paraboloid) give similar values for κ_{th}; the most influential parameter is the ratio of boundary area to gain volume.

Technically, the simulation is implemented in cylinder coordinates, as is naturally suggested by the geometry of the problem. The walks start from random points that are uniformly distributed over the surface of the amplifying volume, and end when they reach either the sample interface or the box boundary. The fraction of walks returning to the boundary of the gain volume is the return probability. The step length is exponentially distributed with average ℓ.

The result of the simulations is shown in figure 2.9. The trends in R_1, R_2, and L_p correspond to what is expected: R_1 is small for small d, because paths that reach deep into the sample will likely miss the amplifying box if they return to the interface, while they have a larger probability of returning to it if d is big. R_2 shows opposite behavior as it largely depends on the boundary area to gain volume ratio. L_p increases for larger box sizes. The combined effect is a κ_{th} that increases for smaller beam diameters, which is in qualitative agreement with the experimental result of figure 2.6.

In order to really compare experiment and simulation we must convert κ_{th} ob-

tained from R_1, R_2 and L_p to a threshold pump intensity. The method we use is adapted from refs. 63, 64 to explicitly include saturation effects: the threshold inversion is a substantial fraction of the total population.

The threshold gain is inserted in a set of laser rate equations where only cavity losses are considered. We analyze the system in steady state for simplicity, corresponding to a CW situation. The pump pulse in our experiments is much longer than the time it takes for a quasi-steady state to develop. This time is of the order of 100 ps, according to earlier simulations [60], and also according to chapter 3. On the other hand, the pump pulse is short enough to neglect population of the triplet state of the dye [64] (buildup time in the order of 100 ns). Isolating the pump intensity I_p in terms of κ_{th} results in the relation

$$I_p = \frac{\eta \hbar \omega_p}{\sigma_a \tau} \frac{\kappa_{th}}{\kappa_0 - \kappa_{th}} . \tag{2.2}$$

Here κ_0 is related to the maximum gain, and has a numeric value of $\kappa_0 = 77\ \mathrm{cm}^{-1} = 0.77\ell^{-1}$. η is the refractive index of the solution, $\hbar\omega_p$ is the pump photon energy, σ_a is the absorption cross section of the dye for pump light, and τ is the excited state lifetime of the dye in methanol. Numerical values for the parameters of Sulforhodamine B may be found in table A.1 on page 111. Because of the steady state character of the analysis, the result is a pump intensity (incident power per area in $\mathrm{W/m^2}$), rather than the fluence (incident energy per area in $\mathrm{J/m^2}$). Intensity is converted into fluence with the help of the pulse duration τ_p. The final result is shown in figure 2.10.

2.5 Discussion

Comparing the results from experiment and simulation, we see that there is an excellent agreement in the behavior of the threshold pump intensity as a function of the excitation spot diameter. The upturn at small diameters that is observed in the experiment is correctly reproduced by the simulation. The dependence of the threshold intensity is well explained by the model described above. Intensities from the experiment are a factor ≈ 2 larger than those from the calculation; the difference is largely caused by two relevant processes that are not included of our model.

The most important aspect is that we assume all incident pump light is absorbed. Because of the method of simulation we chose, i.e. we only simulate propagating emitted light and not the incident pump light, it is not possible to extract the amount of absorbed pump light. However, since the inelastic length ℓ_a is about equal to the transport length ℓ, we expect approximately half of the pump light to be scattered out of the system within the first absorption length. This effect would just cancel

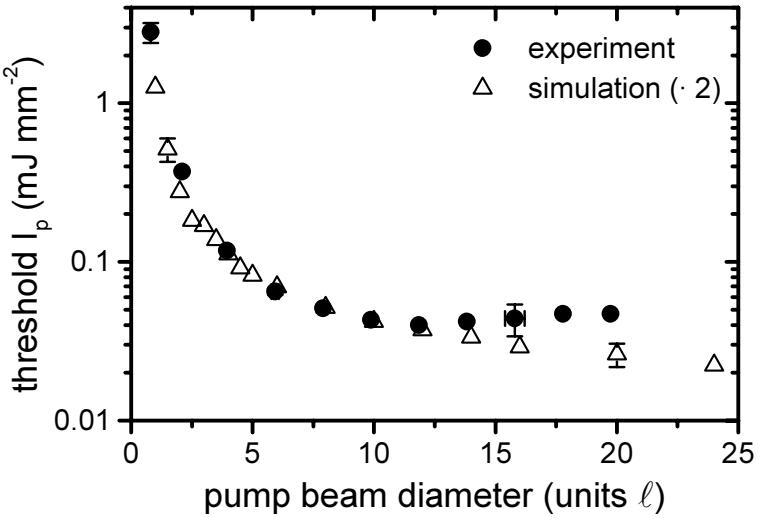

Figure 2.10 The threshold excitation intensity vs. pump beam diameter in units $\ell = 100\,\mu$m; from experiment (●) and from simulation (△). Simulation results have been multiplied by a factor 2 to bring them on the same scale as the experiment.

the difference between experiment and simulation. However, the ratio between the amounts of light scattered and absorbed just behind the interface may vary due to saturation effects leading to a decreased absorption coefficient; the threshold inversions n_1/n close to the interface can be more than 0.5. An a posteriori correction based on estimates like these is the only way to account for the scattering of pump light.

Reabsorption is an additional loss mechanism, while we only consider incomplete feedback (or "cavity" losses). This causes the actual threshold gain to be slightly larger than we estimate. It has not been taken into account here because it is a small effect compared to the gain, and it is only relevant for long paths that do not contribute much to the R_1. There is, however, a feature in the data which we attribute to reabsorption loss: The threshold intensities resulting from the simulation are monotonically decreasing, as is expected from the reasoning used in constructing the model. The experimental threshold I_p's, however, level off for the largest beam diameters and even seem to increase a little. Long paths in the passive part of the system contribute appreciably to the feedback for large pump beam diameters, but are also subject to more reabsorption. This increases the threshold for large pump spots.

We have demonstrated that the excitation intensity, needed to drive a scattering gain medium to its threshold, depends strongly on the beam diameter of the pump.

This effect is due to multiple scattering: it is not observed in the absence of scatterers. Light that propagates diffusively through the medium starts from the excited volume and is amplified less strongly if the amplifying region of the sample has a small diameter, in the order of 5ℓ, giving rise to a threshold that is up to 70 times higher than if the gain volume is large. The experimental data are accurately reproduced by a Monte Carlo random walk simulation.

3. Dynamics of the threshold crossing

Amplification influences light transport in disordered systems. In this chapter we present and interpret detailed calculations of diffusion in a saturable medium that absorbs green light and amplifies red light. The propagation of both pump and laser light are taken into account, coupled to a rate equation for the population inversion. We identify the diffusive analogue of loss in these generalized laser equations, and investigate the threshold crossing. The full dynamics of the interplay between field and population is found to be an essential part of a description of a random laser close to or above the laser threshold. The full transport equations are not very transparent at first sight due to their nonlinearity, and can only be solved numerically. To prevent a "black box" presentation, we start by discussing simplifications and approximations of the complete formalism to demonstrate the physics.

Light is amplified according to the exponential relation $e^{\kappa_g \Lambda}$, where κ_g is the gain coefficient and Λ is the path length traveled in the amplifying medium. This relation was already discussed as Beer's law (1.3), and here we use it with a negative absorption coefficient. It immediately reveals the difference in the effect of gain on long and short paths: with a constant κ_g, the paths of large Λ are amplified much more strongly. The transport characteristics of light change strongly in the presence of gain, as will be discussed below in section 3.1.

The most straightforward way of incorporating gain in multiple scattering is by inclusion of a gain term in the diffusion equation, as in (1.9):

$$\frac{\partial W}{\partial t} = D\nabla^2 W + \kappa_g c W + S\,. \tag{3.1}$$

3.1 The photon bomb

Solutions of (3.1) turn out to exist only for a finite sized systems [48]. The maximum volume for which a solution can be found is called the critical volume V_{cr}. The physical background for this behavior is the possibility of infinitely long paths in diffusion, which will be amplified to infinite intensities in a gain medium. The result is a diverging intensity, occurring whenever the probability for a path to be scattered out of the system is compensated by the gain. Chances of leaving the medium are smaller for larger systems, so the smaller the gain the larger V_{cr}. Because of the similarity with neutron diffusion in fissionable material, exploding at the critical volume, the critical random laser is also called the "photon bomb".

Solutions of (3.1) are found by a method analogous to solving the time dependent Schrödinger equation: first we find the eigenfunctions $\phi_n(\mathbf{r})$ and eigenvalues ε_n of the stationary part. These have the simple time-evolution $\phi_n(\mathbf{r},t) = \phi_n(\mathbf{r},0)e^{-D\varepsilon_n t}$. Then $W(\mathbf{r},t) = \sum_n a_n \phi_n(\mathbf{r},t)$, where the a_n are determined by $W(\mathbf{r},0)$. The exponential time dependence shows that the eigenfunction with the smallest eigenvalue soon dominates the entire sum, and that as soon as there is an $\varepsilon_n < 0$, the intensity grows with time. This is called the generation threshold.

The stationary part of (3.1) is solved for a slab that is finite only in the z-direction with thickness L:

$$-\left[\frac{\partial^2}{\partial z^2} + \frac{3\kappa_{\mathrm{g}}}{\ell}\right]\phi_n = \varepsilon_n \phi_n \,, \tag{3.2}$$

which is like a particle-in-a-box problem with the bottom of the box at a potential $-3\kappa_{\mathrm{g}}/\ell$. The boundary conditions are in principle [20] (1.10), but for demonstration purposes we allow ourselves the small error of just extrapolating ϕ_n to zero a distance z_{e} outside the slab. The ϕ_n are then of the form

$$\phi_n(z) \propto \sin k_n z \quad \text{with} \quad k_n \equiv \sqrt{\varepsilon_n + \frac{3\kappa_{\mathrm{g}}}{\ell}} = \frac{n\pi}{Z} \,. \tag{3.3}$$

Here $Z = L + 2z_{\mathrm{e}}$. The lowest eigenvalue ε_1 reaches zero at $Z = \pi\sqrt{\ell/(3\kappa_{\mathrm{g}})}$, and the critical thickness $L_{\mathrm{cr}} = \pi L_{\mathrm{g}}$, if $L \gg z_{\mathrm{e}}$ and $L_{\mathrm{g}} = \sqrt{\ell\ell_{\mathrm{g}}/3}$ is the diffusive gain length, similar to the diffusive absorption length (1.11).

Connection with the laser threshold The intensity in an actual random laser will of course not diverge, ultimately by energy conservation. The question is what happens instead. The intensity divergence has severely hampered theoretical efforts for systems beyond the critical point, $L > L_{\mathrm{cr}}$. The divergence has been identified with the laser threshold in several theoretical papers [65–70], although none of them

could actually connect to experimental observations. The identification of the explosion with the laser threshold is encouraged by the explosion's origin being the compensation of energy leaving the system by the gain. This balance can be considered as a loose analogy to the laser threshold criterion. Also, the name "generation threshold" coined by Letokhov is suggestive in this respect.

3.2 Transport equations

The essence of (1.3), that was freely employed as the basis of (3.1), is that every slice of thickness $\mathrm{d}z$ should induce a proportional change of the intensity: $\mathrm{d}I = -\kappa I \mathrm{d}z$. This assumes that there is no back-action of the light on the medium. Microscopically, however, for every absorbed photon there is a molecule excited, that will remain excited for the duration of its lifetime τ. For low intensities the change in number of ground state molecules is negligible. But for high intensities, if the absorption rate per molecule $\frac{I}{\hbar\omega}\cdot\sigma_\mathrm{a}$ is comparable to the decay rate τ^{-1}, a significant fraction of the population is excited at any moment. In other words, the absorption is saturated by light intensities larger than $\frac{\hbar\omega}{\sigma_\mathrm{a}\tau}$, the saturation intensity.

Similarly, gain in a medium can be saturated due to de-excitation, hence $e^{\kappa_\mathrm{g}\Lambda}$ is called the *small signal* gain factor. The effect of saturation, vital for the description of a laser, can be incorporated in the diffusion equation by explicitly taking the inversion into account. The amplification term of (3.1) then takes the form $\sigma_\mathrm{e} c n_1(\mathbf{r},t) W(\mathbf{r},t)$, where n_1 is the local and instantaneous density of molecules in the excited state, and σ_e is the stimulated emission cross section.

The pump excites the dye molecules, so we need a diffusion equation for pump light with an absorption term $\sigma_\mathrm{a} c n_0(\mathbf{r},t) W_\mathrm{p}(\mathbf{r},t)$, a saturable version of (1.9). The effects of amplification and absorption on the inversion are accounted for in a population rate equation, like (1.13) but now depending on position. We assume in this chapter that the pump beam has a diameter d that is larger than any other length in the system, allowing the use of a plane wave geometry and discarding transverse directions. Practically $d < L$ may occur, but then L is large and all the phenomena related to gain occur in a shallow front layer of the system. These considerations are embodied in (3.4)–(3.6) below:

$$\frac{\partial W_\ell}{\partial t} = D\nabla_z^2 W_\ell + \left(\sigma_\mathrm{e} c n_1 - \sigma_\mathrm{r} c n_0\right) W_\ell + \frac{\beta}{\tau} n_1 \,; \tag{3.4}$$

$$\frac{\partial W_\mathrm{p}}{\partial t} = D\nabla_z^2 W_\mathrm{p} - \sigma_\mathrm{a} c n_0 W_\mathrm{p} + \frac{1}{\ell} I_\mathrm{in} \,; \tag{3.5}$$

$$\frac{\partial n_1}{\partial t} = \sigma_\mathrm{a} c n_0 W_\mathrm{p} - \left(\sigma_\mathrm{e} c n_1 - \sigma_\mathrm{r} c n_0\right) W_\ell - \frac{1}{\tau} n_1 \,. \tag{3.6}$$

In these equations, W_ℓ and W_p are the "laser" and pump light densities. We speak of laser light because only the light partaking in the amplification process is in (3.4), not all emitted luminescence. The ground state and excited state populations are n_0 and n_1, satisfying $n_0 + n_1 = n$, the total dye concentration.

The spectral dependence is not in (3.4). The real molecular absorption and stimulated emission cross sections vary with wavelength, and so should be read as $\sigma_\mathrm{e} = \sigma_\mathrm{e}(\lambda_\ell)$ and $\sigma_\mathrm{a} = \sigma_\mathrm{a}(\lambda_\mathrm{p})$. The effect of reabsorption on the emission spectrum was presented in section 2.1.2. In these wavelength-independent equations, reabsorption is accounted for by an absorption term with a cross section $\sigma_\mathrm{r} = \sigma_\mathrm{a}(\lambda_\ell)$. This cross section is small, typically a few percent of $\sigma_\mathrm{e}(\lambda_\ell)$ for laser dyes, but its effect is appreciable because of the exponential attenuation of long light paths.

The source terms in (3.4) and (3.5) differ in physical origin. The pump light stems from an incident beam, written here as $\ell^{-1} I_\mathrm{in}(z,t)$. It decays exponentially with z as a result of scattering and absorption. As a result, the pump mainly excites the dye in a layer with a thickness of order L_a near the pump face of the sample. The t-dependence of I_in is the pump pulse profile in time. The source of laser light is the spontaneous emission term $\beta n_1 \tau^{-1}$, where τ is the natural lifetime and β is the spontaneous emission factor, see section 3.3.

The equations (3.4)–(3.6) completely determine the transport of pump and laser light, coupled to the population dynamics, in a diffusive system. They form a set of coupled nonlinear partial differential equations, subject to the boundary conditions 1.10, and need to be solved simultaneously. This is done by numerical integration, as will be described in section 3.4.2.

3.3 β-factor in a random laser

Spontaneous emission is usually the seed for lasing, both in cavity and in random lasers. However, not all spontaneous emission participates in the laser process. The fraction of spontaneous radiation that does contribute to lasing is called β, introduced in section 1.3.1.

Random lasers have been described until now without β [62, 71], yet the observation of a nonzero threshold does clearly necessitate a $\beta < 1$. A reliable numerical value of β is indispensable for a model describing the response of a random laser to an applied pump pulse.

3.3.1 Spontaneous emission seeding in cavity and random lasers

In a cavity laser, light that is emitted outside a resonant mode of the cavity (outside being either of the wrong direction or the wrong wavelength) does not stimulate

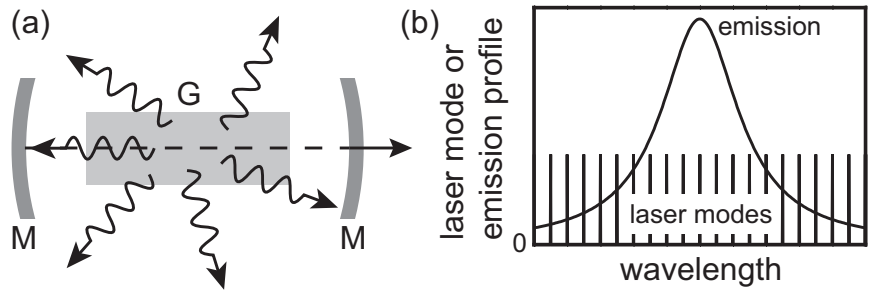

Figure 3.1 Origin of β in a cavity laser. Spontaneous emission that is to contribute to lasing has to be in the correct mode, i.e. there has to be overlap in direction *(a)* and in frequency *(b)*.

further emission and leaves the cavity without contributing to the laser field. Hence, an estimate for β involves geometric parameters like the acceptance solid angle of the lasing modes or the mode volume, as well as frequency [72]. As is illustrated in figure 3.1, β is the overlap in wave vector between spontaneous emission and laser mode.

These geometric restrictions do not apply to the random case, because of the lack of direction in the feedback mechanism: multiple scattering. The only selection criterion is the spectral dependence of the gain. Compared to the spontaneous emission the spectrum narrows above threshold around the maximum of the net gain of the medium. The exponential growth of the emitted intensity with gain coefficient $\kappa_g(\lambda)$ is responsible for the narrowing. Typical (neat dye) spontaneous emission and (high pump fluence) random laser spectra are shown in figure 3.2(a), normalized to their respective maxima. Since spontaneous emission of a wavelength outside the narrowed spectrum can not contribute to the laser process, we use the overlap between below- and above-threshold emission spectra for a definition of β.

3.3.2 Quantitative construction of β in a random laser

The transport of laser light in a random laser is described by (3.4) and (3.6) discussed on page 49. We will now explain what β means in (3.4) and how to obtain it. To incorporate the spectral dependence we rewrite (3.4) in terms of the specific energy density $W_\ell(\lambda) = W_\ell(\lambda;\mathbf{r},t)$.

$$\frac{\partial}{\partial t}W_\ell(\lambda)\mathrm{d}\lambda = D\nabla_z^2 W_\ell(\lambda)\mathrm{d}\lambda + \left(\sigma_\mathrm{e}(\lambda)cn_1 - \sigma_\mathrm{a}(\lambda)cn_0\right)W_\ell(\lambda)\mathrm{d}\lambda + \frac{n_1}{\tau}L(\lambda)M(\lambda)\mathrm{d}\lambda\,. \quad (3.7)$$

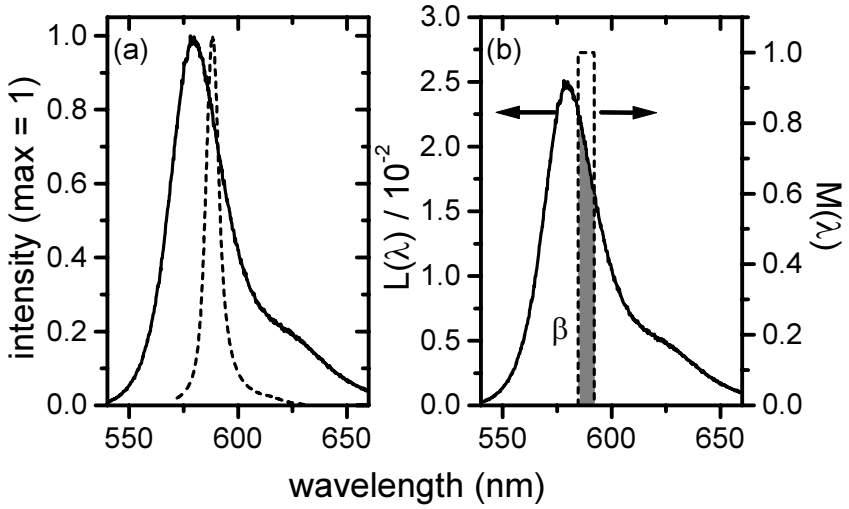

Figure 3.2 Illustration of the construction of β from the overlap between spontaneous emission (solid line) and above-threshold (dashed line) spectra shown in *(a)*. In *(b)*: $\beta = \int_{\lambda_\ell-\delta}^{\lambda_\ell+\delta} M(\lambda)L(\lambda)\mathrm{d}\lambda$, where $L(\lambda)\mathrm{d}\lambda$ is the specific spontaneous emission spectral density (solid line, left axis) and $M(\lambda)$ is the coupling to the random laser process (dashed line, right axis). In this example we use for $M(\lambda)$ a step function, yielding $\beta = 0.14$.

Here, $L(\lambda)\mathrm{d}\lambda$ is the spontaneous emission spectral density function, with $\int_0^\infty L(\lambda)\mathrm{d}\lambda = 1$. Integration over the entire spectrum yields (3.4) from (3.7). Since W_ℓ should only include the laser light (not all spontaneous emission), $L(\lambda)$ is multiplied by a "spectral participation factor" $M(\lambda)$, describing the coupling of the spontaneous emission to the laser process. $M(\lambda)$ excludes spontaneous emission outside the lasing band from W_ℓ. The exact shape of $M(\lambda)$ is immaterial for the current discussion, as long as it is peaked in a small wavelength range $\pm\delta$ around the central wavelength above threshold λ_ℓ, and $M(\lambda) \leq 1$. Following these arguments, we can restrict the integration domain to $\lambda_\ell \pm \delta$, where λ is the center wavelength of the emission spectrum above threshold. Outside this range $W_\ell(\lambda), M(\lambda) \approx 0$. In this small wavelength domain we can take all cross-sections to be constant.

$$\begin{aligned}\frac{\partial}{\partial t}\int_{\lambda_\ell-\delta}^{\lambda_\ell+\delta} W_\ell(\lambda)\mathrm{d}\lambda = D\nabla_z^2 \int_{\lambda_\ell-\delta}^{\lambda_\ell+\delta} W_\ell(\lambda)\mathrm{d}\lambda \\ + \left(\sigma_\mathrm{e}(\lambda_\ell)cn_1 - \sigma_\mathrm{r}(\lambda_\ell)cn_0\right)\int_{\lambda_\ell-\delta}^{\lambda_\ell+\delta} W_\ell(\lambda)\mathrm{d}\lambda \\ + \frac{n_1}{\tau}\int_{\lambda_\ell-\delta}^{\lambda_\ell+\delta} M(\lambda)L(\lambda)\mathrm{d}\lambda\,.\end{aligned} \tag{3.8}$$

Now $W_\ell = \int_{\lambda_\ell-\delta}^{\lambda_\ell+\delta} W_\ell(\lambda)\mathrm{d}\lambda$, so to equate (3.4) and (3.8) we define

$$\beta \equiv \int_{\lambda_\ell-\delta}^{\lambda_\ell+\delta} M(\lambda)L(\lambda)\mathrm{d}\lambda \tag{3.9}$$

and $\sigma_\mathrm{e} = \sigma_\mathrm{e}(\lambda_\ell)$, $\sigma_\mathrm{r} = \sigma_\mathrm{a}(\lambda_\ell)$.

For (3.6) the same procedure is followed, except for the multiplication by $M(\lambda)$ of the spontaneous emission term, since n_1 is not spectrally dependent. Thus, β does not appear in (3.6), as it should not.

3.3.3 Discussion

In the treatment of a cavity laser, β appears not only in the spontaneous emission term but also in the gain coefficient [34, 73] as in (1.14). This is because of the fundamental requirement that, if the average occupation number of the laser mode is 1, the spontaneous and stimulated emission be equal. Via this back door, which cannot be locked in a system with discrete modes, the β that was intuitively introduced for the spontaneous emission seed, enters in the stimulated emission term. In the derivation above we have only worked with energy densities, without having to refer to photon numbers. This is allowed by the absence of discrete modes in a random laser, due to the continuity of the space variables. If $g(\lambda,\lambda_0)$ is the lineshape function centered at λ_0, then our use of $\sigma_\mathrm{e}(\lambda_\ell)$ instead of $\sigma_\mathrm{e}(\lambda_0)\int_0^\infty g(\lambda,\lambda_0)d\lambda$ may be seen as the analogue of the β in the gain coefficient, see also (1.18).

From (3.9), it is obvious that the spectral shape of $M(\lambda)$ will quantitatively influence β. The above-threshold spectrum is in principle the outcome of several wavelength dependent processes: amplification $\kappa_g(\lambda)$, seeding by spontaneous emission via $L(\lambda)$, and possibly even scattering via $D(\lambda)$. The spectral participation factor $M(\lambda)$ is clearly a simplification of this complex problem, foregoing many sublteties. But the bottom line—spontaneous emission outside the laser spectrum does not contribute to W_ℓ—is encompassed in the $M(\lambda)$ construct. It therefore suffices to say that $M(\lambda)$ must be similar to the normalized above-threshold spectrum.

β reflects the narrowing of the spectrum above the threshold, indeed connected to the sharpness of the laser threshold, as was discussed in section 2.2. So, β takes into account the spectral redistribution in a calculation that is not wavelength-dependent; the coupling between different wavelengths in (3.4)–(3.6) would make them much less compact numerically. As will be seen in chapter 4 this use of β yields quantitatively correct results.

If the scattering mechanism is wavelength dependent, as can occur in a system in which the scatterers are monodisperse Mie-spheres, the resulting narrowed spectrum may be altered due to the improved feedback, or, equivalently, smaller transport term,

near scattering resonances. Effectively, this means that $D = D(\lambda)$, where D decreases near a resonance. The definition of β is not changed by this process, because it uses the experimentally obtained laser spectrum to determine the overlap with the spontaneous emission spectrum of the active medium.

Quantitative estimate The numerical value for β is needed for the full calculation of the inversion. It typically turns out to be of the order of 0.1. Our method to construct β from the spectra is outlined in figure 3.2. For demonstration purposes we take $M(\lambda)$ to be 1 (perfect coupling) inside $\lambda_\ell \pm \delta$, where 2δ is the FWHM of the spectrum. This yields almost certainly to an overestimation of β, but only by factors of order unity. With this $M(\lambda)$ we get from (3.9) $\beta = \int_{-\delta}^{\delta} L(\lambda - \lambda_\ell) \mathrm{d}\lambda \approx 0.14$. Using the spectrum normalized to the maximum as shown in figure 3.2(a) for $M(\lambda)$ yields $\beta \approx 0.07$.

These numbers are quite sizeable compared to the β-factors encountered in conventional lasers, typically 10^{-8} for gas lasers, 10^{-5} for commercial semiconductor lasers and up to 10^{-1} for (hardly "conventional") microcavity systems [34]. The physical background for this large magnitude is of course the "soft" selection mechanism solely by spectral overlap in random lasers, in contrast with the much more stringent requirements on the wave vector **k** imposed by discrete modes. However, the lack of direction in the emission (while making a large β possible) renders the random laser useless for the purposes large-β lasers are desired for, such as thresholdless directional emission and controlled QED experiments.

3.4 Closer investigation of the transport equations

We now return to (3.4)–(3.6). In this section, we will present the method to obtain the dynamic solution of these transport equations. In addition, we discuss an attempt at a stationary solution method, which does not provide a quantitative answer for all pump energies but does give insight in the analogy with normal lasers, connecting to section 1.3. Numerical estimates and examples apply to the random lasers consisting of scatterers in laser dye with a concentration in the order of 1 mM, and transport mean free paths of 1–10 μm, applying to most of our experiments as described in chapter 4 and part of chapter 5.

We rescale (3.4)–(3.6) in dimensionless quantities. To do this, we choose a coordinate scaling derived from transport properties, rather than laser properties such as τ or κ_g. The space coordinate z is scaled to $\zeta = \frac{z}{L_z}$, where L_z is a measure of the size of the amplifying part of the system; a more precise choice for L_z will be made in section 3.4.2. Consequently, the time scale is set to be the transport time over a distance L_z: $\tau^s = \frac{L_z^2}{D}$ and $\theta = \frac{t}{\tau^s}$. We write $\partial_\theta \equiv \frac{\partial}{\partial\theta}$ and $\nabla_\zeta^2 \equiv \frac{\partial^2}{\partial\zeta^2}$.

The dynamic quantities are scaled with respect to numbers derived from laser physics. We use the notation $\tilde{x} = \frac{X}{X^s}$. The pump and laser light scales are the respective saturation densities $W_\ell^s = (\sigma_e c\tau)^{-1}$ and $W_p^s = (\sigma_a c\tau)^{-1}$. The population scale is derived from the stimulated emission rate, $n^s = (\sigma_e c\tau^s)^{-1}$. The result is:

$$\partial_\theta \tilde{w}_\ell = \nabla_\zeta^2 \tilde{w}_\ell + \left(\tilde{n}_1 - \tfrac{\sigma_r}{\sigma_e}\tilde{n}_0\right)\tilde{w}_\ell + \beta\tilde{n}_1\,; \tag{3.10}$$

$$\partial_\theta \tilde{w}_p = \nabla_\zeta^2 \tilde{w}_p - \tfrac{\sigma_a}{\sigma_e}\tilde{n}_0\tilde{w}_p + \tilde{w}_{in}\,; \tag{3.11}$$

$$\partial_\theta \tilde{n}_1 = \frac{\tau^s}{\tau}\left[\tilde{n}_0\tilde{w}_p - \left(\tilde{n}_1 - \tfrac{\sigma_r}{\sigma_e}\tilde{n}_0\right)\tilde{w}_\ell - \tilde{n}_1\right]. \tag{3.12}$$

All terms in (3.10)–(3.12) are of order 1, except the ratios $\frac{\sigma_r}{\sigma_e}$ and $\frac{\tau^s}{\tau}$. The former is $\sim 10^{-2}$, which just means that absorption at the emission wavelength is relatively unimportant. For the discussion of the main properties of this model we will disregard the reabsorption for the rest of this section, to bring it back in section 3.5. The latter, $\frac{\tau^s}{\tau}$, is of the order 10^{-3} if we assume that $L_z \approx L_a \sim 10\ \mu$m for typical materials with $\ell \sim \mu$m and $\ell_a \sim 100\ \mu$m. Then the transport time through the excited layer $\tau^s \sim$ ps, while the natural lifetime $\tau \sim$ ns. This large deviation of $\frac{\tau^s}{\tau}$ from unity signals a slow coupling between population and field, with far-reaching consequences.

3.4.1 Analogy with conventional lasers

We apply the same scaling as described above to the ordinary laser rate equations (1.12) and (1.13), with the substitution for the pump rate $R = \sigma_a c W_p$ (see appendix B), so $R^s = \tau^{-1}$ is the saturation pump rate. If we make the identification for the time scale $\tau_c^s \equiv \gamma_{loss}^{-1} = \tau_c$, we arrive at relations that can easily be compared with (3.10) and (3.12):

$$d_\theta \tilde{w} = -\tilde{w} + \tilde{n}_1\tilde{w} + \beta\tilde{n}_1\,; \tag{3.13}$$

$$d_\theta \tilde{n}_1 = \frac{\tau_c^s}{\tau}\left[\tilde{n}_0\tilde{r} - \tilde{n}_1(\tilde{w}+1)\right]. \tag{3.14}$$

There is no spatial coordinate to scale, as (1.12) and (1.13) are formulated for a cavity mode. The field density, gain coefficient, pump rate and loss rate do not depend on position but rather on mode index. There is no interaction between the modes.

Upon comparing (3.10) and (3.13), it is immediately apparent that the transport in a random laser maps directly on the loss in a cavity system. The loss now varies locally, rather than per mode. The role of transport as a local loss is quite natural: it is the net rate of energy removed from a specific position. However, the fact that diffusive transport is driven by density variations introduces a coupling with the field density in the neighborhood that does not occur in the single mode system to which

(3.13) applies. The steady state transport on the length scale of the entire system is directed towards the interfaces, there is a net flow of energy from any position inside the medium. As a consequence, $\nabla^2 W \leq 0$ in a finite, nonabsorbing system, as a loss term should be. The transport time τ^s is the diffuse analogue of the cavity decay time τ_c.

A sketchy analysis of (3.10) and (3.12) in the steady state fashion of section 1.3.1 already reveals some qualitative similarities between the kinetics of random and cavity systems. More details on the mapping of a random laser on a cavity system will be filled in in figure 3.3 and the accompanying discussion on page 56.

Below threshold, the density of laser light is far less than the saturation density, $\tilde{w}_\ell \ll 1$. Then (3.12) shows the inversion below threshold to be nearly proportional to the pump density for small $\tilde{w}_p$.

$$\tilde{n}_1 = \tilde{n} \frac{\tilde{w}_p}{1+\tilde{w}_p}\,, \tag{3.15}$$

to be compared with (1.15). For $\tilde{w}_\ell$ we encounter a relation like (3.1), the details of which have been discussed in section 3.1.

Above threshold $\tilde{w}_\ell \gg 1$. The random laser analogue of (1.16) is

$$\tilde{n}_1 = -\frac{\nabla^2 \tilde{w}_\ell}{\tilde{w}_\ell}\,; \qquad\qquad \tilde{w}_\ell = \frac{\tilde{n}_0}{\tilde{n}_1}\tilde{w}_p - 1\,. \tag{3.16}$$

Like in a cavity system, $\tilde{w}_\ell$ depends linearly on $\tilde{w}_p$, and the threshold inversion $\tilde{n}_1$ is the ratio between loss and generation terms. If we assume that the pump energy does affect the magnitude of W_ℓ but not the z-dependence (an assumption that will turn out to be correct well above threshold), then $n_1(z) = n_{th}(z)$, independent of pump fluence.

Matrix inversion A conceptually simple analogue to the solution of the rate equations of a cavity system is matrix inversion. It is found to stall near the laser threshold, but does give reliable and intuitively appealing results well below threshold.

For matrix inversion, the space coordinate z is discretized in intervals h that are a few times smaller than ℓ, and for $\nabla^2 f = \frac{d^2 f}{dz^2}$ we use the simplest form of a second derivative on a grid $\frac{1}{h^2}[f(z-h) - 2f(z) + f(z+h)]$ [76]. In matrix form this is a tridiagonal square matrix Δ with a dimension equal to N, the number of discretization points, and $\Delta_{i,i} = -2$ and $\Delta_{i,i-1} = \Delta_{i,i+1} = 1$. $\tilde{\mathbf{w}}_{\boldsymbol{\ell}}$, $\tilde{\mathbf{w}}_{\mathbf{p}}$ and $\tilde{\mathbf{n}}_{\mathbf{1}}$ are column vectors of length N, containing the local light and inversion densities.

We reformulate (3.10)–(3.12) as matrix equations and invert them directly, solving the system by iteration. As an example we give the equivalent of (3.10):

$$\tilde{\mathbf{w}}_{\boldsymbol{\ell}} = \left(\Delta + \mathbb{I}\tilde{\mathbf{n}}_{\mathbf{1}}\right)^{-1} \cdot \beta \tilde{\mathbf{n}}_{\mathbf{1}}\,, \tag{3.17}$$

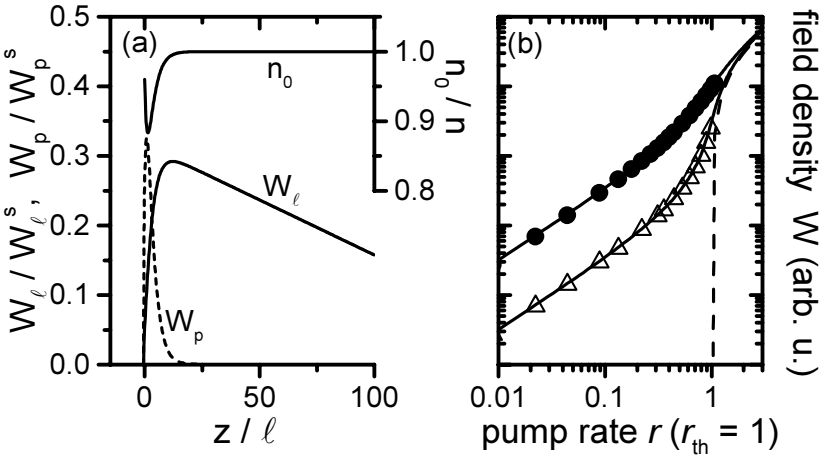

Figure 3.3 Results from a steady state solution below threshold of (3.10)–(3.12), for a medium of thickness $L = 200\ell$ and $\sigma_r = 0$. *(a)* $W_\ell(z)$, $W_p(z)$ and $n_0(z)$, for $\beta = 0.1$ and a pump energy of about a third of the threshold value. $W_\ell(z)$ extends linearly to L. $W_p(z)$ and $n_0(z)$ are concentrated in a thin layer near the interface. *(b)* Mapping of a random laser on a cavity system. The maximum of $W_\ell(z)$ for $\beta = 0.1$ (●) and $\beta = 0.01$ (△). The lines are solutions for W of (3.13) and (3.14) for the same values of β, the dashed line is the solution for $\beta \to 0$. The units for W_ℓ are not easy to determine in this comparison because $\max W_\ell(z)$ is a rather arbitrary measure for the magnitude of $W_\ell(z)$.

where $\mathbb{I}$ is the identity matrix. The matrix to be inverted is the sum of the matrices representing transport and stimulated emission, or loosely speaking, the difference between gain and loss, tending to zero near the threshold. $\Delta + \mathbb{I}\tilde{\mathbf{n}}_\mathbf{1}$ becomes singular at this point and cannot be inverted. Below threshold the matrix inversion does work. The z-dependence of W_ℓ, W_p and n_0 is displayed in figure 3.3 on the left. The magnitude of W_ℓ behaves identically to W obtained from normal laser equations, as can be seen in the right plot.

3.4.2 Intrinsic dynamics

A cavity laser with $\tau_c \ll \tau$ is said to be in the "bad-cavity limit": the dynamics of the field are governed almost completely by τ_c, the cavity decay time. The population, subject to the timescale τ, reacts much slower. A laser with this characteristic exhibits spiking or relaxation oscillations at switch-on and in response to sudden disturbances of the equilibrium state [74]. Relaxation oscillations are a general phenomenon occurring in nonlinear oscillators off equilibrium [75]. In a laser, the population inversion and field density oscillate around their equilibrium values. The oscillation is usually damped in four-level lasers.

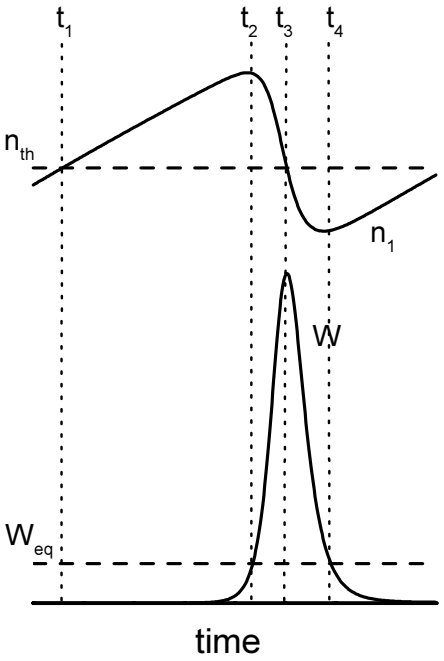

Figure 3.4 Anatomy of a laser spike: at t_1 the inversion (upper curve) reaches the threshold level $n_{\rm th}$, but because the field (lower curve) is still very much smaller than the equilibrium W, the gain does not saturate immediately: $n_1 > n_{\rm th}$, enhancing the growth of the field. When at t_2 W crosses the equilibrium value $W_{\rm eq}$, n_1 begins to drop because of saturation, but as long as $n_1 > n_{\rm th}$ the intensity continues to grow. Only when the inversion is driven below the threshold at t_3 W starts to decrease due to the net cavity loss, and when $W < W_{\rm eq}$ at t_4 the pump can replenish the population inversion. The oscillation arises because W can change with the fast rate $\tau_{\rm c}^{-1}$, whereas the growth rate of n_1 is the much slower $r\frac{\tau_{\rm c}}{\tau}$.

The sequence of events in one laser spike is shown in figure 3.4. The oscillation is produced because of the large difference between the response time of the field $\tau_{\rm c}$ to a change in inversion, and the response time of the inversion $r^{-1}\frac{\tau}{\tau_{\rm c}}$ to the driving pump. The pump rate r is normalized at threshold. What results is an exchange of stored energy between the gain medium and the laser field. An example of a damped relaxation oscillation obtained from a numerical integration of (3.13) and (3.14) is given in figure 3.5. The parameters used are those appropriate for a random laser as on page 55, and $r = 10$. The pump is suddenly switched on at $t = 0$.

For small oscillations, (3.13) and (3.14) can be linearized [33], and yield estimates for the oscillation frequency $\omega_{\rm r}$ and decay rate $\gamma_{\rm r}$. These are

$$\omega_{\rm r} = \sqrt{\frac{r-1}{\tau\tau_{\rm c}}}\,; \qquad \gamma_{\rm r} = \frac{r}{2\tau}\,. \tag{3.18}$$

Apparently, it is not possible to stationarily cross the threshold in a laser with a fast cavity decay, and consequently also the random laser threshold is intrinsically dynamic. This is witnessed by the impossibility to generally solve (3.4)–(3.6) in steady state by simple matrix inversion. Saturation alone does not suffice to prevent a diverging intensity. The slow response of the inversion forbids that the saturation takes effect instantaneously, again creating the condition discussed in section 3.1 which produces infinite amplification.

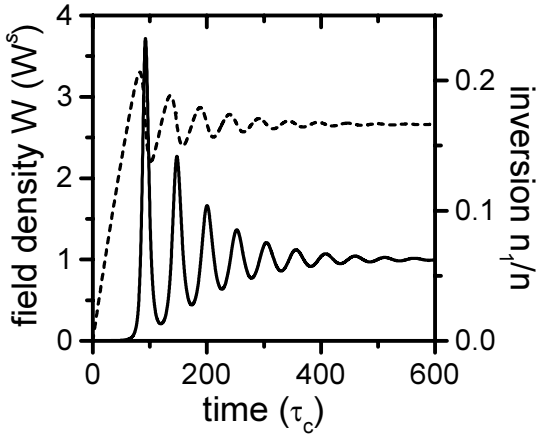

Figure 3.5 Relaxation oscillation in field density W (solid line) and population inversion n_1 (dashed line) obtained from a numerical integration of the (non-diffusive) laser equations (3.13) and (3.14).

Solution by the method of lines The transport equations can be integrated for z and t simultaneously by the method of lines [77]. In this method a set of partial differential equations (maximally of second order in z, first order in t) with boundary conditions in z is solved in the following way: The system is separated in first order ordinary differential equations, possibly nonlinear, in the time coordinate. The space coordinate is discretized in N steps, and the $N-1$ ordinary differential equations in t are coupled via the second derivative, discretized in the form discussed on page 56. The set of differential equations in t can then be numerically integrated by a suitable method. In our case the time dependence is stiff, i.e. there are two very different time scales on which the variables change [78].

The method of lines is available as the IMSL routine DMOLCH [79]. This routine performs the separation mentioned above and then uses a backward differentiation method [77], stable with stiff systems, to integrate the time dependent equations. The algorithm is quite fast, experimentally realistic situations can be calculated on a 600×500 ($t \times z$) grid in 10 seconds on a Pentium 600 MHz system with 128 Mb of RAM. By realistic we mean that the modeled system is large enough in space and time to display the macroscopic dynamics. ∎

The scaling parameters that were introduced on page 54 are now fixed. We choose L_z to be the diffusive absorption length at an inversion of $\frac{n_1}{n} = 0.5$: $L_z = \sqrt{\ell/(3n_1\sigma_a)}$. For a discussion of the properties of the model we use results obtained with the parameters of the experiment in section 4.3: $\ell = 3\ \mu$m and a dye concentration of 1 mM ($n = 6 \cdot 10^{23}\ \mathrm{m}^{-3}$). In that case $L_z = 15\ \mu\mathrm{m} = 5\ell$, indeed roughly the thickness of the gain layer in figure 3.3. With this choice for L_z, $\tau^s = 1$ ps, much smaller than $\tau = 3.2$ ns. We measured all parameters appearing in the transport equations (3.4)–(3.6). Their numerical values are listed in appendix A. The pump pulse is modeled

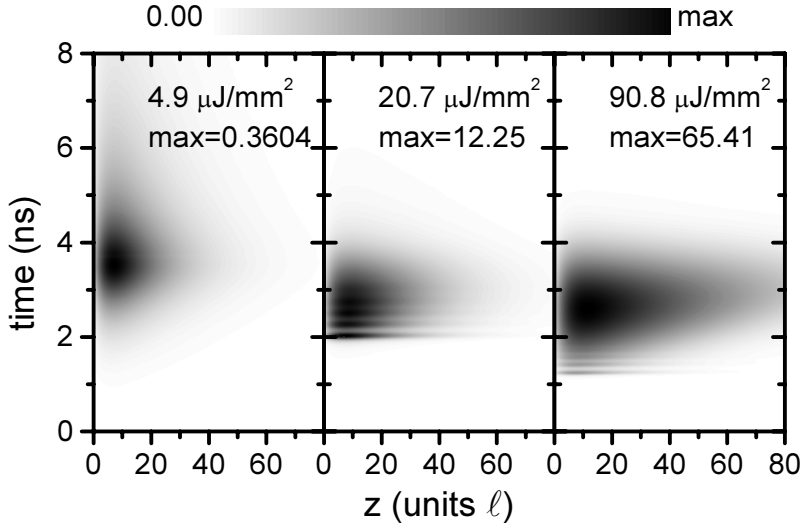

Figure 3.6 Density of laser light $\tilde{w}_\ell$ in a random laser as a function of time t (vertical axis) and position z (horizontal axis), for the three different pump fluences, indicated in the figures. The grayscale runs from 0 to maximum density, the maxima are also indicated in the plots. The threshold pump fluence is 10 μJ/mm^2.

as a plane wave that is gaussian in time, with a FWHM of 2 ns, corresponding to experiment. We reinstate the reabsorption σ_r for obtaining quantitatively correct results. The calculation covers a time span of up to 12 ns and a medium thickness of $L = 200\ell$. The results for laser light and inversion are shown in the figures 3.6 and 3.7.

3.5 Transport properties of random lasers

This section is dedicated to an analysis of the solution of the transport equations. In the following sections 3.5.1–3.5.3 the quantitative features of the inversion, pump, and laser light densities will be discussed thoroughly. We first give a brief qualitative review of the data in figures 3.6 and 3.7. It is important to realize that, although in other locations our language may have been a little sloppy, in this section the words "intensity" and "fluence" are used according to the definition of appendix B. Fluence is the amount of energy in a pulse per unit area, while intensity is the *instantaneous* rate of energy flow during the pulse, a power per unit area.

The most important observation is that for any pump rate a finite equilibrium value for the luminescence density exists: there is no photon bomb. Before reaching equilibrium, the system may go through a series of relaxation oscillations in which

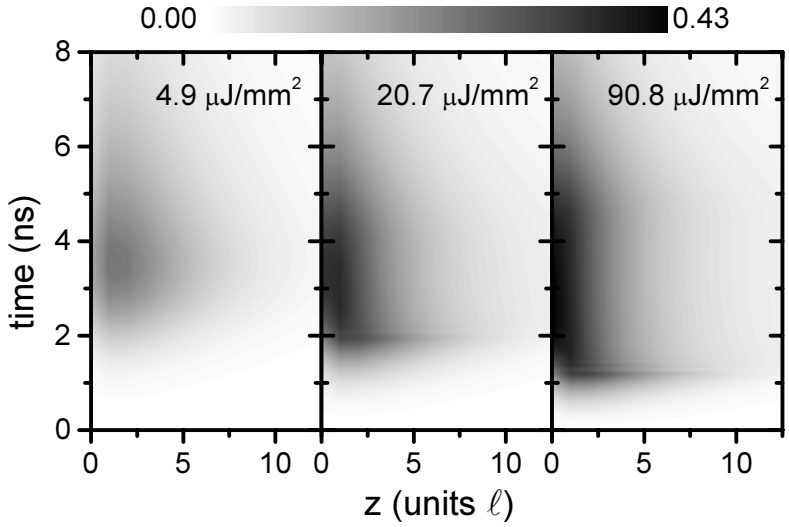

Figure 3.7 Inversion $\frac{n_1}{n}$ in a random laser as a function of time t (vertical axis) and position z (horizontal axis), for the three different pump fluences, indicated in the figures. The maximum inversion obtained for above threshold pump fluences ($> 10\ \mu\mathrm{J/mm^2}$) is about 0.43.

the intensity and inversion can become larger than the equilibrium level, but only for a short time. A threshold is experimentally (as in figure 2.2) found to be at a pump fluence of $10\ \mu\mathrm{J/mm^2}$, which we take as the *laser* threshold. This is also the pump fluence at which the oscillations start to appear.

The pump fluence in the leftmost plots is below threshold. The inversion follows the gaussian pump pulse on its rising side, and later decays with time constant τ. This behavior reflects the below threshold estimate for n_1 of (3.15). W_ℓ lags with respect to the inversion due to the characteristic time τ with which it is generated. Note the difference in z-scale between figure 3.6 and 3.7.

For larger pump fluences, shown in the middle and right plots of figures 3.6 and 3.7, relaxation oscillations appear, most clearly in W_ℓ, but also in n_1. These oscillations shift forward in time with increasing pump fluence, indicating that the threshold intensity is crossed at an earlier instant if the gaussian pulse has a larger energy content. The inversion is approximately constant in time after the oscillations, until the pump pulse vanishes. The laser light switches on sharply, reaches increasingly higher densities with larger pump intensity, and diminishes smoothly when the pump intensity decreases.

The more detailed presentation below will concentrate on the inversion density and the laser light. Only the overall magnitude of W_p depends strongly on the inci-

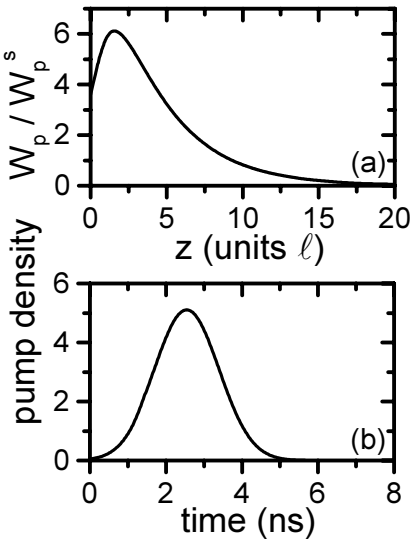

Figure 3.8 Dependence of the pump light density on *(a)* z ($t = 3$ ns) and *(b)* t ($z = 3\ell$) for a pump fluence of 53.6 μJ/mm^2. The behavior for other pump fluences is similar due to the gain saturation of n_1 above threshold.

dent pulse energy, its behavior in z and t are largely unaffected by a change in pump fluence. The generic dependence of $W_\mathrm{p}(z,t)$ is shown in figure 3.8. The pump light interacts with $n_0 = n - n_1$, for which relative changes with pump light density are small. The largest variation that we found is a factor 2 in n_1, see figures 3.9(a) and (c), amounting to a relative change in n_0 of 1.3, and only for $z < 5$.

3.5.1 Spatial behavior

The dependence of the dynamic quantities on the position in the medium can be shown more quantitatively by looking at cross sections through the data for constant t. Figure 3.9 shows such cross sections through the inversion and laser light density for four different pump fluences. We discuss the salient features brought out by this slice of the data.

Only a relatively thin ($< 10\ell$) layer with significant inversion, and, consequently, a high gain coefficient, develops at the arrival of the pump pulse. This layer provides the net gain, and also serves as a source by spontaneous emission. The inversion's z-dependence is exponential: n_1 is nonvanishing only where the pump light can reach it. The laser light density obeys a diffusion equation, cf. (3.15), with a small absorption term due to σ_r, attentuating W_ℓ for large z.

For pump fluences below threshold, the local inversion rises linearly with the local pump light density. Above threshold, the inversion does not increase anymore, but is instead fixed at a level that varies with z, depending on the local losses. The inversion rises to such a level $n_\mathrm{th}(z)$ that the corresponding gain cancels those losses

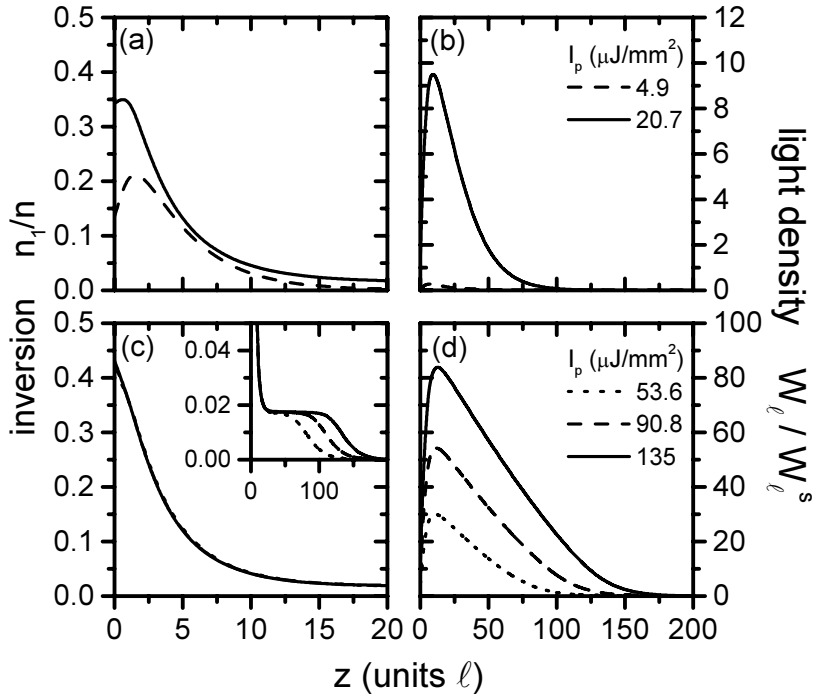

Figure 3.9 Spatial dependence of the inversion and laser light densities. The cross sections through the spatiotemporal profiles as shown in figures 3.6 and 3.7 are taken at $t = 3$ ns, after the oscillation has died out. In *(a)* and *(b)* , data are shown for pump fluences of 4.9 and 20.7 μJ/mm^2, in *(c)* and *(d)* for 53.6, 90.8 and 135 μJ/mm^2. Plots *(a)* and *(c)* contain the n_1 for $z < 20\ell$, *(b)* and *(d)* $\tilde{w}_\ell$ through the entire system. The n_1 for pump fluences above threshold coincide, due to the clamping of n_1 at the threshold level $n_{\rm th}$ as in a normal laser. The inset in *(c)* is the same inversion data as the main graph, except that z now goes up to 200ℓ, bringing out the effect of reabsorption.

locally. Near the boundary, the loss is dominated by the large transport term, giving rise to a high threshold inversion level, but deeper in the medium only reabsorption plays a role. There, the emitted light pumps the population to an inversion providing a gain that exactly compensates the reabsorption. The lack of curvature in $W_\ell(z)$ for intermediate depths, for z ranging from 20ℓ up to 120ℓ for the largest pump fluence, signifies the absence of a net absorption (since $\nabla_z^2 W_\ell = 0$ far from the boundary). The depth to which the reabsorption can be compensated in such a way depends on the local W_ℓ: if large enough, it can counter the absorption by "repumping" the dye to such a level that the gain cancels the absorption.

This mechanism is seen in the inversion in the inset in figure 3.9(c). Close to the boundary the inversion is large due to the large transport term, but for large z there

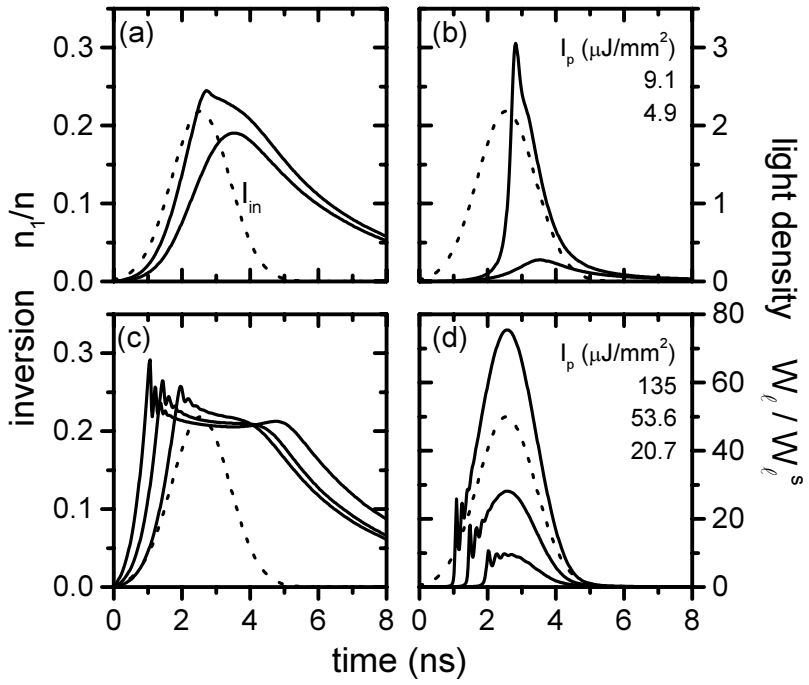

Figure 3.10 Graphs of the t-dependence of the inversion and laser light densities between 0 and 8 ns. Cross sections through figures 3.6 and 3.7 are taken at a depth $z = 3\ell$. *(a)* and *(b)* contain data for pump fluences of 4.9 (lower) and 9.1 (upper trace) $\mu J/mm^2$, below and at threshold, *(c)* and *(d)* for (bottom to top:) 20.7, 53.6 and 135 $\mu J/mm^2$ (all above threshold). Graphs *(a)* and *(c)* display the n_1/n, *(b)* and *(d)* $\tilde{w}_\ell$. As a reference, the time profile of I_{in} is shown as a dotted line. $\tilde{w}_\ell$ has a linear dependence on the pump intensity above threshold. n_1 grows proportionally to the pump intensity up to the threshold. Above threshold, n_1 is approximately constant at the threshold level, $n_{th}/n \approx 0.23$ for this position.

is a low plateau of inversion that reaches deeply into the system. The transport term $\nabla_z^2 W_\ell = 0$ here, and the only loss is the constant reabsorption $\sigma_r c n_0$.

3.5.2 Temporal features

A close investigation of the temporal behavior reveals that the dynamics of a random laser are very similar indeed to those of a conventional laser system. The first observation we make on the basis of figures 3.6 and 3.7 is that the time variation occurs simultaneously throughout the system. The transport is the fastest of all interacting processes, so any intensity fluctuation propagates fast, actually instantaneous compared with the time scales associated with pumping or amplification.

Cross sections through the spatiotemporal data for constant z are given in figure

3.10. The population inversion increases proportionally to the pump intensity until the threshold inversion n_{th} is reached, $n_{\text{th}}/n \approx 0.23$ for $z = 3\ell$ as in figure 3.10. $n_{\text{th}}(z)$ can be found in figure 3.9(c). Then the system goes through the relaxation oscillation, of which the details will be discussed later. As can be seen in the data in figure 3.10(c), the above-threshold inversion level is approximately constant. Once the pump threshold intensity is crossed in the downward direction, i.e. the energy supply rate is insufficient to keep up a gain that compensates the losses, the population starts to decay spontaneously, seen here as an exponential tail for $t > 5.5$ ns in figures 3.10(a) and (c).

The laser light density for low pump fluence is very small, basically only spontaneous emission, and has a delay τ with respect to the pump pulse, cf. the lower trace in figure 3.10(b). For 9.1 $\mu\text{J}/\text{mm}^2$ the system just touches on threshold, after one spike the pump intensity has already dropped below the threshold level. Above threshold, for higher pump fluence, the laser light density depends linearly on the pump intensity, as shown in figure 3.10(d).

Slicing figures 3.6 and 3.7 along the time direction allows a quantitative comparison of the relaxation oscillation with the predictions from cavity laser equations with small fluctuations. The linearization is unfortunately not as easy in the random laser transport equations (3.4)–(3.6), because of the space derivative. But it is possible to compare the results obtained from the numerical solution with (3.18).

As suggested by the analogy between transport and loss, noted on page 56, we use the characteristic transport time $\tau^s = 1$ ps for the cavity loss time τ_c in (3.18). For pump rates r between 1 and 10 (with the threshold $r_{\text{th}} = 1$), the range discussed above, we estimate an oscillation period $2\pi/\omega_r \sim 100$ ps, and a decay time $\gamma_r^{-1} \sim 1$ ns, to be compared with results from the dynamic calculation as displayed in figure 3.11. The γ_r^{-1} from the calculation is actually about a factor 2 smaller than estimated, caused by the rising pump rate at threshold, which enhances the damping during the oscillation. In general the agreement between the estimate from elementary laser theory and numerical result for random lasers is satisfactory.

3.5.3 Laser threshold and the explosion

In the previous section, we have identified two regimes for random lasers, as a function of pump intensity: a low pump rate regime where the inversion and the emitted light density behave as in a normal laser below, and a high pump rate regime corresponding to a laser above threshold. The transition between the two is accompanied by an oscillatory instability. We can therefore say that a random laser does have well-defined threshold, and that it comes about in a way that is similar to the threshold in a normal laser: a balance between gain and loss. What is particular to a random laser is the transport nature of the loss, necessitating a local description of the laser

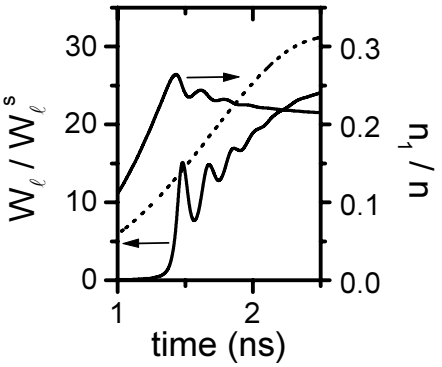

Figure 3.11 Close-up of the relaxation oscillation for a pump fluence of 53.6 μJ/mm^2.

process rather than a formulation in laser modes, and introducing an "off-diagonal" coupling to the density in neighboring positions. This coupling is absent in a cavity with orthogonal modes. Laser cavity modes may interact, as in multimode lasers, but that interaction usually occurs via the gain, e.g. through spatial hole burning [80].

The random laser threshold we find is obtained from a transport formalism, taking into account the local gain in a population rate equation. This shows that the "laser view" [46, 57, 58, 62, 81, 82] and the "multiple scattering view" [66, 68, 83, 84] on random lasers can be united into one. The theoretical results presented in this chapter show the analogy with normal lasers, and connect to experimental observations in offering an explanation for measurements like the proportionality of the laser output with the pump above threshold (figure 2.2). In chapter 4 we will demonstrate the success of this diffusive random laser model in quantitatively reproducing multiple scattering experiments. Another experimental observation that is replicated by the transport theory is the absence of the explosion, that does follow from the elementary diffusion equation with a gain term. The saturation of the gain at high laser light density restores the equilibrium, preventing an indefinite growth of W_ℓ.

Actually, the problems encountered with a direct stationary solution of the system by matrix inversion show that saturation is not enough to prevent a diverging intensity. Dynamics are absolutely necessary to treat the system above threshold. A random laser is intrinsically time-dependent due to the very different time scales of transport and population dynamics. The population is slow to react, and consequently the above-threshold equilibrium is not established instantaneously. The relaxation oscillation acts as a safety valve in random lasers.

This shows that the photon bomb is purely an artifact of stationary random laser theories. The fact that a more careful description can circumvent the divergence exposes a serious flaw of static formulations, and actually renders them invalid for investigating phenomena connected to the laser threshold. The pump rate at which the explosion occurs is related to and even close to the pump rate at the onset of the

oscillation that signals the threshold crossing, but is not the same per se.

3.5.4 Comparison with earlier work

In this chapter we have demonstrated that in a realistic system the explosion does not exist, and consequently is *not* the same as a laser threshold, which does exist. At the laser threshold the population inversion is fixed at a level where the (local) gain exactly compensates the (local) loss, like in an ordinary laser the modal gain equals the modal loss. We have introduced β for a random laser, the fraction of spontaneous emission contributing to the laser process. The validity of the model will be established by a quantitative comparison with measurements in chapter 4.

Earlier explorations of the realm of dynamic random laser theory were made, the important references are the works of Letokhov [48], Berger, Kempe, and Genack [60], and Wiersma and Lagendijk [71]. There are three aspects to the work described in this chapter by which it augments the theory of these references:

- the definition of the β-factor, using experimentally accessible quantities;
- the elaborate interpretation of transport phenomena in terms of laser terminology, most importantly the identification of the transport as the quantitative equivalent of cavity loss;
- the possibility to compare directly with experiments, also by inclusion of the reabsorption term.

We give a brief review of other theoretical work to compare it with our own.

Our theory, like the one in ref. 71, can not treat emission line narrowing or other spectral features in detail. We take the effect of spectral narrowing into account in β, but the occurrence of e.g. a second laser peak [81, 85] can not be handled. The works by Letokhov [48] and by Berger and coworkers [60] make it possible to study spectral dependence. Berger *et al.* use a Monte Carlo simulation to study the dynamics of the system, and this can be done for a distribution of frequencies. But the method suffers from a general limitation of Monte Carlo simulations: it is very time consuming to study long times and large systems. This makes it difficult to use the results for a study of the common experiments with nanosecond excitation pulse lengths. They do explain the short pulse output observed by Siddique *et al.* [58], that is due to the occurrence of one laser spike during the picosecond pump pulse. Letokhov develops a formalism that is very general, but only numerically tractable for weak scattering and small gain. For a solution he assumes homogeneous pumping, negligible saturation and a spherical geometry which makes comparison with real systems difficult. Unlike Berger and coworkers, Letokhov does not find a limit to the linewidth above threshold.

John and Pang [86] calculate the line narrowing with a theory that models the population dynamically, but uses a static description for the transport. Their results for the laser threshold, which is not very accurately defined, depend strongly on dye parameters which we find to be of no importance, such as the rate at which the triplet state is populated. In their calculation they do use a formalism which resembles our discussion of the β-factor.

Wiersma and Lagendijk [71] integrate a set of equations like (3.4)–(3.6) in a manner that is similar to our calculation, for parameters that are appropriate to a system consisting of Ti:sapphire powder. The pump energies needed to reach the threshold are however not easy to realize, unfortunately precluding an experimental test of the model. They include a probe beam, separate from the emitted laser light. Because we distinguish between spontaneous emission and laser light by β, a probe beam could be added in our equations by a simple source term like I_{in}.

A completely different, but dynamic nonetheless, approach is taken by Jiang and Soukoulis [87]. They solve the Maxwell equations for the field coupled to four-level rate equations for the gain in a one-dimensional disordered system by the finite-difference time domain (FDTD) method. This technique is basically a direct numerical integration in time of the Maxwell equations, in a medium with a variation in dielectric constant on a space grid. One calculates the microscopic field, so the space and time discretizations have to be very finely grained, much smaller than the wavelength and the optical cycle. Because the time step is so small, one has to take all four levels of the gain medium into consideration. The time of evolution one can calculate is consequently much smaller than with a diffusion theory, on the other hand the amount of detail is much larger. This detailed information is used to obtain the frequency spectrum by Fourier transforming the field in time.

This approach is used to explain the observation of narrow frequency structure in the emission of random lasers, supposedly due to Anderson localized modes. Jiang and Soukoulis find strong localized modes that are very sharp due to the amplification in the system. They use parameters appropriate to a concentrated dye solution with ZnO scatterers, modeling a system consisting of randomly spaced layers. The frequency spikes are the subject of chapter 5, but we discuss the calculations of ref. 87 here, because they can be used to illustrate the interpretation of our own results. In disordered materials the dimensionality of the system is crucial [88]: in 1D and 2D random media waves are always localized. This is caused by the fact that, whatever the strength of the disorder, a one- or two-dimensional random walk will eventually return to its starting point with probability one. Transport is inhibited in such a system. The only way for the wave to escape is to make the sample shorter than the localization length, i.e. the extent of the localized state. The localization length depends on the strength of the disorder.

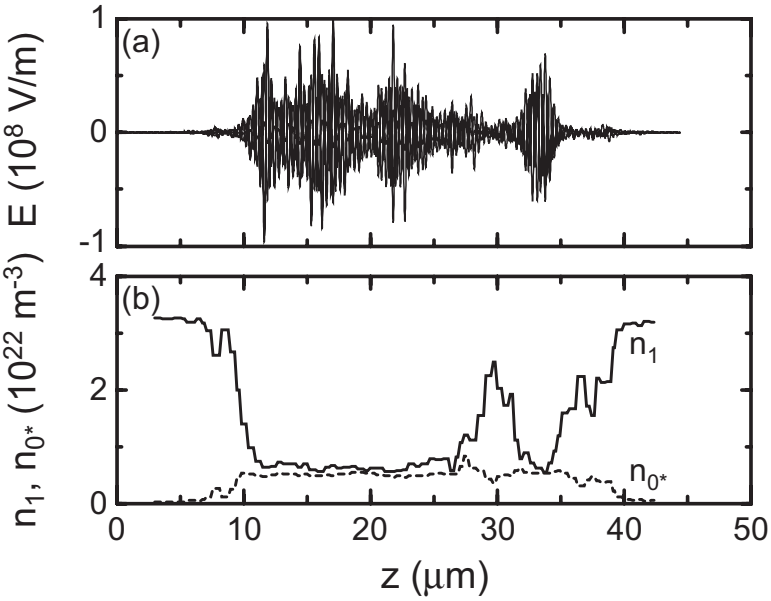

Figure 3.12 Local field strength *(a)* and population in the upper and lower laser levels *(b)* in a 1D disordered medium, from ref. 87. The localized field does not suffer loss by transport and thus the above-threshold gain is saturated to zero value ($n_1 = n_{0^*}$) at positions with a high field strength.

In the discussion of diffusion with gain, especially section 3.4.1, we emphasized that transport is the dominant loss mechanism in a random laser. In a localizing medium this loss mechanism is absent, and hence the equilibrium above-threshold gain should be zero for it to equal the loss. This can be seen clearly in figure 3.12, where the population difference on the lasing transition is reduced to zero in places with a large field strength. The rate of downward transitions becomes very large, comparable to the vibrational $n_{0^*} \rightarrow n_0$ relaxation (see figure 1.12) resulting in a significantly populated n_{0^*} level. Hence $n_{\text{th}} = n_{0^*}$ ($\neq 0$) fits the requirement of zero gain above threshold, set by the absence of transport as a loss mechanism.

4. Interference in random lasers

This chapter describes experiments in which the amplification of a probe beam is used for studying light propagation in a random laser. We have performed measurements on speckle in the scattered and amplified light, which is discussed first. The second part of this chapter is about enhanced backscattering. We present the first high quality enhanced backscattering measurements in a random laser that can be driven above the laser threshold, providing experimental insight in the effect of the threshold on light transport. The results of these measurements are shown to be in quantitative agreement with the theory developed in chapter 3.

In the experiments described in chapter 2 we observed the fluorescence emitted by a random laser to infer the influence of the characteristic length scales in diffuse transport on the laser threshold. The fluorescence is generated by the system itself and consequently details like directionality, coherence or spectral content can not be used as experimental parameters. When studying the light transport itself, it is desirable to have the ability to control the properties of the light source. This is most conveniently done by using an external beam incident on the sample. We then have a source of diffusing light with known properties, and by measuring the scattered light we can investigate the transport of light in the medium. Much is known about transport in passive disordered systems from light scattering experiments, and we can assess the effect of amplification in multiple scattering by comparing data from random lasers with results for ordinary random systems.

4.1 Experimental considerations

Probe beams are used in the experiments presented in this chapter, with a wavelength that can be amplified by the dye in the medium. The intensity of the incident probe

Table 4.1 Pulse characteristics of frequency-doubled Nd:YAG and OPO. Specific requirements of the experiment determine which is to be the pump and which the probe. The main advantage of the OPO is of course its tunability, allowing it to be used with a variety of dyes. A benefit of the Nd:YAG is its coherence, making speckle measurements possible.

Characteristic		Nd:YAG	OPO
wavelength	(nm)	532	410–700
max. energy	(mJ)	100	35
duration (FWHM)	(ns)	2.0	1.6–5[a]
temporal profile		gaussian	
spatial profile		"top hat"	elliptic[b]
divergence	(mrad)	≈ 0.5	< 1–10[c]
spectral width		$\sim$ GHz[d]	0.1–5 nm
coherence length[e]	(cm)	40	0.01–0.2

[a] Gradual increase, tuning from blue to red.
[b] Long axis is vertical; relatively flat top but not sharply bounded.
[c] The spectral width and divergence increase sharply towards the red end of the tuning range.
[d] $1.5 \times$ transform limited
[e] Derived from the spectral width.

pulse is chosen small with respect to the pump intensity, and preferably also with respect to the generated fluorescence. With this provision the probe actually probes the system instead of affecting the gain saturation.

We work with a setup in which the pump and probe pulses are incident simultaneously on the sample. The light in the medium then consists of amplified probe light, in which we are interested, and fluorescence. Because we want to do our experiments at large amplification, and the maxima of the gain curve $\sigma_e(\lambda)$ and the fluorescence spectrum $L(\lambda)$ of a dye are usually close in wavelength, the probe and fluorescence can not be fully separated spectrally. The fast decay of the dye also precludes a distinction in time to be made. We have to tell the probe and the fluorescence apart in other ways; in this chapter that will be done using interference in the probe light.

The pump and probe pulses are provided by one laser system, an optical parametric oscillator (OPO) pumped by a Q-switched Nd:YAG laser (Coherent Infinity 40–100/XPO). The Nd:YAG laser has a maximum pulse energy of 600 mJ at the fundamental wavelength, 1064 nm, and a pulse length of 3 ns. The repetition rate is variable from single shot to 100 Hz. The Nd:YAG pulse is subsequently frequency-doubled to 532 nm (green) and tripled to 355 nm (UV). After the third harmonic generation the energy in the green pulse is still more than sufficient, approximately 100 mJ, to serve as a pump pulse in our experiments. The UV pulse is used to pump the OPO, which is a light source tunable through the visible part of the spectrum, with pulse energies up to 35 mJ. If the OPO is not needed, the third harmonic can be employed as a pump for UV absorbing materials.

Depending on the requirements on the pump and probe beams, we can choose to use either the second harmonic of the Nd:YAG laser as a pump and the OPO as a probe or vice versa. There are a number of characteristics in which the pulses differ; a summary is given in table 4.1. It shows that the properties of the OPO pulse depend strongly on the set wavelength, and in general degrade towards the red side of the tuning range. The energy in the OPO pulse is large, but the moderate beam quality necessitates spatial filtering (except perhaps for $\lambda < 480$ nm), which reduces the usable energy by a factor 50.

For OPO power regulation we use a set of polarizing Glan laser prisms. The first is rotated to vary the amount of power, while the second selects the transmitted polarization, compatible with the mirrors used. A drawback of this setup is the steep intensity change at small transmission ($I \propto \sin^4 \alpha$, where α is the rotation angle). The advantage is its wavelength independence. For the Nd:YAG we use a rotating $\lambda/2$ retardation plate mounted between two crossed Glan prism polarizers. In this case the sensitivity for small transmissions is better ($I \propto \sin^2 \alpha$).

Getting pump and probe pulses from the same laser system has the advantage that the timing of the experiment becomes particularly simple. The jitter between the pulses is minimal and the difference in arrival times can be easily compensated by optical delay. We put a delay line in the pump beam path, because the probe beam alignment is much more precarious than the pump, and might be disturbed by moving a slightly imperfectly aligned delay line. The Nd:YAG pulse is the leading one. Several ns of variable delay is convenient for optimization; the delay line has a length of maximally 2×1.5 m.

4.2 Speckle in random lasers

Speckle is the strongly fluctuating, grainy intensity pattern resulting from the interference of a randomly scattered coherent wave. It can be observed in space, time and frequency. Some statistical characteristics of the speckle pattern contain information about the transport process [89]. We discuss only speckle in space, i.e. a fluctuating intensity with angle.

If a coherent plane wave falls on a rough surface, a speckle pattern can be seen on a screen positioned at some distance from the scattering object. The scattered fields at a certain position on the screen comes from all points of the rough surface, and its random phases distributed uniformly between 0 and 2π. The speckle is the addition of the electric field vectors of all the N contributing partial waves. The summation constitutes a random walk in the complex plane, with a resulting field $E = 1/\sqrt{N} \sum_k a_k \exp(i\phi_k)$ [90].

The sum results in a gaussian distribution for E, with most probable value $E = 0$

and variance $\langle |E|^2 \rangle = \lim_{N\to\infty} (2N)^{-1} \sum_k \langle |a_k|^2 \rangle$. The observed intensity $I = |E|^2$ then follows a Rayleigh distribution:

$$P(I) = \frac{1}{\langle I \rangle} e^{-\frac{I}{\langle I \rangle}} . \tag{4.1}$$

The typical speckle spot size depends on the characteristic distance along the screen on which the fields that contribute to the speckle dephase. The largest path length difference at a spot on the screen is caused by the partial waves arriving from opposite ends of the illuminated region of the scattering surface. Consequently, the typical angular size of a speckle spot is λ/d [90], if d is the diameter of the illuminated region. This demonstrates that a measurement of the speckle spot size, for instance by the autocorrelation of the speckle pattern, does not usually give information about light *inside* a scattering medium. The spot size in reflection depends mainly on the incident beam diameter. In transmission the most influential parameter is the sample thickness, which determines the degree to which an incident point source spreads in transport to the rear interface.

The field of speckle experiments in random lasers is largely uncharted territory. The only data available of the effect of gain on a speckle pattern produced by a probe beam are those of ref. 91. Refs. 92 and 93 study the related subject of coherence properties of the generated light. In this section we present experimental results concerning the intensity statistics and speckle spot size. In contrast with passive systems, these measurements do depend on parameters of light transport. There is no theory to compare the measurements with. We will give qualitative explanations of the results.

Theoretical studies of speckle in random lasers [66, 94–96] invariably investigate speckle correlations. While interesting, these correlations are exprimentally not easily accessible, for reasons that will be discussed in section 4.2.4. A further limitation of the theoretical efforts in this field is that they all rely on a stationary formalism, with fixed gain, so they encounter the explosion when approaching the laser threshold.

4.2.1 Sample and setup

Spatial speckle can only be observed if the coherence length of the light is much larger than the maximum path length difference between partial waves contributing to speckle. In the region where the rhodamine dyes fluoresce the OPO beam has a linewidth that is too large to produce speckle with a good contrast: its coherence is insufficient. The frequency-doubled Nd:YAG can be amplified by a dye with a large gain at 532 nm, such as Coumarin 6 (see appendix A). In dye lasers it is usually dissolved in ethylene glycol, but unfortunately our TiO_2 [44] colloid is not suspended

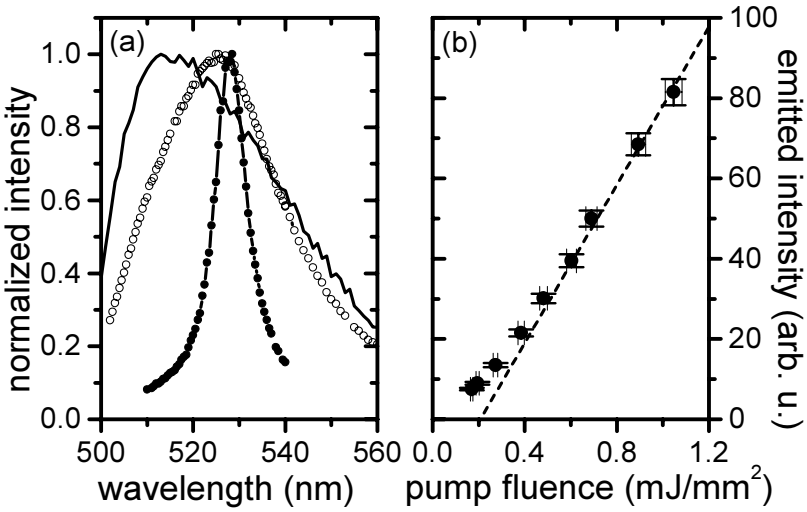

Figure 4.1 *(a)* Line: normalized emission spectrum of a Coumarin 6 solution in hexylene glycol, with CW 488 nm excitation. Points: normalized emission spectra of the solution with TiO_2 scatterers, $\ell = 10\ \mu$m; below (○) and above threshold (●). The pump source is a 482 nm pulse of duration 2.6 ns. *(b)* Emitted intensity from the scattering solution at 527 nm, near the maximum, as a function of pump intensity. The threshold is found to be at approximately 0.22 ± 0.05 mJ/mm^2.

well in this liquid. Hexylene glycol is a good alternative. The fluorescence spectrum of Coumarin 6 in hexylene glycol, cf. figure 4.1(a), is nearly equal to that in ethylene glycol. Hexylene glycol also slows sedimentation of the scatterers by its high viscosity.

The suspension is contained in a round plastic container with dimensions 6 mm depth $\times$ 10 mm diameter, covered with a 4 mm thick glass window. The sample is rotating slowly to prevent sedimentation and dye degradation. Coumarin 6 can be pumped with blue light, we use the OPO tuned to 482 nm. The dye concentration is 2 mM, providing a gain and absorption comparable to the 1 mM Sulforhodamine B solutions of chapter 2 and section 4.3. The transport mean free path is 10 μm, from enhanced backscattering (this technique will be explained in figures 4.7 and 4.8). This sample has a rather high threshold pump intensity of $I_\mathrm{p} = 0.22$ mJ/mm^2, determined from the measurements shown in figure 4.1. We could not find a reliable, durable combination of dye and solvent that amplifies well at 532 nm, and would suspend the colloid, with a lower threshold.

The speckle is recorded on a Kappa CF 8/1 FMC 8-bit CCD camera. The light from the sample passes through an aperture, blocking stray light, a 532 nm interference filter with a transmission FWHM of 1.0 nm to remove most of the fluorescence,

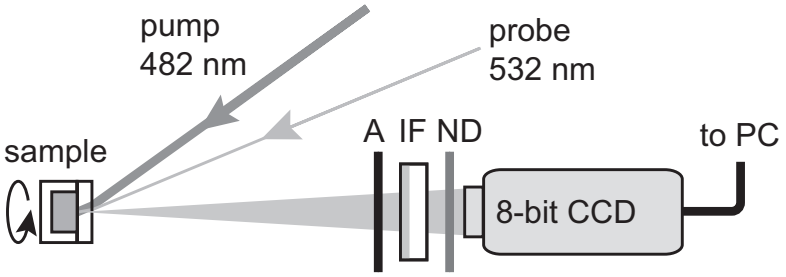

Figure 4.2 Schematic of the setup for speckle experiments. The pump (diameter 2 mm) and probe (diameter 0.8 mm) reach the sample simultaneously. The sample is mounted on a motor, spinning it slowly to prevent sedimentation. The scattered and amplified probe light is collected on an 8-bit 752×582 pixel CCD camera (Kappa CF 8/1 FMC), through an aperture (A), a 532 nm interference filter (IF) and one or more neutral density filters. The distance between sample and camera is 10 cm.

and a neutral density filter. The image is a single shot exposure, because the sample is liquid so the speckle changes continuously. The probe beam diameter is 0.8 mm. This produces a speckle that can be resolved well on the camera, with a large number of speckle spots. The pump spot is chosen to be larger, 2 mm, to provide a large amplifying region for the probe light to propagate in. Figure 4.2 is a schematic of the experimental arrangement of sample and detection.

4.2.2 Intensity statistics

The Rayleigh distribution of speckle is a very robust phenomenon. The only requirements are uncorrelated phases of the scattered light and the independence of the amplitude a_k and phase ϕ_k. It does not make a principal difference whether the scattered light has actually traveled inside the scattering medium or is just reflected off the surface. Considered this way, a measurement of speckle intensity statistics does not promise to be an effective method to obtain new information about random lasers. It does, however, provide access to a measurement that is otherwise difficult to perform: the degree to which the incident probe is amplified by the system.

We make use of the coherence of the Nd:YAG frequency doubled output as a probe pulse, producing a speckle with good visibility. Figure 4.3(a) shows an image of the speckle pattern in scattered and amplified probe light from a Coumarin6/TiO_2 random laser. The drawback of the large pump spot is a larger fluorescence component in the image.

The intensity histogram of the speckle in figure 4.3(a) is shown in figure 4.3(b). The histogram has an unusual feature: it only starts to show Rayleigh statistics above intensity 50. The lower intensities are incoherent fluorescence, giving each pixel an

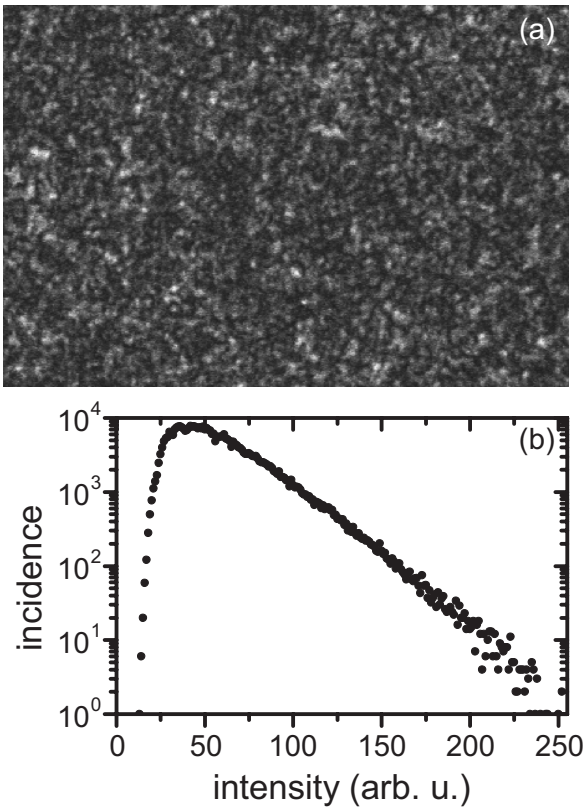

Figure 4.3 *(a)* Speckle pattern on an 8-bit CCD camera of frequency-doubled Nd:YAG scattered and amplified by a 2 mM Coumarin 6 solution in hexylene glycol, with TiO_2 scatterers, $\ell = 10$ μm. The pump pulse from the OPO of wavelength 482 nm has an energy of 0.32 mJ/mm^2. *(b)* Intensity histogram of the image in *(a)*. The Rayleigh distribution is offset by a background of incoherent fluorescence. The slope of the linear decrease is $1/\langle I \rangle$.

offset. The average intensity can be determined from the slope of the exponential decrease for higher intensities. A plot of the fluorescent intensity (the offset) as a function of pump fluence reproduces figure 4.1(b), providing evidence that the gain dynamics of the system are not significantly influenced by the probe pulse.

We extract the average intensity of the amplified probe from the slope of the intensity statistics plotted in the manner of figure 4.3. The dependence of the average intensity of the speckle, or the intensity of the amplified probe, on pump fluence is plotted in figure 4.4. The exposures taken at the highest pump intensities are overexposed, but if the average intensity can still reliably be obtained from the low intensity part of the negative exponential it is included in the figure. A measurement in which the intensity on the camera is attenuated using a neutral density filter shows that the linear behavior of figure 4.4 persists up to the highest pump intensity 2.9 mJ/mm^2, amounting to an amplification factor ≈ 10.

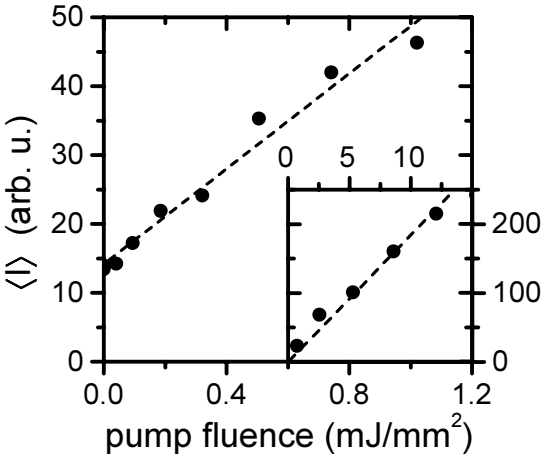

Figure 4.4 Average intensity derived from Rayleigh statistics as a function of pump fluence, for a fixed probe intensity of 59 μJ/mm^2. The amplified intensity grows linearly with pump fluence. For comparison, we plot the mean intensity as a function of the *probe* fluence (in units of 0.01 mJ/mm^2) in the inset. The pump intensity is high: 2.9 mJ/mm^2. The lines are linear fits to the data.

4.2.3 Speckle spot size

As discussed on page 74, a measurement of the speckle spot size yields the transverse dimension of the coherent source on the scattering surface. In a random laser this may very well depend on the pump energy, since a larger gain allows the light to spread further, enhancing long paths. The results of chapter 2 clearly show the relation between the transverse dimension of the amplifying volume and the threshold.

The spot size is measured by calculating the two-dimensional intensity autocorrelate $G_{\mathrm{I}}(\Delta\theta) = \langle I(\theta)I(\theta+\Delta\theta)\rangle$ of a speckle pattern as in figure 4.3(a). For a circular illumination spot of diameter d by purely coherent light the autocorrelation is

$$G_{\mathrm{I}}(\Delta\theta) = \langle I\rangle^2 \left[1 + A\left(\tfrac{d}{\lambda}\Delta\theta\right)\right] , \tag{4.2}$$

where $\Delta\theta$ is the angular distance between two points on the screen, and $A(u) = (2J_1(u)/u)^2$ with J_1 the first order Bessel function. $A(u)$ has the same functional dependence as the Airy diffraction pattern of a circular aperture, and so the first zero is expected at $\Delta\theta = \theta_0 = 1.22\lambda/d$, providing a measure for the speckle spot size. The contrast between the maximum at zero and the value at large $\Delta\theta$ is a factor 2: $G_{\mathrm{I}}(\Delta\theta \gg \lambda/d) = \langle I\rangle^2$, and $G_{\mathrm{I}}(0) = 2\langle I\rangle^2$.

Our diffuse light source is, however, partly incoherent due to the contribution of fluorescence. The consequences for the intensity autocorrelate are shown in figure 4.5, showing a cross section through the autocorrelate of the data in figure 4.3(a). The speckle contrast is reduced [97] to $1 + (\langle I\rangle/\langle I_{\mathrm{T}}\rangle)^2$, where $\langle I\rangle$ is the average intensity of the amplified probe and $\langle I_{\mathrm{T}}\rangle = \langle I\rangle + I_{\mathrm{F}}$ is the average total intensity, including the fluorescence intensity I_{F}. For the data in figure 4.3 $\langle I\rangle \approx I_{\mathrm{F}}$ and so the contrast in the autocorrelate is reduced to a factor 1.25. The position of the first zero in the autocorrelate becomes hard to determine due to this lower contrast.

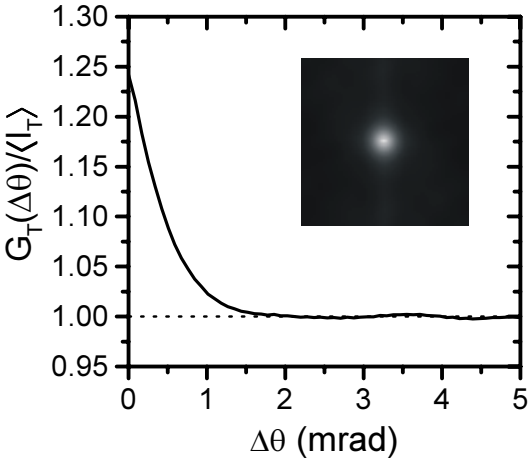

Figure 4.5 A cross section through the autocorrelate $G_{\mathrm{T}}(\Delta\theta)$ of the data in figure 4.3, normalized to the average total intensity $\langle I_{\mathrm{T}}\rangle$. The contrast is reduced from 2 to 1.25 due to the incoherent background, complicating the determination of the first zero θ_0. The two dimensional autocorrelate itself is shown as the inset.

Another change with respect to the fully coherent situation is the disappearance of the flat top for $G_{\mathrm{I}}(\Delta\theta = 0)$. There is no explanation for this sharpening, except perhaps the remark in ref. 97 that the details of the autocorrelation function of speckle in partially coherent light depend to a large degree on the particulars of the contributing fields. The resulting $G_{\mathrm{T}}(\Delta\theta)$ $(= G_{\mathrm{I_T}}(\Delta\theta))$ is normalized to $\langle I_{\mathrm{T}}\rangle$ and analyzed quantitatively by modelling it with a function

$$G_{\mathrm{m}}(\Delta\theta) = 1 + \left[\frac{\langle I\rangle}{\langle I_{\mathrm{T}}\rangle}\right]^2 e^{-\Delta\theta/\theta_{\mathrm{c}}}. \tag{4.3}$$

$\langle I\rangle$ and $\langle I_{\mathrm{T}}\rangle$ are determined directly from the data, so θ_{c} is the only free parameter in a fit with G_{m}, providing a way to determine the speckle spot size. The characteristic angle θ_{c} is smaller than θ_0 by a constant factor ≈ 1.

The θ_{c} are plotted as a function of pump fluence in figure 4.6(a). The speckle spots are found to shrink as the pump fluence is increased from 0 to 1 $\mathrm{mJ/mm^2}$, after which their size is approximately constant. The optical resolution of the imaging system is ≈ 0.1 mrad. Apparently the source of diffuse light producing the speckle becomes larger if the pump fluence is larger. This is consistent with the notion that mainly the long paths are amplified in a random laser. If only the intensity is increased, without actually changing the amount of amplification the speckle size is constant, as shown in figure 4.6(b).

Without the pump, the speckle size is set by the probe beam diameter of 0.8 mm (80ℓ), and for the highest pump energies the equivalent source size increases to approximately 1.5 times this value. For high pump fluence the speckle does not get smaller. This is consistent with the result obtained in chapter 3 that far above threshold the local equilibrium gain is clamped at the local loss level, so $\kappa_{\mathrm{g}}(\mathbf{r})$ does not depend on the pump fluence.

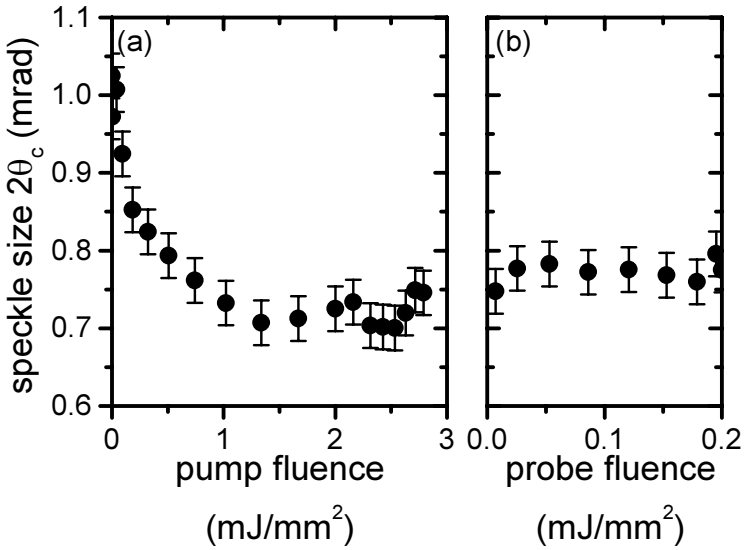

Figure 4.6 Characteristic decay angle of the autocorrelate, as measured by a fitting G_{T} with G_{m}, given in (4.3). *(a)* For large pump fluence the speckle spots get significantly smaller compared to the case without gain, signifying that the amplification assists the spatial spreading of the probe light. The probe fluence is 59 $\mu\mathrm{J}/\mathrm{mm}^2$. *(b)* With varying probe energy at a pump fluence of 2.9 $\mathrm{mJ}/\mathrm{mm}^2$, the speckle size is constant, demonstrating the role of the amplification in the effect in *(a)*.

A quantitative assessment of the modification of the path length distribution $P(\Lambda)$ is not possible with the available theory. The formalism of chapter 3 takes into account only one spatial variable, whereas the transverse dimensions are clearly needed for describing the lateral spreading of the probe. Even in one dimension $P(\Lambda)$ can not be determined, in absence of a stationary form for the diffusing density. Recalling that the rms traveled distance in a random walk of length Λ is $\sqrt{\ell\Lambda/3}$, we conclude that the average path length $\langle\Lambda\rangle$ becomes $(1.5)^2 = 2.25$ times larger in this sample.

4.2.4 Possible experiments?

We conclude the discussion of speckle in random lasers with a suggestion for a possible experiment, investigating intensity correlations in amplifying random media. It is derived from the classic C_1 short range speckle correlation measurement, see ref. 98 for an introduction.

The effect of a changing gain on the intensity correlation can be measured by $C_1(\Delta I_{\mathrm{p}}) = \langle I(I_{\mathrm{p}})I(I_{\mathrm{p}} + \Delta I_{\mathrm{p}})\rangle$. This will reflect the change in spot size presented

above, but then with a method that is theoretically better controlled. We expect a change in speckle pattern to occur while $\kappa_g(z)$ changes, far above threshold it should be constant and only increase in average intensity.

$C_1(\Delta k_\perp)$ has a weak dependence on the absorption, appreciable if $1/L_a^2$ is not negligible compared to $k_\perp^2$, so for small angles. Upon replacing L_a by $-L_g$, which is allowed for a weak probe that does not saturate the gain, we gauge that C_1 should be appreciably larger than the passive case for rotation angles smaller than $(kL_g)^{-1}$. This estimate applies to the transmission of a relatively thin sample ($L \approx 2L_a$ for pump light) with two-sided pumping as proposed by Wiersma [71], so κ_g is approximately constant. The analysis of Burkov and Zyuzin [66] suggests the same relative change due to gain for short and long range correlations.

An experimental obstacle is the need for a solid sample, in order to be able to correlate different speckle patterns in a well-defined measurement. We have not managed to make a high gain solid random laser, in spite of several attempts based on both silica glass and PMMA plastic matrices. We find that in the plastic the dye degrades too fast, while in the glass the scatterers coagulate during sol-gel synthesis. Working with powdered dye-doped glass is a possibility if the mean free paths required are not too small. Another complication is the need for large dynamic range detection, which is problematic in pulsed experiments.

4.3 Enhanced backscattering in random lasers

In this section we describe our enhanced backscattering measurements, probing the gain dynamics in a random laser. Experimentally they are similar to the speckle measurements, which is why we present both in one chapter. We focus specifically on the laser threshold, experimentally investigating the role of the threshold for light propagation, with a technique that allows a detailed and quantitative analysis of the results. Enhanced backscattering (EBS) has evolved from being a subject of study in itself [99] into a tool that can be put to use for studying transport of waves in random media in a very precise and quantitative manner [27]. The principle of EBS is explained in figures 4.7 and 4.8.

The shape of the backscatter cone is determined by the characteristic transport distance of the light in the medium. The exponential amplification of the intensity with path length Λ in a gain medium results in a larger contribution of long light paths compared to light in passive material. The long light paths constitute the top of the EBS cone: a relatively larger contribution of long paths yields a sharper and narrower EBS line shape [70, 83]. This sensitivity to long paths makes EBS particularly well-suited for testing the alleged divergence behavior.

We then compare the measurements with EBS cones calculated from the dy-

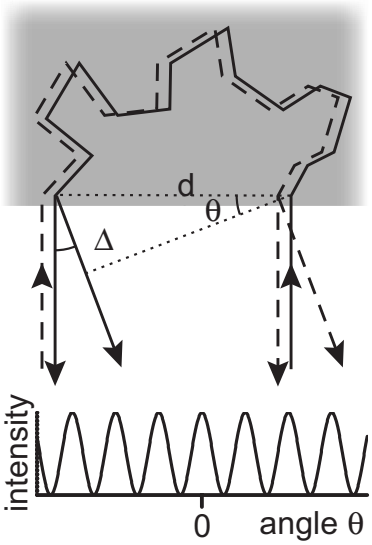

Figure 4.7 Sketch of the principle of enhanced backscattering: a plane wave is incident on a multiply scattering medium. Every random "path" in the medium (gray, assumed semi-infinte) can be traversed in two ways, forward and backward. These two waves exiting the medium are always in phase, since their path lengths are equal. Only outside a path length difference Δ develops, depending on the transverse distance d between both ends of the path: $\Delta = d\sin\theta$, where θ is the angle with respect to the incident direction. Each path serves as two in-phase point sources (regardless of the longitudinal coherence of the wave, since it interferes with itself), separated by a distance d, producing an interference pattern in the far field $I(d;\theta) \propto 1+\cos(2\pi\Delta/\lambda)$. The contribution of long paths (with large d) varies quickly with θ. *(Continued in figure 4.8.)*

namic random laser theory of chapter 3. This allows us to validate the theory, and provides a way to show experimentally that the explosion does not exist. We infer $\kappa_g(z)$ from the results.

4.3.1 Experimental details

Our measurements of EBS in high gain amplifying random media are performed with samples consisting of 220 nm diameter TiO_2 [44] colloidal particles suspended in 1.0 mM Sulforhodamine B laser dye in methanol. The samples are contained in a cell as in the speckle experiments. The cell is slowly spinning to prevent sedimentation, dye degradation and also to assist speckle averaging. When measuring EBS it is important to average out the speckle, which has a much larger intensity variation than the cone, and so will obscure it. A source with short coherence length produces a speckle with less contrast, so it is easier to average. In this case the short coherence length of the OPO is actually an advantage, and the use of the OPO allows us to take Sulforhodamine B as a gain medium, which is easier to work with than Coumarin 6.

The setup is similar to the one used in the speckle experiment; we highlight only the differences. The dye/TiO_2 suspension is optically pumped with the frequency doubled Nd:YAG pulse. The pump fluence range at the sample position is 0–140 μJ/mm^2. The pulse repetition rate is 20 Hz. The probe pulse has a low energy of $3\,\mu\mathrm{J}/\mathrm{mm}^2$, a duration of 4.4 ns, and is tuned to the maximum of the fluorescence band of the dye (590 nm). The pump and probe beams with a diameter of 3 mm coincide on the sample front interface. Rising edges of both pulses arrive simultaneously. A

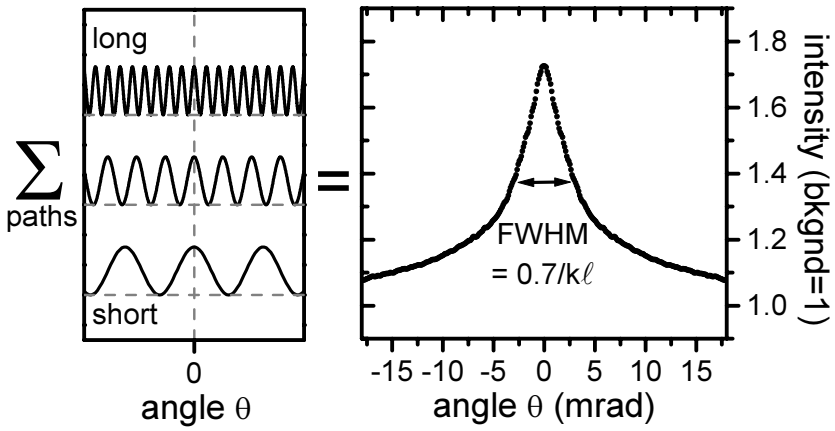

Figure 4.8 *(Continued from figure 4.7:)* All these interference patterns are summed, weighted according to the probability for a path to span a certain transverse distance d. The fringes average to a flat ("diffuse") background for all angles, except for a range of width $1/k\ell$ around $\theta = 0$ where interference is always contructive. The result is an intensity distribution as measured in the right hand plot, called the backscatter cone, rising to a height of maximally two times the diffuse background. In principle d can be infinite, which produces a cusp at the top of the cone. In the measurement the top is rounded due to the instrument resolution of 1 mrad. The peak intensity relative to the background, or enhancement factor E, is reduced due to stray light. The information about light transport is in the distribution of traveled distances: for plain diffusion the cone's FWHM $= 0.7/k\ell$. An absorbing medium removes long paths and rounds the cone, while in an amplifying medium the weight of longer paths is enhanced compared to shorter ones, making the cone narrower. It is important to realize that E does not depend on gain or absorption, since the background and the cone are produced by the same source, with only one path length distribution.

schematic of the setup is shown in figure 4.9.

The probe beam enters the sample via a beamsplitter to allow intensity measurements in the exact backscattering direction. The sample is tilted forward by $\approx 2^\circ$ to keep the specular reflection out of view of the detection. The scattered light is collected through an interference filter and a focusing lens on the CCD camera to record the EBS cone. We accumulate 51 to 204 different speckles (realizations) in each exposure, depending on the collected intensity. The angular resolution is 1 mrad, limited by the probe beam divergence.

4.3.2 Results from experiment

In figure 4.10 an example of a measurement is shown. The image clearly shows the larger intensity near the backscattering direction. For analysis we manually find the

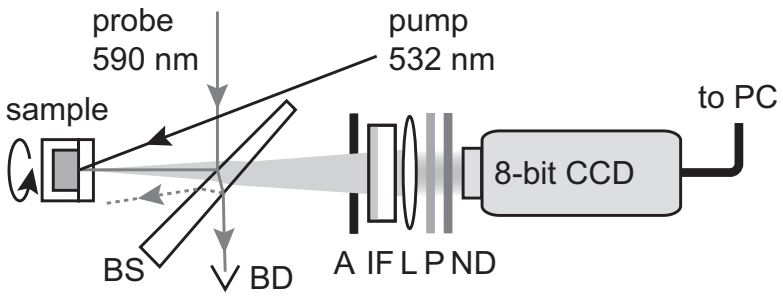

Figure 4.9 Schematic of the setup used for random laser EBS. The pump and probe (both diameters 3 mm) arrive simultaneously at the sample. The probe is incident via a beam splitter (BS), with a wedged shape to eliminate spurious reflections. The sample is spinning slowly. The scattered and amplified probe light is recorded on the CCD camera, after passing through the beam splitter, an aperture (A), a 589.6 ± 0.5 nm interference filter (IF), a focusing lens (L), a polarizer (P) selecting in the scattered light the incident polarization, and one or more neutral density filters (ND). Exposure times of the camera vary from 2.56 to 10.24 s, depending on the amount of incident light.

center of the peak, since this proves to be the most reliable method, and integrate on concentric circles around it. For visual inspection a symmetric picture is more appealing, so we mirror the data in the $\theta = 0$ axis.

From the backscattering cone obtained without pump, taking into account the reabsorption, we infer that the transport mean free path $\ell = 3$ μm. Earlier EBS experiments [83, 100] have been performed with materials in which the laser threshold could not be reached. In our sample the laser threshold is found to be at a pump fluence of 10 μJ/mm^2 from the width of the fluorescence spectrum as a function of the pump pulse energy.

The salient features of the influence of gain can be seen in figure 4.10. Both the width and enhancement factor E become smaller with increasing pump energy. The enhancement factor has a (gain-independent) value of maximally 2 that is diminished by angle-independent contributions to the intensity. The width is related to the transport length: for a cone without gain it is $\propto \ell^{-1}$, and provides a measure to compare the cones at varying pump energy. The larger fraction of long light paths at high gain reduces the width of the EBS cone, but there is no sign of a divergence or a sudden change in behavior at the threshold crossing. After the initial cone narrowing, the width saturates far above threshold at a value that is a third of the width of the cone without gain. The decrease of E from 1.65 to 1.25 is due to the incoherent fluorescence component in the collected light, which becomes stronger for higher pump energies.

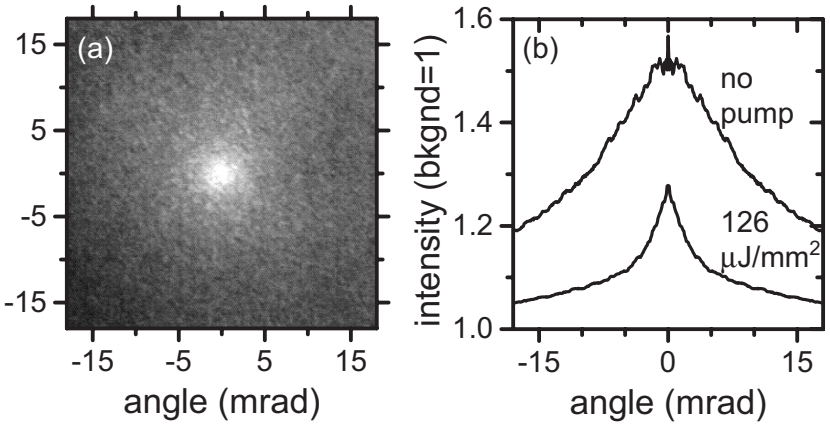

Figure 4.10 *(a)* CCD image in scattered probe light, containing the EBS cone. The sample is described in the text, $\ell = 3$ μm, pump fluence 126 μJ/mm^2. The exposure is the sum of 72 shots, averaging out most of the speckle. *(b)* The cone derived from this image (bottom curve) by averaging over the azimuthal angle around the top. The resulting curve is mirrored around $\theta = 0$, and the background is normalized. For low intensities residual speckle may be a problem, especially around the top of the cone where the amount of pixels contributing to the average is small. As an example the cone without pump is shown (top curve). $E < 2$ due to single scattering, stray light, and fluorescence (cf. figure 4.3(b)).

4.3.3 Comparison with theory of chapter 3

For a comparison with the theory of chapter 3 we need to extract EBS cones from the calculated time- and position-dependent inversion data, providing the spatiotemporal gain-profile reflected in the cone.

The z-dependence of $\kappa_g(z,t)$ in EBS can be treated with the method due to Deng *et al.* [101]. It is an extension of the formalism presented in section 3.1, the expansion of a solution of the diffusion equation in eigenmodes. If the constant κ_g is replaced by one depending on z, the method can still be applied, only for general $\kappa_g(z)$ the eigenfunctions $\phi_n(z)$ and eigenvalues ε_n must be found numerically. Furthermore the x- and y-directions are reintroduced to allow the calculation of EBS. The geometry is still translation invariant in the transverse dimensions, so these are Fourier transformed to $k_\perp = k\sin\theta$. The EBS contribution to the intensity $\gamma_E(\theta)$ is then given in terms of $\phi_n(z)$ and ε_n, and angle-dependent factors:

$$\gamma_E(\theta) = \frac{3}{\ell^2}\sum_{n=0}^{\infty}\frac{1}{k_\perp^2+\varepsilon_n}\left|\int_0^L \mathrm{d}z\,\phi_n(z)e^{-(v-iu)z/\ell}\right|^2 . \tag{4.4}$$

Here $v(\theta) \equiv \frac{1}{2}[1+(\cos\theta)^{-1}] = 1+O(\theta^2)$ and $u(\theta) = k\ell(1-\cos\theta) = O(\theta^2)$ are constants for $\theta^2 \ll 1/k\ell$.

The recipe of ref. 101 is, however, a stationary description. The gain profile is static and also the diffusion equation it uses is time-independent. We need to work around the first problem, but as a small digression we will first say some things about the second.

Path length distribution The path length distribution $P(\Lambda)$ in a disordered medium can be regarded as a time-of-flight spectrum for multiply scattered light. What $P(\Lambda)$ for a random laser looks like has been a long-standing question [102]. The path length distribution is important for diffusive wave spectroscopy (DWS) [103], and a useful concept in general when describing multiple scattering as a sum of light paths. It can be measured directly in time-resolved experiments. γ_{E} and $P(\Lambda)$ for backscattering are related by [104]:

$$\gamma_{\mathrm{E}}(\theta) = \int_{t_{\mathrm{f}}}^{\infty} \gamma_{\mathrm{E}}(\theta;t)\mathrm{d}t = \int_{t_{\mathrm{f}}}^{\infty} P(t)e^{-Dk_{\perp}^2 t}\mathrm{d}t\,, \tag{4.5}$$

where $t_{\mathrm{f}} \equiv \ell/c$ is the mean free time and $P(t) = P(\Lambda/c)$.

When calculating EBS from a time-dependent diffusion equation, one can find a form for $P(t)$ in terms of the eigenfunction expansion, also for an amplifying system, as long as κ_{g} is time-independent. From a dynamic diffusion equation we can find $\gamma_{\mathrm{E}}(\theta;t)$, and identify $P(\Lambda)$ from (4.5):

$$\gamma_{\mathrm{E}}(\theta) = \frac{3D}{\ell^2}\sum_{n=0}^{\infty}\int_{t_{\mathrm{f}}}^{\infty}\mathrm{d}t e^{-D(k_{\perp}^2+\varepsilon_n)t}\left|\int_0^L \mathrm{d}z\,\phi_n(z)e^{-(\nu-iu)z/\ell}\right|^2 \quad \Rightarrow \tag{4.6}$$

$$P(\Lambda) = \sum_{n=0}^{\infty} e^{-\varepsilon_n \ell\Lambda/3}\left|\int_0^L \mathrm{d}z\,\phi_n(z)e^{-(\nu-iu)z/\ell}\right|^2 \tag{4.7}$$

For long light paths ($\theta^2 \ll 1/k\ell$ in the EBS cone) $P(\Lambda)$ is angle-independent, as a path length distribution should be. The requirement of long light paths physically means that the transport must be described well by the diffusion approximation, known to fail near the boundary and for short paths.

Using this method for an amplifying medium with a model $\kappa_{\mathrm{g}}(z) = \kappa_{\mathrm{g}} > 0$ in a layer $0 < z < L_z$ (with $L_z < L'_{\mathrm{cr}} \equiv \frac{\pi}{2}L_{\mathrm{g}}$, the critical thickness for an amplifying layer, backed by a semi-infinite passive medium with the same transport properties), and $\kappa_{\mathrm{g}}(z) = 0$ for $z > L_z$, we find the behavior shown in figure 4.11. From the well-known $P(\Lambda) \propto \Lambda^{-\frac{3}{2}}$ for a passive medium, the large Λ tail rises gradually towards $P(\Lambda) \propto \Lambda^{-\frac{1}{2}}$ when approaching $L_z = L'_{\mathrm{cr}}$, but by then the limits of the small-gain assumption are stretched already beyond breaking. ∎

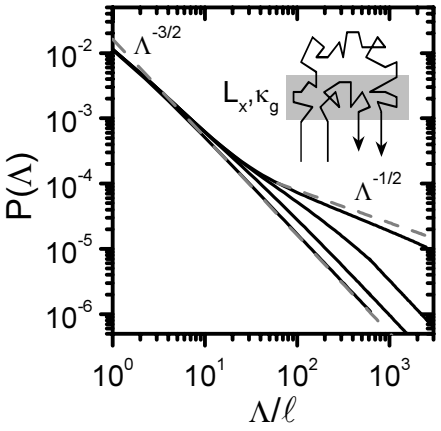

Figure 4.11 Path length distributions in backscattering $P(\Lambda)$ calculated for a thick medium with an amplifying layer of thickness L_z near the source interface. Plotted are 4 curves for different κ_g, $L_z/L'_{cr} = 0$, 0.47, 0.78, and 0.97 (solid lines, bottom to top) and the limiting curves $P(\Lambda) \propto \Lambda^{-\frac{3}{2}}$ for zero gain ($L'_{cr} \to \infty$) and $\propto \Lambda^{-\frac{1}{2}}$ for $L_z \to L'_{cr}$. For intermediate κ_g, $P(\Lambda)$ returns to $\Lambda^{-\frac{3}{2}}$ for long paths. These reach the passive part of the system, and are thus amplified as much as the paths of medium length, as sketched in the inset.

In the analysis of $\kappa_g(z)$, the time variation is a subtle issue. The similarity of time scales of gain dynamics and light transport make it very difficult to solve the time-dependent EBS cone in a varying gain-profile. Extending the method outlined above to $\kappa_g(z,t)$ would mean that the ϕ_n and ε_n become time-dependent. We chose instead to use the averaging property by the time-integrated detection method in the experiment to simplify the analysis.

Since the EBS process itself samples the medium on the time scale needed to build up a cone, it only senses slow variations in $n_1(z)$. The longest paths that contribute in an experiment with an angular resolution of 1 mrad have a separation between entrance and exit points of $d = 10^3\lambda \approx 600\ \mu$m. The diffusive transport time over this distance is $d^2/D \approx 1.7$ ns. We mimic this property by low-pass filtering the data, and subsequently averaging $n_1(z,t)$ in time windows of length d^2/D, and use this mean inversion profile to calculate a "partial" EBS cone. The partial cones are summed, each weighted with the mean probe intensity in its window. This procedure largely overcomes the dominance of the nearly critical $\kappa_g(z)$ occurring in the relaxation oscillation: long paths, needed for the divergence to happen, do not have the time to build up in the ≈ 50 ps that the "supercritical" inversion lasts. This demonstrates once more that the dynamic picture, although allowing for high inversion densities, prevents the explosion. We stress that a theory that does not incorporate the full dynamics, fails to reproduce the cones completely. In particular a static approach predicts an extremely small width and diverging height using the same parameters.

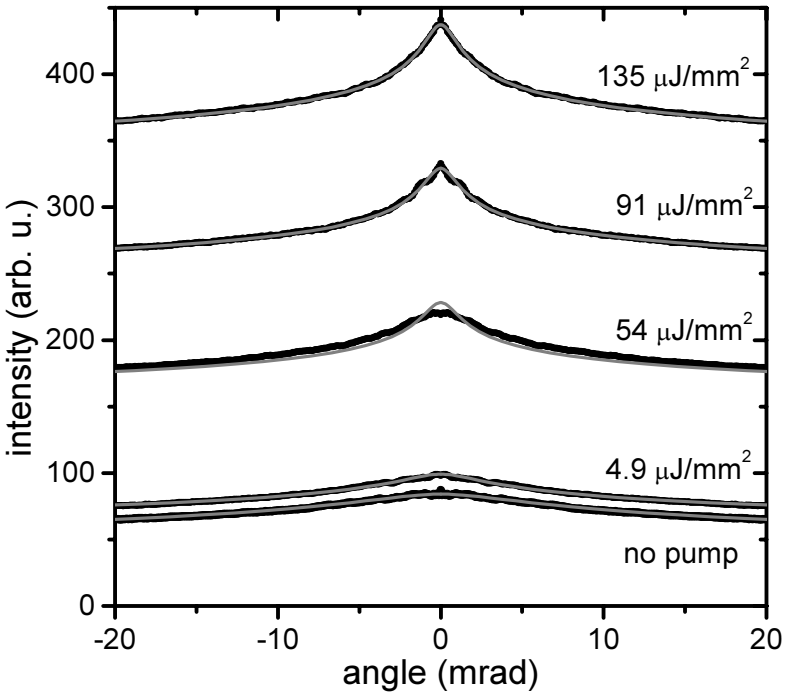

Figure 4.12 Black points: enhanced backscattering cones for pump fluences ranging from 0 to 135 μJ/mm^2. Gray lines: cones calculated from the dynamic theory of chapter 3. The experimental results are accurately reproduced by the theory, except for intermediate pump energies (ca. 20–70 μJ/mm^2; one example shown) where the relaxation oscillations dominate the temporal inversion profile.

4.3.4 Discussion

The lines in figure 4.12 are obtained from the $n_1(z,t)$ found from the model of chapter 3 with the methods of section 4.3.3. The agreement between experimental data and theoretical description is excellent for low and high pump energies. Initially, the width of the EBS cone drops quickly with increasing pump pulse energy. Far above threshold, the FWHM saturates (at ≈ 10 mrad, depending on system parameters) due to the pump-independence of the above-threshold $n_1(z)$.

For pump fluences between 20 and 70 μJ/mm^2 the theory deviates from the experimental results, see figure 4.13. This discrepancy is due to the entanglement of the time scales of transport and variation of $n_1(z)$. Since $n_1(z)$ changes faster than the time needed for the formation of a backscatter cone, the reversibility of transport in the medium is affected. A wave traversing the medium along a certain path experiences a spatiotemporal gain profile that is in principle different than the profile

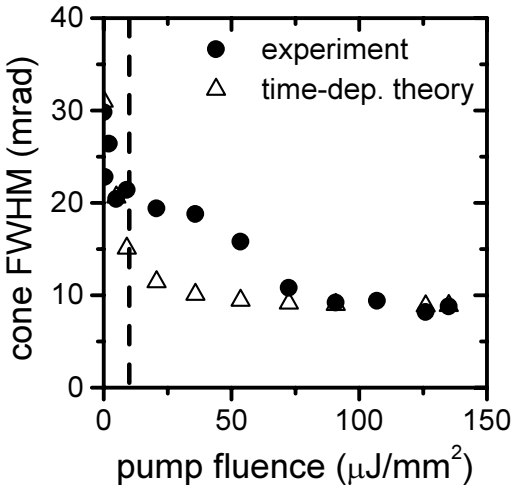

Figure 4.13 The full widths at half maximum of the backscatter cones as a function of pump fluence. The dashed line indicates the threshold, obtained from an independent measurement. Circles are obtained from experiment, triangles from the theory in chapter 3.

seen by the wave in the reversed path. This reduces the interference contrast in the scattered light, as the two waves no longer have equal amplitudes when exiting the medium. This unbalance is especially prominent just above threshold, where the long-lived oscillations make up an important part of the temporal gain profile. Long light paths are most strongly influenced by the changing $n_1(z)$. Their interference contribution is smaller than inferred from the averaged gain profile, and the actual, measured EBS cone is broader than given by our theory. A simulation of dynamic EBS backs up this explanation, showing a cone broadening of the correct magnitude due to the inequality of interfering paths.

4.4 Conclusions

In this chapter, we have reported on speckle and enhanced backscattering experiments on high gain random lasers, consisting of a laser dye with TiO_2 colloidal scatterers. The cone width becomes smaller with increasing gain, and saturates above threshold at a value that is three times smaller than the width of the cone without gain. We find that a cone shape that fits the EBS data well is only given by a time-dependent calculation of the population inversion $n_1(z)$ in the medium, even though the experiment integrates out the temporal variations. Contrary to what is expected from an extrapolation of the known low-gain stationary description to the high amplification coefficients of organic dyes, the experimental data show no sign of a divergence of the intensity.

The speckle experiment also reflects the saturation behavior above the laser threshold. The speckle spots shrink with increasing amplification, due to the in-

creased contribution of long light paths. This trend, too, saturates far above threshold, where the speckles have a constant angular size of 1.5 times smaller than the speckles from a passive sample. The speckle retains its Rayleigh intensity statistics. The analysis of the speckle autocorrelation in terms of a coherent amplified probe on an incoherent fluorescence background is consistent.

These results show that the spatial gain profile can be investigated well with probing techniques, allowing a quantitative study of light transport in random lasers. The theory developed in chapter 3 is validated by these measurements, and the interpretation of experimental data with the help of comparisons with that theory provides insight in the actual dynamics of a random laser, even by the stationary experiments reported here.

5. Narrow peaks in fluorescence from scattering systems

Recently, several articles have appeared reporting on the observation and interpretation of narrow peaks in the emission spectrum of random lasers. The phenomenon was said to be a manifestation of Anderson localization. This is a bold claim, needing a solid experimental backing. We performed a series of experiments trying to replicate the results and to investigate these peaks more quantitatively and systematically than in the published research. The outcome of our experiments can be explained in terms of material properties, and we assert that this explanation can be generalized to the literature results.

The combination of Anderson localization and amplification has been appealing since the idea was brought up [71]. The picturesque view of Anderson localized light being captured in "loops" suggests the possibility of random ring laser cavities [52, 105], providing resonant feedback, i.e. light experiences a phase shift of an integer times 2π in a round trip. This would permit a "coherent random laser", a third, qualitatively different regime in scattering amplifying systems (first and second being the single, post-ASE scattering as in section 2.3.2, and multiple scattering as in the other experiments described in this thesis). The suggestion that Anderson localization might be facilitated by the presence of gain—localization being destroyed by absorption, and gain being negative absorption, in a way—has been present for a long time, but up to today nobody has theoretically pursued the idea to its full (3D) extent.

Experimentalists have put a tremendous amount of effort into achieving localization of light, until now without undisputed success. Furthermore, the knowledge about the phenomenology of the localized state in an actual measurement is very limited. These considerations call for wariness when interpreting experimental results in terms of Anderson localization. Fluorescence is sensitive to microscopic changes

in the electronic structure of the sample (e.g. specific defects, surface adsorption). For this reason material parameters should only be ruled out as an explanation for a spectroscopic phenomenon after very careful inspection.

5.1 Critical review

5.1.1 Observations and interpretations from the literature

In this section we present an overview of relevant results and interpretations from the literature, followed by a discussion. The reported phenomena are summarized in figure 5.1: sharp peaks appear in the emission spectrum of a random laser, on top of the narrowing ASE spectrum, near the maximum of the emission spectrum. Such observations have been made in multiply scattering samples made of ZnO and GaN powders [52, 106–110], and dye solutions with ZnO scatterers [53], but also in transparent samples, such as thin films of nanocrystalline ZnO [105, 110–113], dye-doped gel, active polymer, or index-matched opal [114, 115]. A distinction has to be made between the multiply scattering materials and thin films, that have become part of the same discussion. The observations are similar for both types of samples, although the optical properties differ strongly.

The measurements have been explained in terms of resonant feedback induced by disorder. A dominant idea is that of microscopic ring cavities, light trajectories that return to the same scatterer with a round trip phase lag of $n \cdot 2\pi$, with n an integer. Recurrent scattering events (loop paths of *any* length) have been shown to exist as a single-scattering-like contribution to the backscattered intensity [116] for $k\ell \lesssim 10$. We will discuss this interpretation in some more detail in section 5.1.2.

Recently some results were reinterpreted [108] in terms of the system's electromagnetic eigenstates, characterized by a spectral width $\delta\omega$ and a spacing Ω. The eigenmodes overlap in frequency, $\delta\omega > \Omega$, for less than very strong disorder—said to result in the incoherent-feedback multimode random laser as in our chapter 2—to decouple for strong disorder, $\delta\omega < \Omega$—allowing a coherent random laser working in a single electromagnetic mode of the system. See also our discussion of the random laser vs. cavity laser β-factor, section 3.3.1. $\delta\omega/\Omega < 1$ for the transport eigenstates of a disordered medium is the Thouless criterion for Anderson localization [88], implying that a random laser exhibiting the narrow peaks should be in the localized regime.

To substantiate the proposal of a disorder-induced resonant feedback, one has attempted to reduce the amount of disorder and so make the effect disappear. One method is already mentioned in figure 5.1: to change the amount of scatterers in the dye solution, which indeed has an effect on the occurrence of the frequency peaks.

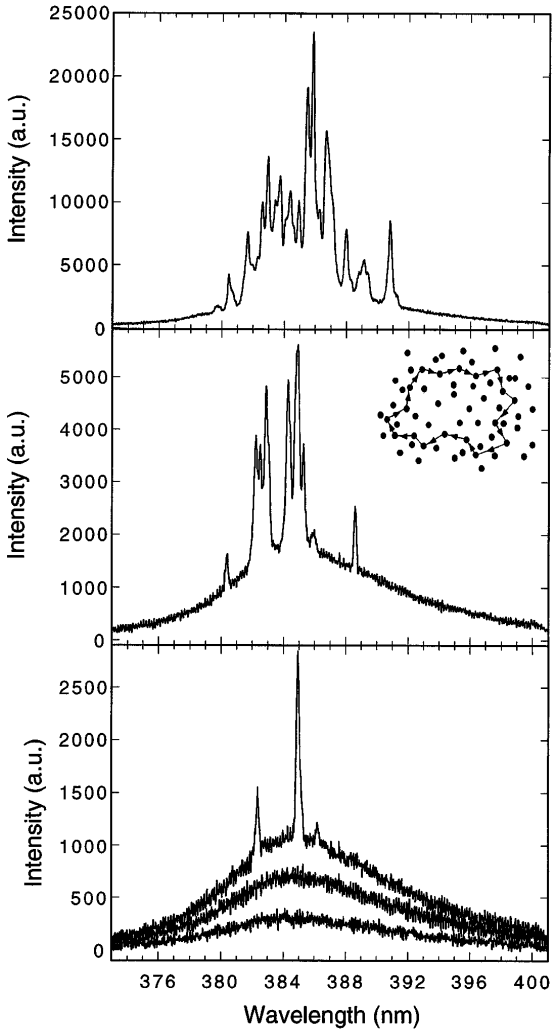

Figure 5.1 Narrow frequency spikes (FWHM$\approx$ 0.2 nm) appearing in the emission spectrum of a random laser consisting of ZnO powder, from ref. 52. The particle size is $\approx$ 50 nm, the refractive index $\eta = 2.2$; $k\ell = 5$ is claimed. The pump intensity increases (bottom to top) from 400 to 1387 kW/cm^2. Narrow peaks appear at 763 kW/cm^2. Pump data: $\lambda = 355$ nm, beam diameter ≈ 45 μm, pulse duration 15 ps.
The phenomenology: microscope images [107] show the field at the frequency of the peaks to be concentrated in small spots (~ 0.5 μm). The spectrum varies with emission angle, and the pump intensity at which the peaks appear decreases for larger pump spots. The number of peaks grows with pump intensity and the pump area. A measurement in a system of Rhodamine 640 perchlorate dye with ZnO scatterers [53] investigates the dependence on ℓ, or scatterer density. The peaks are absent for the largest $k\ell \approx 70$, but do appear for $k\ell = 47$ and smaller. The photon statistics of the peaked emission exhibit the Poisson distribution of coherent light [108].

Another method is to anneal the powder film [106], increasing the particle size. This either eradicates the peaks or increases the amount of pump light needed to produce them by up to factor 10.

In both methods—changing scatterer density and annealing the sample—the disorder is not the only varying quantity. Besides the question whether one actually *reduces* the disorder when the grain size changes from 50 nm to 150 nm by annealing, the effect of the reducing number of (surface) defects could be much more important, if defects play a role. The influence of defects on ZnO luminescence is an active area of research [117, 118]. Many semiconductor excitations, related to the surface,

Figure 5.2 Illustration of Anderson localization in loops. *(a)* The probability to go from A to B via path 1 (amplitude P_1) or path 2 (P_2) is $\propto P_1^2 + P_2^2$, without interference terms because all contributing fields have a random phase. *(b)* Only paths returning to A always interfere constructively with their reversed counterparts, resulting in a return probability $\propto (P_1 + P_1)^2 = 4P_1^2$.

defects, or microscopic disorder (i.e. non-crystallinity) are optically active, possibly exhibit a nonlinear response, and could influence the emission spectrum [109, 119]. A cleaner way to change the mean free path in ZnO powders is to reduce the refractive index contrast by filling them with a transparent liquid [27, 120].

For varying the scatterer density in a dye a similar remark can be made: it also changes the surface area of the scatterers in contact with the solution. If the dye adsorbs to the surface of the scatterer, its electronic structure may change, affecting its optical properties in hardly predictable ways, especially on semiconductors [121].

The influence of material properties has not been ruled out with these experiments. In fact, the evidence presented for an explanation of the data in terms of multiple scattering is debatable: the scattering strengths in different samples vary widely. All reported values of $k\ell$ indicate classical diffusive transport.

5.1.2 Localization and random ring cavities

Localization is an inhibition of transport due to interference, we said on page 22. The current discussion necessitates a little more detail. The criterion for localization is $D = 0$. The principle of Anderson localization is usually illustrated with the following picture [122], see also figure 5.2.

The probability $P(\mathbf{r_A}, \mathbf{r_B})$ to get from a position $\mathbf{r_A}$ to $\mathbf{r_B}$ is the squared sum of all contributing probability amplitudes P_i. For all points $\mathbf{r_B}$ but one, each random path i starting at $\mathbf{r_A}$ has a random phase, and so the interference terms do not contribute in the ensemble average; $P(\mathbf{r_A}, \mathbf{r_B}) = \sum_i P_i^2$. The one exception is $\mathbf{r_B} = \mathbf{r_A}$, where every path is in phase with its time-reversed counterpart $-i$ (of course $P_i = P_{-i}$), so the interference terms do contribute: $P(\mathbf{r_A}, \mathbf{r_A}) = \sum_i (P_i + P_{-i})^2 = 2\sum_i P_i^2$, like in EBS. The higher resultant intensity at $\mathbf{r_A}$ can not have gone somewhere else and so the transported intensity is smaller than given by diffusion theory. The diffusion

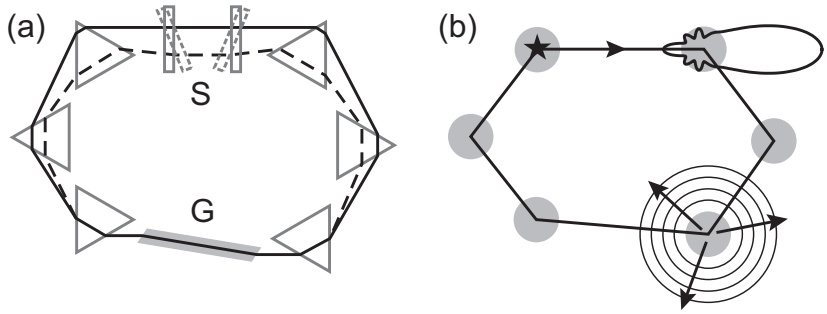

Figure 5.3 Comparison between a ring cavity contructed with prisms *(a)* and the closed loop light paths *(b)* proposed as an explanation for the narrow peaks observed in random laser fluorescence. In *(a)* the losses at every prism, at the dispersive frequency selection S and the gain cell G are $\sim 1\%$ due to reflection losses. In *(b)*, however, light emitted in a scatterer (★; depicted is the case of amplifying scatterers, as in ZnO powder) is radiated from every scatterer in a spherical wave (bottom right) the amplitude of which is modified by the differential scattering cross section (top right). The result is a huge loss, resulting in a very broad frequency profile.

constant is reduced by interference, and when $D = 0$ at $k\ell \sim 1$, transport stops and the system is in the localization regime.

The paths featuring in this handwaving picture for localization are the supposed random ring cavities, proposed as a mechanism providing coherent feedback in a random laser. However, these trajectories in localization are not actual, traceable light rays from scatterer to scatterer. It is not possible to construct such paths in wave diffusion; a propagation line drawn in multiple scattering is the normal to the spherical wavefronts emanating from the scatterers. The lines are rather the curves along which the propagation of the field amplitude is evaluated, not unlike the multiple scattering approach to the refractive index [123]. Each individual path has measure zero. The inhibition of transport only emerges in the summation of the infinite number of possible paths. A localized wave is better regarded as an exponentially decaying field state [124] with an extent that is the localization length.

One can assess the probability of a loop to function as a random ring microlaser, by resorting to a classical wave propagation picture between scatterers and trying to create the threshold condition in such a ring cavity. The estimation is illustrated in figure 5.3. Imagine a short path of N scatterers, starting on scatterer 1 and meeting $N-1$ other scatterers before returning to 1. Every scatterer j radiates a spherical wave subject to its differential scattering cross section $\frac{d\sigma_j}{d\Omega}$, which together with the solid angle spanned by scatterer $j+1$ determines the fraction R_j of the wave continuing in the ring. The round trip loss factor of such a ring "cavity"

is $(\prod_{j=1}^{N} R_j)^{-1}$, which is an enormous number for any realistic estimate for the R_j. Two consequences: firstly, the threshold condition in this ring with a length of a few λ is only satisfied by an impossibly large gain. Secondly, with such a large loss the frequency spectrum is so broad that one cannot speak of a resonant wavelength for which a round trip shifts the phase by $n \cdot 2\pi$. Of course, a rare event with smaller loss may exist, but the major characteristic of such a random laser is unlikelyhood. The essence is not that the loops do not exist, it is that they are a scarce and unimportant subclass of all possible events.

Incidentally, the picture just sketched also shows that the proposed mechanism is an amplitude property, since only one propagating field is needed to demonstrate it. Localization is an intensity effect. Contributions to it always arise out of interference between two or more paths.

5.1.3 Thin film "random" laser

Since the optical properties of the semiconductor, polymer, and dye-doped gel thin films, in which the phenomena of figure 5.1 have been observed, differ strongly from the multiply scattering systems, we discuss them separately. The measurements were explained [105, 110–112, 114] in terms of the same random ring cavities, but now supposed to occur in-plane. We will present a different interpretation for the observations in ZnO thin films.

First, it is important to realize that the samples essentially do not scatter. Estimated scattering lengths range up to 0.5 mm [109, 114], compared to thicknesses of 0.1–1.0 μm. The films are transparent, and homogeneous in the direction normal to the plane. The ZnO films are polycrystalline, consisting of "columnar" grains (reaching from substrate to top), with sizes of 20–150 nm. Experiments are done by illuminating the film with a *stripe* of pump light, imposing a preferred direction for the amplification process.

The role of the transparency is exemplified by the sensitivity to external feedback [112], the difference in characteristics in directions in the plane of the film and normal to it [111] and the importance of the stripe excitation. The narrow peaks of stimulated emission can only be caused by direct optical feedback, for instance by reflection off the film edges or even off external objects, known to influence the mode structure in high-gain semiconductor lasers [125]. The variability of the output spectrum can be attributed to details of the film, such as (macroscopic) imperfections or edge structure [114]. However, we can be a little more specific, at least for the ZnO films.

In ZnO layers with a known hexagonal morphology of the grains, Tang *et al.* [126] have shown that the film microstructure induces laser action upon pumping with a stripe, without external mirrors. They measure an emission spectrum consist-

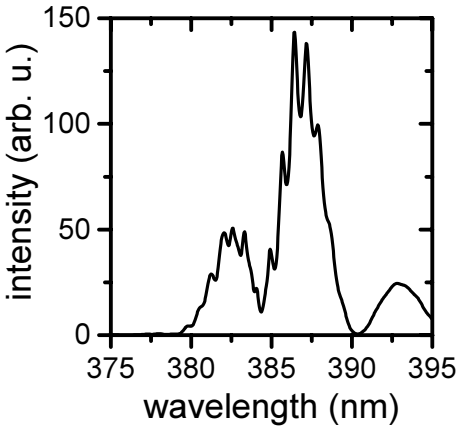

Figure 5.4 Spectrum produced by superposition of the fields (in all modes) of 4 amplifying Fabry-Pérot cavities of nearly equal length, 50 ± 5 μm, calculated for a film of ZnO. The phenomenology of the spectrum is the same as measured in the emission spectrum of disordered ZnO thin films.

ing of regularly spaced narrow lines, and attribute this to Fabry-Pérot (FP) resonators formed by the parallel facets of the hexagonal ZnO microcrystallites. In the pumped region, the high free carrier density reduces the refractive index to minimally the lattice value, creating a partially reflecting boundary between pumped and unpumped grains. This explanation is backed by a measurement of the mode spacing as a function of stripe length, and a measurement of the intensity as a function of direction of the pump stripe along the film, beautifully replicating the hexagonal structure.

We contend that this mechanism is at work in the disordered ZnO films in which the emission spectrum shows peaks at irregular distances. In a disordered layer like the one described above, parallel facets can occur, and if they do near the ends of the pump stripe, they set up a FP-type cavity, with ends reflecting due to the refractive index change induced by the high exciton density along the pump stripe. One cavity produces a comb of peaks, one for each longitudinal mode, but since the pump stripe is wide enough to contain a number of cavities of similar length, the sum of the fields can produce a spectrum that has lost its regular aspect.

We calculate the resonance spectra of such FP cavities, formed by the combination of free carrier generation and film microstructure. The real part of the refractive index of ZnO $\eta(\lambda_\ell = 385 \text{ nm}) = 2.285$ [127, 128], which in the pumped region (i.e. in the cavity) is reduced to 1.90, the value far from resonance [129]. The imaginary part ζ contains gain and absorption: gain is only in the pumped region, a Lorentzian spectrum with a FWHM of 10 nm centered on λ_ℓ; $\zeta(\lambda_\ell) = -0.019$, from the measured gain coefficient in this kind of ZnO films [126]. The absorption rises steeply on the blue side of $\lambda = 378$ nm [127]. The resulting intensity of four such cavities is in figure 5.4. Its features are remarkably similar to those of the spectra in e.g. ref. 105.

There is no carrier transport through the grain boundaries, providing a truly

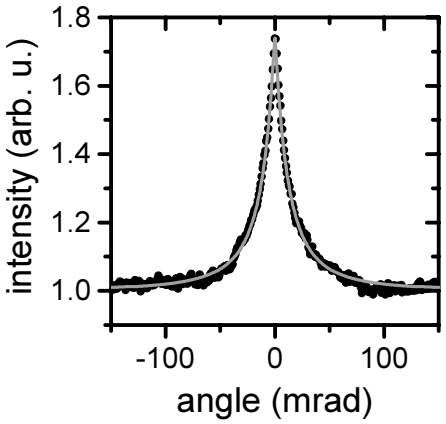

Figure 5.5 EBS cone of ZnO powder (CW, no gain), measured with the off-centered rotation technique [130], measurement by J. Gómez Rivas. The sample thickness is ≈ 1 mm. With this wavelength ($\lambda = 632.8$ nm) the best fit indicates $k\ell = 25$, including internal reflection correction. This number is to be compared with data in ref. 52, where the same measurement was done on a thin sample, on the basis of which $k\ell = 5$ was claimed. See also ref. 131.

discontinuous refractive index step. The refractive index contrast between pumped and unpumped grains is quite small, resulting in a small 1.5% reflectance of the "mirrors". The result is a lossy cavity with an correspondingly large threshold gain, i.e. a high carrier density, exerting a large effect on the refractive index.

5.2 Experimental results

In this section we present our experimental results on the luminescence of ZnO powder films and scattering dye solutions. We try to reproduce the results of refs. 52 and 53, to do more quantitative measurements and so to establish whether multiple scattering has a role in the occurrence of the narrow peaks.

5.2.1 ZnO powders

We measure the luminescence spectrum of ZnO powder upon excitation with a UV pulse. The samples are commercially obtained ZnO, supplied by Aldrich [132] (ZnO-A) and Nanophase [133] (ZnO-N). These powders differ in the methods of synthesis, particle size distribution and morphology. The mean free paths as determined by EBS, however, are similar: $\ell \approx 2.5$ μm at $\lambda = 632.8$ nm ($k\ell = 25$), see figure 5.5. At the ZnO emission wavelength ($\lambda_\ell = 385$ nm) the refractive index of the scatterers $\eta_1 = 2.28$ instead of 2.0 at the wavelength of the EBS measurement, and probably also the average particle scattering cross section σ_s is larger at λ_ℓ. We estimate the reduction of $k\ell$ to be at most a factor 2 [131, 134].

Samples are made from a thick suspension in chloroform. A drop is put on a glass slide and the liquid is let to evaporate. This method produces smoooth samples of a uniform density.

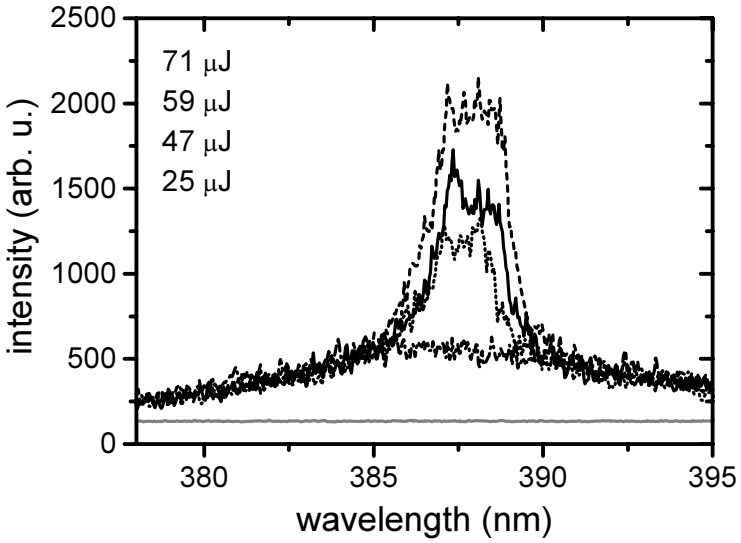

Figure 5.6 Narrow features in the emission spectrum of ZnO. For low pump energies only the broad fluorescence band is seen, which develops narrow frequency structure if the pump energy is increased. For the highest pump energy shown the narrow features have merged. The rep. rate is 2 Hz, the pump energy increases from bottom to top. The instrument resolution is 0.3 nm.

Both powders fluoresce upon illumination with the UV pump beam, though the ZnO-A does so more readily than the ZnO-N, compare figures 5.6 and 5.7. For this reason most measurements were done on ZnO-A, and all data shown are obtained from this sample, unless otherwise noted. Single-shot fluorescence spectra of ZnO-A for different pump energies are shown in figure 5.6. The pump spot is focused to a diameter of $\approx 50\ \mu$m.

The pump source is a frequency-tripled (355 nm) Nd:YAG laser (Coherent Infinity 40–100), with a pulse duration of 1.7 ns and a variable pulse repetition rate. The fluorescence is picked up by an Ocean Optics 200 μm core UV-silica fiber, positioned at a distance of 5 cm from the pump spot on the sample, so the collection angle is 4 mrad (smaller than a speckle spot). The directions of incident pump light and detection make an angle of $\approx 30^\circ$. The fluorescence is analyzed using an Oriel MS-257 0.25 m, f/4 single grating spectrometer, using a 2400 lines/mm grating, and detected with a Princeton Instruments Intensified CCD camera. The instrument resolution is 0.3 nm. The image intensifier on the camera amplifies not only the signal, but also the relative uncertainty in the signal: at the gain setting we use the error in a count c is $2\sqrt{c}$.

As shown in figure 5.6, narrow frequency structure is observed in the fluores-

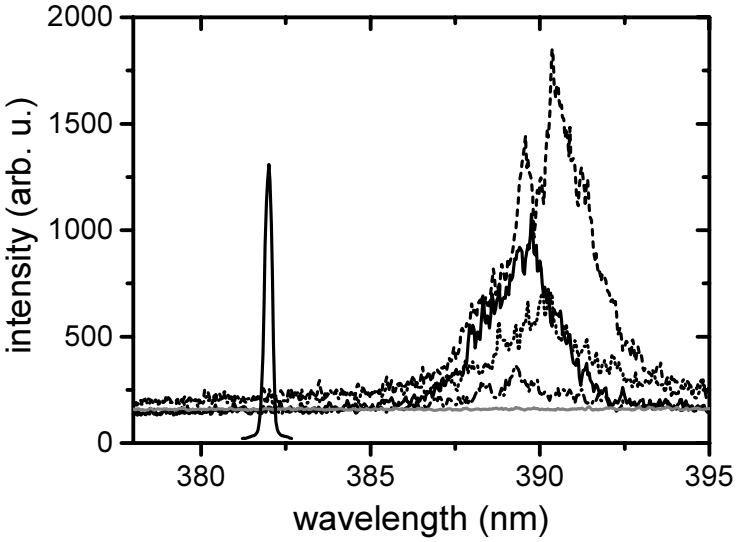

Figure 5.7 Fluorescence from ZnO-N. The pulse energy is (a very high) 0.58 mJ, different spectra are taken from different locations on the sample. Again, the gray curve is the camera dark count level. The instrument function is also shown. The broad fluorescence background is not observed (see figure 5.6), but the variability of the luminescence yield precluded a systematic study in this sample. The rep. rate is 1 Hz.

cent emission of ZnO powder upon excitation with a UV pulse. It appears only for pump intensities higher than a certain threshold, low pump intensities only give the broad spontaneous emission spectrum. The peaks are not as pronounced as those of Cao and coworkers [52, 107], which we attribute to limitations in the resolution and detection efficiency of our setup. Our pump intensities (in W/m^2) are approximately 20 times higher than in ref. 52. The explanation for this strange discrepancy is given in figure 5.8 and the accompanying discussion.

For comparison the luminescence of the ZnO-N powder is shown in figure 5.7. This powder has the same scattering characteristics as ZnO-A, but differs in other material parameters. The threshold for narrow peaks is much larger here, and the spectra show more pronounced structure. The spectrum is redshifted by ≈ 3 nm with respect to the data shown in figure 5.6, possibly because the luminescence originates from an electron-hole plasma (EHP), formed at this high excitation pulse energy. At lower pump energies no reliable signal could be obtained, so a systematic study of the peaks on power dependence could not be done in this sample.

Both series of data (figures 5.6 and 5.7) were measured with low pulse repetition rates of 2 and 1 Hz. Changing the pulse rate f_p to higher values turns out to have a profound effect on the emission spectrum, see figure 5.8. It displays two spectra,

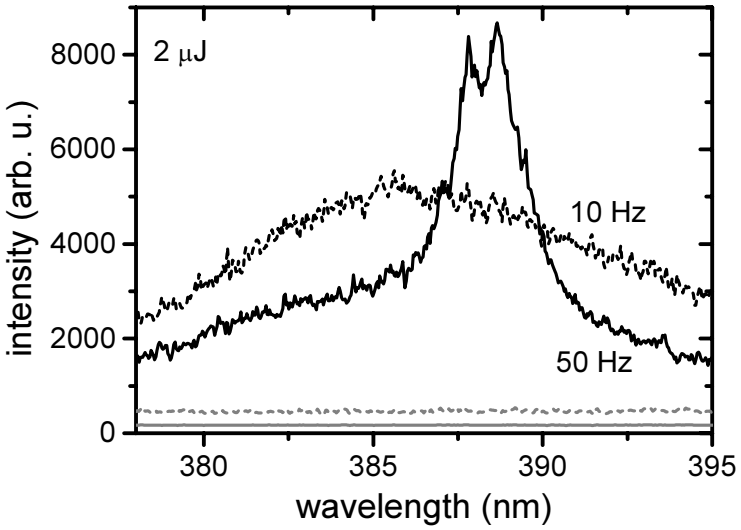

Figure 5.8 Effect of the pulse repetition rate f_p on the ZnO emission. At a pulse energy of 2 μJ, vastly different spectra are produced with $f_p = 10$ Hz (broken line) and $f_p = 50$ Hz (solid line). The number of spectra averaged in each curve is 50, all spectra (10 Hz and 50 Hz) are taken on the same location of the sample. Individual spectra at 50 Hz show the narrow peaks, averaging out to some degree in the accumulated data, although at this pump energy the count rates are too low to make out fine details. The camera dark counts for both exposure times are shown as broken (5 s) and solid (1 s) gray lines.

consisting of multiple shots, one taken at $f_p = 10$ Hz, the other at $f_p = 50$ Hz, with the same pulse energy (2 μJ), at the same location on the sample, accumulating the same number of shots. The low f_p spectrum is basically the spontaneous emission spectrum of ZnO, while the high f_p spectrum has a narrowed intensity distribution, with narrow features in the single-shot spectra that partially average out in the sum of 50. The integrated intensity at $f_p = 50$ Hz is 16% lower than at $f_p = 10$ Hz.

The pump intensity is much lower than in figures 5.6 and 5.7, and now also a factor 2 smaller than in ref. 52. Cao *et al.* used $f_p = 10$ Hz. We find that the threshold for the narrowing and the onset of the frequency spikes decreases with increasing pulse rate. We currently do not have an explanation for this remarkable influence of the repetition rate on the emission spectrum. Speculations are postponed until the discussion in section 5.3.1.

A more elaborate study of the emission spectrum as a function of pump energy exposes the strong nonlinearity of the response of the luminescence to an excitation pulse. In figure 5.9 a series of spectra is shown, taken at 50 Hz, each containing the accumulated emission of 50 shots. This procedure again washes out finer details of the individual spectra, but it allows us to concentrate on the overall features.

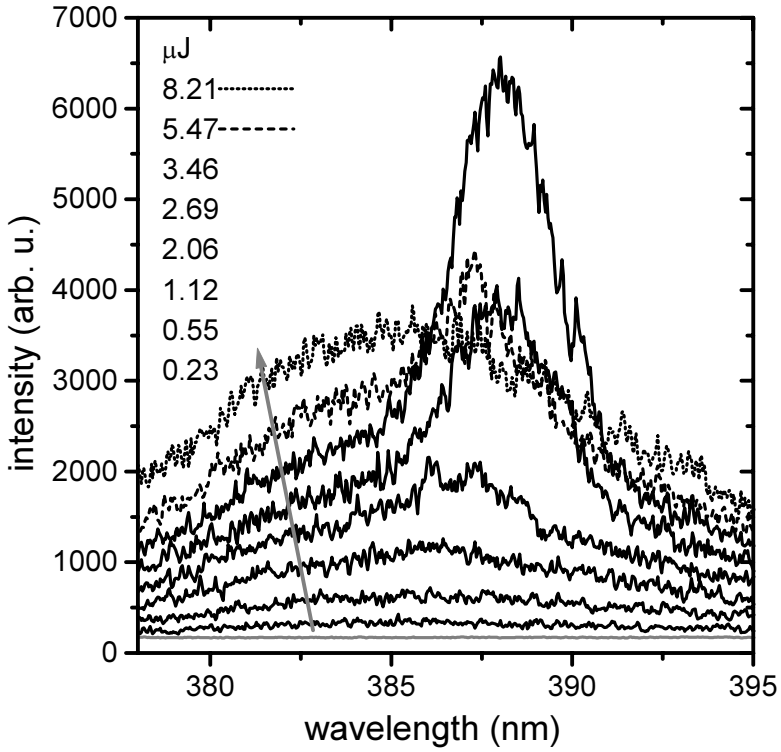

Figure 5.9 Peak intensity decrease, blueshift and rebroadening of ZnO fluorescence with increasing pump energy. $f_p = 50$ Hz, exposure 1 s. The averaging of many spectra washes out the details of the single-shot response. Pulse energies are indicated in the figure. The spectra obtained with the highest pump energies are shown as broken lines to avoid confusion where the lines cross.

At low pump intensities the system responds as expected: it emits a spectrum corresponding to the energy distribution of spontaneous emission. Increasing the excitation energy above 2 μJ narrows the spectrum, with frequency spikes visible in the individual spectra (the pulse energy at which the spectral narrowing occurs, differs from that in figure 5.8 because the location on the sample was changed). Above 3 μJ the peaks begin to merge, like in figure 5.6, but at 5 μJ the fluorescence starts to *decrease* in intensity, to shift to higher energies and to broaden, finally resulting in a blueshifted spontaneous-emission-like spectrum at 8 μJ.

The peak intensity decrease, blueshift and rebroadening of the fluorescence spectrum is not an effect of radiation damage. 8 μJ is still a low excitation energy compared to the pump energies of figure 5.6, which produced reliable and reproducible fluorescence for extended periods of time. Also, the effect seen in figure 5.9

dye	scatt.	$k\ell$	n (cm^{-3})	comment	shorthand
SRB	TiO_2	15	$1.8 \cdot 10^{13}$	good quality	ST
SRB	ZnO	70	$8.7 \cdot 10^{14}$	good quality	SZ
R640	TiO_2	–	–	inhomogeneous	RT
R640	ZnO	70	$8.7 \cdot 10^{14}$	low fluorescence	RZ

Table 5.1 Samples made for the investigation of the narrow peaks in scattering dye solutions. SRB is Sulforhodamine B, R640 is Rhodamine 640. Dyes are 5 mM solutions in spectroscopic methanol, scatterers are colloidal particles [44, 133]. Both powders are suspended in densities of 320 mg powder per ml dye solution. $k\ell$ is measured by EBS with $\lambda = 632.8$ nm, n is the scatterer density. The shorthand is used for reference in the text.

is insensitive to whether the series is measured with increasing or decreasing pump energy. At high pump energies, the spectrum does take some time to equilibrate. Suddenly switching on the pump at an energy of 8 μJ initially produces a narrowed spectrum, which subsequently relaxes, in about 2–3 s, into the spectrum shown as the dotted line in figure 5.9. A sudden decrease from 8 μJ back to ≈ 3 μJ only makes the peaks reappear after a similar amount of time. This slow response suggests a thermal origin.

5.2.2 Scattering dye solutions

The role of scattering in random lasing can be tested if the scattering and amplification are independent, e.g. in a dye solution with scatterers. To also test a possible material dependence of the narrow peaks in a dye-based random laser, we test different combinations of dye—5 mM Sulforhodamine B or Rhodamine 640 in methanol—and scatterers—320 mg/ml TiO_2 or ZnO-N colloid. We do not use ZnO-A because it is not suspended well in methanol. The samples are listed in table 5.1.

The high dye concentration is chosen to facilitate the comparison with the work by Cao *et al.* [53], although the results of chapter 3 indicate that the above-threshold gain does not increase substantially, but the reabsorption does. Also, the thickness of the amplifying layer decreases.

As a pump source we use a frequency-doubled Q-switched mode-locked Nd:YAG laser (Quantel YG-501 30), pulse duration < 40 ps, wavelength 532 nm, maximum pulse energy 0.7 mJ, pulse rate 10, 20 or 30 Hz. The pump beam is focused to a spot of ≈ 20 μm diameter (barely out of, or still in, the small-spot limit of figure 2.10, depending on the ℓ of the material). The detection setup is the same as in the ZnO experiments, see page 99. The fiber is positioned 1 cm from the sample.

The energy stability of the pump laser is poor: the relative standard deviation from the mean pulse energy is 30–35%. We do use this laser as excitation source,

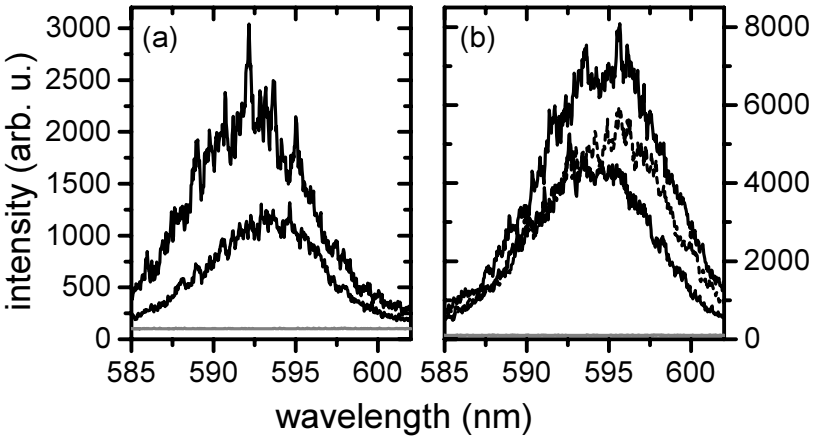

Figure 5.10 Single-shot fluorescence spectra from ST sample (see table 5.1). *(a)* Low to medium pump energies; medium $\approx$ 180 nJ. Increasing pump (signal) intensity is accompanied by the emergence of peaks in the spectrum. The gray line is the dark count level. *(b)* At high pump intensities (up to $\sim 7\ \mu$J), the peaks' relative intensity decreases. The middle spectrum is shown with a broken line for clarity.

because the use of picosecond excitation pulses turns out to be essential for the observation of the narrow peaks. With a nanosecond pump laser only the smooth spectra as shown in figure 2.1(a) are observed. With picosecond excitation, however, some of the spectra do show evidence of narrow frequency structure. Figure 5.10 contains an example, obtained with the ST sample.

As the pump energy increases from zero to $\approx$ 180 nJ, we see sharp peaks appearing on top of a broad (FWHM $\approx$ 9 nm) background of "normal" amplified fluorescence in figure 5.10. The peaks are not as pronounced as in the data in ref. 53, owing to a limited resolution. At higher pump energies the intensity in the peaks decreases with respect to the broad background: they either disappear or merge. The exact pump energies are unknown because of the pulse-to-pulse energy variation in the laser. We assume the usual correspondence between fluorescence intensity and pump pulse energy, in accord with the input-output power relation in a laser as measured in figure 2.2. The relatively large spectral width of the background (all measurements with an appreciable signal are above threshold) and the redshift compared to other fluorescence data of the same sample are consequences of the large dye concentration.

The large noise level makes it difficult to say whether the positions of the peaks are correlated between different spectra. This would be a sure sign of a material excitation. The positions are certainly not the same in the emission spectra of all shots, but a comparison of, for instance, the upper solid and broken lines of figure

5.10(b), does suggest that the peak positions are not completely random.

The spectra in figure 5.10 differ in the position of the center of the broad fluorescence band. It shifts randomly over a range of 2–3 nm. We did not observe this kind of shift with nanosecond excitation. The differences are possibly chemical in origin, stemming from an interaction of the dye with the surface of the scatterers [135]. Note that the TiO_2 particles are surface treated with an (insulating) alumina/silica layer. The scatterer surface is amorphous, hence many specific adsorption sites exist. A small shot-to-shot variation at the onset of the emission-amplification process could persist in the resulting measured spectrum due to the nonlinearity of the ASE process at high gain. Owing to the large intrinsic emission linewidth of the dye, such a process does not seem a likely candidate as an explanation for the narrow peaks.

Repeating this experiment with the SZ sample—same dye, different scatterer, larger ℓ—yields qualitatively the same outcome. Compared to the ST measurements, the emission spectrum is redshifted by 6 nm, the recorded intensities are a factor 1.5–2 lower at the same pump intensity, and the number of peaks is smaller. The lower intensity is a consequence of the higher threshold in this sample, caused by a larger ℓ. An interaction of the dye with the ZnO surface is readily apparent as the sample is prepared: upon addition of the scatterers the dye solution changes color from bright red/pink to deep purple. No change of color is observed if the coated TiO_2 scatterers are used. This interaction of the dye with the scatterer surface could influence the emission spectrum.

The scatterers in the RT sample aggregate, and even after ultrasonic shaking the suspension remains inhomogeneous. The RZ sample is identical to the material used by Cao *et al.* [53]. We find that it luminesces weakly, and does not produce any convincing peaks at pump energies up to 50 μJ; above this energy the pump pulse damages the glass of the sample container. We do not have an explanation for the discrepancy between our measurements and those of ref. 53. The stability of the suspension is markedly worse than the ST and SZ samples.

The pump pulse repetition rate profoundly influenced the ZnO emission. A variation from 10 to 30 Hz is, however, found to have no effect on the appearance of the spikes in the dye-based ST and SZ samples.

5.3 Discussion and conclusions

In the previous section we have presented measurements, augmenting the data from the literature reviewed in section 5.1. Here we discuss how the additional experiments fit in or modify the picture sketched in earlier publications. We do not try to answer the question whether or not the narrow peaks in ZnO are related to lasing; in ref. 108 they were shown to be. The issue we address is the role of multiple

scattering in the laser process.

First, we remark that all samples studied, by us and by others, are far from localization: the smallest values for $k\ell$ are achieved in the ZnO powder samples [131] and the dye samples with TiO_2 scatterers, $k\ell \approx 14$. Considering that materials with $k\ell$ =3–4 still show predominantly diffusive behavior [26, 27], it is hasty to attribute any observation in less strongly scattering materials to localization. Even if the handwavingly substantiated hunch that gain facilitates localization (see page 91) turns out to be legitimate, the gap from $k\ell \geq 14$ to the transition is huge, and observable effects are at best improbable.

5.3.1 ZnO powders

The two ZnO powder samples react very differently to UV excitation, while their $k\ell$ values are the same. ZnO-N only emits at high pump energy with an EHP-like spectrum. ZnO-A shows many narrow peaks in the exciton luminescence band.

In ZnO-A, we observed a surprisingly strong dependence of the emission spectrum on the pump pulse repetition rate (figure 5.8) and an extreme nonlinearity as a function of pump pulse energy (figure 5.9). Both phenomena are reversible, and both respond slowly, with a time constant of 2–3 s. The only likely candidate to produce such a slow response is a thermal process. The absorbed pump energy is partly converted into heat, producing a local temperature increase. This effect should be more pronounced in a powder than in any other phase, on account of the poor thermal conductivity of an inhomogeneous structure.

Underlying process? What the elevated temperature might effectuate is a matter of speculation, which we will pursue only briefly. Narrow sub-gap peaks in photoluminescence spectra have been observed in disordered or alloy II–VI semiconductors [136], and even lasing has been reported [137]. The intensity in the peaks shows the characteristic laser-like nonlinearity as a function of pump power. These narrow spectral features have been attributed to complex states consisting of an exciton bound to a localized defect. The peaks are observed only up to a maximum temperature, depending on the material, above which the exciton dissociates thermally from the defect and the emission disappears.

The stability of excitons in II–VI semiconductors under lasing conditions, however, is disputed [138]. Exciton absorption is seen to bleach above the laser threshold in quantum well lasers [139, 140]. Electron-hole recombination across the energy gap, that is renomalized due to the Coulomb interaction, produces gain and luminescence at the exciton energy, without an actual exciton population [141]. At room temperature, excitons are shown to be *always* unstable in these materials, owing

to the large coupling to other (continuum) states. On the other hand, the theory is done for materials with a perfect crystal lattice, so defect-related excitations can not be reproduced. Localized (bound) excitons have a much smaller coupling to other states, with dephasing times up to 4 orders of magnitude larger than extended (free) excitons [118].

Our experiments do not contain sufficient detail to decide whether the emission we see is excitonic or free carrier recombination across a renormalized energy gap, nor is this our prime interest. We do see a nonlinearity with a thermal-like time response. Temperature-dependent excitations may seem peculiar in semiconductors at room temperature, since most features are only observed at low temperatures. Two energy scales in ZnO are larger than the thermal energy $k_{\mathrm{B}}T = 25$ meV: the bulk exciton binding energy $E_{\mathrm{b}} = 60$ meV, and the Urbach tailing parameter $E_{\mathrm{U}} = 40$ meV [142], describing the exponential decay of the electronic density of states at the band edge due to defect states.

We propose that the pumping of the sample populates luminescent levels, and that this process is facilitated by the heating of the powder by the pump absorption, enhancing the luminescence at high rep. rates, cf. figure 5.8. The narrow linewidths observed suggest a role for localized defect states. An increase of the pulse energy or rep. rate raises the temperature further, thermally dissociating the luminescent state, which we assume consists of one or more charge carriers bound to a lattice defect. Consequently, the emission vanishes.

Stimulated emission from a compound defect state is possible by the narrow linewidth and concomitant large gain. ref. 108 shows the light to be coherent, so a resonant (amplitude) feedback mechanism is present. At these high gain levels, however, even a weak external reflection can be sufficient to provoke lasing.

An example of defect-exciton complex luminescence is donor-acceptor pair (DAP) emission. In this process an electron on a donor recombines with a hole on an acceptor nearby [109, 143]. The result is a regular series of peaks at fixed positions due to the $1/r$ Coulomb energy term contributing to the emitted photon energy, with $\mathbf{r}$ on the lattice. This regularity could not be established by an inventory of literature data or our own. On the other hand, a signature of DAP emission is a blueshift with increasing pump energy, as clearly observed in figure 5.9. ■

Above, we have presented a speculative proposal for an origin of the narrow peaks in ZnO powders. The optics of highly excited semiconductors is a rich and complex field of research [144], and especially the nature of the gain mechanism in II–VI materials is a matter of debate, that we do not aspire to settle here. To summarize, we remark that we did not find evidence for a crucial role for multiple scattering in the occurrence of the narrow peaks in ZnO powder luminescence, and that our

results suggest a thermally activated mechanism with a strongly nonlinear response. Which semiconductor electronic process produces these spectral features, and has a compatible temperature or intensity dependence, remains speculative. Similar peaks have been seen in homogeneous alloy semiconductors.

5.3.2 Dye suspensions

The results of the experiments on dyes with scatterers are not as conclusive, or suggestive, as those on ZnO, partially on account of the lesser data quality. Based on the observations presented in section 5.2.2, the most straightforward conclusion is that the narrow peaks in this system *are* caused by scattering. The most strongly scattering (ST; cf. table 5.1) sample shows the strongest peaks, the scatterers in which happen to have a surface coating, reducing the interaction of the surface electronic structure with the dye. We tried to test the influence of the material more stringently by increasing the scatterer concentration in the SZ sample but found that a denser ZnO suspension is unstable and the colloid aggregates.

On closer inspection of the data in section 5.2.2, and comparing with the article by Cao and coworkers [53], two issues arise:

- The peaks are only observed with a picosecond excitation pulse, only the normal narrowed spectrum appears with a nanosecond pump.
- The RZ sample on which the published experiments by Cao *et al.* were performed showed no peaks in our experiments, and low luminescence. Even though its $k\ell$ is large, the absence of a convincing signal up to these high pump energies is surprising. On the other hand, the SZ sample does show peaks, but has the same $k\ell$ (from EBS) as a sample where Cao *et al.* did not observe any. The difference is the dye, the turbidity is the same.

The latter point only seems to indicate, if anything, a very sensitive dependence of the narrow-peak appearance on material and preparation. The former is an observation that needs to be explained if the phenomenon is to be given a theoretical backing in multiple scattering. If multiple scattering is to be responsible for the narrow peaks, we must find a process causing the peaks, that happens on a time scale $\gtrsim 50$ ps, because the peaks do not average out with this excitation pulse length, but $\lesssim 500$ ps, because there is no trace of the peaks with a nanosecond pump pulse.

In a nanosecond, a scattering medium is essentially static: particle motion in a colloidal suspension has a typical time scale of milliseconds. There are two processes in a diffusive random laser with time constants of the correct order. The longest detectable paths in a multiply scattering liquid medium dephase at a rate in the GHz range; these dynamics are used in DWS. Constructive interference between

long paths is a particular speckle, which is not sufficiently wavelength specific. Another process at a 10–100 ps time scale is the relaxation oscillation. This is not spectrally selective either.

Material-related processes with subnanosecond dynamics exist in great variety in a system of dye on an oxide surface. It is not always clear whether these are accompanied by narrow spectral features. Dye-like excitations have a large intrinsic linewidth, maybe a combination with the surface electronic structure of the scatterer can give rise to narrow features. Our experiments are not sufficient to decide whether a particular type of excitations causes the sharp peaks.

5.3.3 Conclusions

We find a striking difference in luminescence properties of the two ZnO powders, differing in method of synthesis, particle size distribution, and surface properties, but not in purity or scattering characteristics. The light transport is undoubtedly diffusive at $k\ell \approx 14$.

Furthermore, we measure a strong nonlinearity with a thermal-like time response in the fluorescent emission of ZnO powders. These observations lead us to an interpretation of the narrow peaks in terms of material excitations, rather than one based on the random laser concept. The explanation is compatible with, and even supported by [109, 117] the data on these samples in the literature, and could be applied to ZnO thin films. However, for the occurrence of narrow peaks in thin films there is another, more elegant candidate, that is supported by direct experimental evidence [126]: the formation of Fabry-Pérot cavities by grain boundaries between pumped and unpumped material, proposed in section 5.1.3. The only data that lack a consistent interpretation are those on scattering dye suspensions. Our findings partially contradict the results in the literature.

Superfluous as it may seem, there could be three different mechanisms at work, producing very similar-looking narrow peaks in different materials. One can also resort to the semi-skeptical statement that it must be some electronic excitation in all cases, the nature of which can be speculated on in ZnO, and is left unspecified in the dye materials. We opt for two processes: the cavities in the transparent films and an electronic excitation in the multiply scattering materials. The latter explanation is adopted for the dye suspensions only because the alternatives must be discarded; for the ZnO powders it is quite firmly supported by experimental data.

A. Properties of Sulforhodamine B and Coumarin 6

In the work described in this thesis two laser dyes were mainly used: Sulforhodamine B (synonym: Kiton Red S) for the experiments in chapter 2 and sections 4.3 and 5.2.2 and the theory in chapter 3; Coumarin 6 (synonym: Coumarin 540) for the speckle experiments of section 4.2. Table A.1 lists the most important dye properties and experimental parameters.

The absorption and emission cross sections of Sulforhodamine B were obtained by measurement of the absorbance $\varepsilon_a(\lambda)$ ($\sigma_a = \ln(10) \cdot \varepsilon_a / n_0$) of a 4 μM solution, and the fluorescence spectrum $L(\lambda)$ ($\sigma_e(\lambda) = \frac{\lambda^4 L(\lambda)}{8\pi c \tau \eta^2}$, with the normalization

Quantity		SRB	C6	Ref.
pump wavelength	λ_p (nm)	532	482	
solvent		MeOH	HG	
solvent ref. ind.	η	1.329	1.425	
emission max.	λ_ℓ (nm)	590 ± 5	527 ± 2	exp.
natural lifetime	τ (ns)	3.2 ± 0.1		exp.
quantum efficiency	*QE*	0.8	0.85	43, 145, 146
Cross sections (in 10^{-20} m^2*):*				
pump absorption	$\sigma_a(\lambda_p)$	1.6 ± 0.1	2.1	exp., 146
stim. emission	$\sigma_e(\lambda_\ell)$	4.0 ± 0.4		exp.
reabsorption	$\sigma_a(\lambda_\ell)$	0.073 ± 0.01		exp.

Table A.1 Parameters of Sulforhodamine B (SRB) and Coumarin 6 (C6). MeOH = methanol; HG = hexylene glycol (2-methyl-2,4-pentanediol). The last column lists the reference to the data; exp. means experimentally determined by us. Fluorescence maxima are those as measured in a strongly scattering solution ($\ell \sim 10$ μm) with a pulsed excitation source.

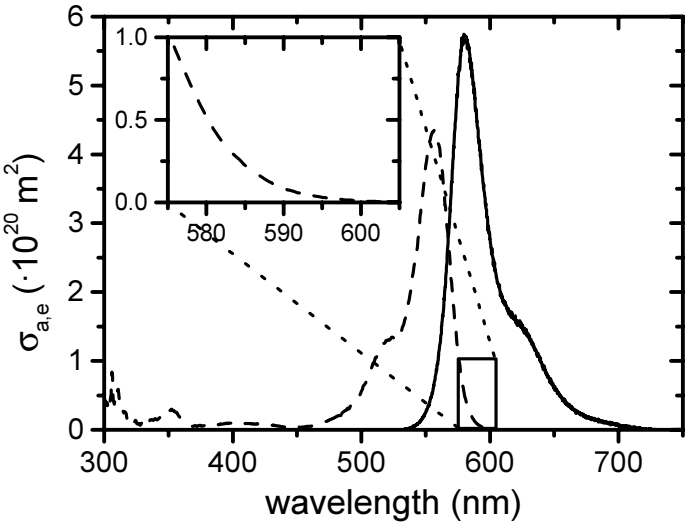

Figure A.1 Absorption (dashed) and emission (solid) cross sections of Sulforhodamine B. The inset shows the non-zero absorption cross section near the laser wavelength $\lambda_\ell = 590$ nm.

$\int L(\lambda)\mathrm{d}\lambda = QE$, and η the refractive index [64]). Absorption is measured by broadband transmission of a pulsed flashlamp, fluorescence with the 514.5 nm line from an Ar^+ laser.

B. Pump units and terminology

In experiments related to the laser threshold, it is important to correctly quantify the pump energy supply. The most basic mechanism involved in introducing and maintaining gain in the laser is the transfer of population from the ground state to the excited state. Laser rate equations usually incorporate a term that describes this process as the pump *rate*: number of dye molecules excited per second. The number of excited dye molecules is proportional to the amount of supplied energy and to N_0, the number of available molecules in the ground state. Power (P), the rate of energy supply, is the crucial quantity.

We use optical pumping, so the energy is supplied by photons. The number of excited molecules is equal to the number of absorbed photons, and probability of an incident photon being absorbed is given by the absorption cross section, which is an area, relative to the total area A of the exciting beam. Apparently, we have to consider the flux density F of photons, number per unit time per unit area. Then the pump rate becomes $r = F \cdot N_0 \cdot \sigma_a$. F is related to the intensity I by $I = F \cdot \hbar\omega_p = P/A$. For homogeneous optical pumping, the intensity (in $\mathrm{W} \cdot \mathrm{m}^{-2}$) is the most straightforward quantity to use.

In an inhomogeneous system like ours there is a catch: we have to consider the energy supply to a small volume around each point because quantities vary locally. This is most easily done by working in terms of volume densities, i.e. number of dye molecules and amount of pump energy per unit volume. Writing the pump energy density as $W_p = I \cdot c/\hbar\omega_p$, we arrive at a pump rate density $R_d = W_p \cdot c \cdot \sigma_a \cdot n_0$, where c is the propagation speed of light in the medium and n_0 is the density of dye molecules in the ground state. R_d is the number of dye molecules per unit volume excited per unit time ($\mathrm{m}^{-3}\mathrm{s}^{-1}$).

This pump rate density depends on the pump light density, resulting from the incident beam, which is measured in our pulsed experiments in units of fluence,

$J \cdot m^{-2}$. The connection between these two quantities, flux density in a plane wave and light density in a diffusing field is a well-studied problem, see ref. 15. Incident light is usually introduced by placing a diffuse source at a distance of one mean free path from the surface, or like in our calculations, by using an exponentially decaying source intensity [147]. The source has to be properly normalized to make quantitative comparison with experiments possible. The local and instantaneous light density is a solution of the diffusion equation, see chapter 3.

R. References

[1] M. Born and E. Wolf, *Principles of Optics*, 6th ed., Pergamon, Oxford (1980), sect. 2.3.4.

[2] J. D. Jackson, *Classical Electrodynamics*, 2nd ed., John Wiley & Sons, New York (1975), sect. 4.3–5, and 6.7.

[3] R. Loudon, *The Quantum Theory of Light*, 2nd ed., Oxford University Press, Oxford (1983), sect. 8.2, 8.6 and 8.7.

[4] D. P. Craig and T. Thirunamachandran, *Molecular Quantum Electrodynamics*, Academic Press, London (1984), p. 131.

[5] J. D. Jackson, *op. cit.* [2], pp. 418–422.

[6] A. Lagendijk and B. A. van Tiggelen, *Resonant multiple scattering of light*, Phys. Rep. **270**, 143–216, sect. 2.

[7] C. F. Bohren and D. R. Huffman, *Absorption and Scattering of Light by Small Particles*, John Wiley & Sons, New York (1983), pp. 130–132.

[8] Lord Rayleigh, *On the Light from the Sky, its Polarization and Colour*, Philos. Mag. **41**, 107–120, 274–279 (quoted in ref. 7); *On the Scattering of Light by Small Particles*, *ibid.*, pp. 447–454.

[9] H. C. van de Hulst, *Light Scattering by Small Particles*, Dover Publishing, New York (1981), p. 114.

[10] R. P. Feynman, R. B. Leighton, and M. Sands, *The Feynman Lectures on Physics*, Addison-Wesley, Reading (1963), vol. 1, sect. 32-5.

[11] C. F. Bohren and D. R. Huffman, *op. cit.* [7], chapter 4. The book also gives a Fortran program to calculate scattering and absorption cross sections, scattering angles, etc.

[12] H. C. van de Hulst, *op. cit.* [9], sect. 13.2.

[13] V. Sandoghar, F. Treussart, J. Hare, V. Lefèvre-Seguin, J. M. Raimond, and S. Haroche, *Very low threshold whispering-gallery-mode microsphere laser*, Phys. Rev. A **54**, R1777–R1780 (1996).

[14] M. Born and E. Wolf, *op. cit.* [1], sect. 13.1 and 13.2.

[15] A. Ishimaru, *Wave Propagation and Scattering in Random Media*, Academic Press, New York, 1978, pp. 175–183.

[16] B. A. van Tiggelen and A. Lagendijk, *Analogies between light and electrons?* and *Coherent beam, diffuse beam and speckles: the old view*, sect. 1.1 and 1.2, in: POAN Research Group (Ed.), *New Aspects of Electromagnetic and Acoustic Wave Diffusion*, Springer Tracts in Modern Physics, vol. 144, Springer, Berlin (1998).

[17] M. P. van Albada, B. A. van Tiggelen, A. Lagendijk, and A. Tip, *Speed of propaga-*

tion of classical waves in strongly scattering media, Phys. Rev. Lett. **66**, 3132–3135 (1991). This paper shows how to calculate the actual energy velocity v_E. For our type of materials the departure from the phase velocity c_0/η is negligible.

[18] A. Z. Genack, *Optical transmission in disordered media*, Phys. Rev. Lett. **58**, 2043–2046 (1987).

[19] N. Garcia, A. Z. Genack, and A. A. Lisyanski, *Measurement of the transport mean free path of diffusing photons*, Phys. Rev. B **46**, 14475–14479 (1992).

[20] A. Lagendijk, R. Vreeker, and P. de Vries, *Influence of internal reflection on diffusive transport in strongly scattering media*, Phys. Lett. A **136**, 81–87 (1989).

[21] J. X. Zhu, D. J. Pine, and D. A. Weitz, *Internal reflection of diffusive light in random media*, Phys. Rev. A **44**, 3948–3959 (1991).

[22] M. B. van der Mark, *Propagation of light in disordered media: a search for Anderson localization*, Ph. D. thesis, Universiteit van Amsterdam (1990), p. 26. Available on the web [150].

[23] P. W. Anderson, *Absence of diffusion in certain random lattices*, Phys. Rev. **109**, 1492–1505 (1958).

[24] P. W. Anderson, *The question of classical localization: a theory of white paint?*, Philos. Mag. B **52**, 505–509 (1985).

[25] See, e.g., D. S. Wiersma, P. Bartolini, A. Lagendijk, and R. Righini, *Localization of light in a disordered medium*, Nature **390**, 671–673 (1997); A. A. Chabanov, M. Stoytchev, and A. Z. Genack, *Statistical signatures of photon localization*, Nature **404**, 850–853 (2000).

[26] J. Gómez Rivas, R. Sprik, A. Lagendijk, L. D. Noordam, and C. W. Rella, *Mid-infrared scattering and absorption in Ge powder close to the Anderson localization transition*, Phys. Rev. E **62**, R4540–R4543 (2000); *Static and dynamic transport of light close to the Anderson localization transition*, *ibid.* **63**, 046613 (2001).

[27] F. J. P. Schuurmans, M. Megens, D. Vanmaekelbergh, and A. Lagendijk, *Light scattering near the localization transition in macroporous GaP networks*, Phys. Rev. Lett. **83**, 2183–2186 (1999).

[28] E. Yablonovitch, Phys. Rev. Lett. **58**, 2059–2062 (1987).

[29] M. S. Thijssen *et al.*, *Inhibited light propagation and broad band reflection in photonic air-sphere crystals*, Phys. Rev. Lett. **83**, 2730–2733 (1999); A. Blanco *et al.*, *Large-scale synthesis of a silicon photonic crystal with a complete three-dimensional bandgap near 1.5 micrometers*, Nature **405**, 437–440 (2000); H. P. Schriemer, H. M. van Driel, A. F. Koenderink, and W. L. Vos, *Modified spontaneous emission spectra of laser dye in inverse opal photonic crystals*, Phys. Rev. A, 011801(R) (2001).

[30] F. P. Schäfer, *Principles of dye laser operation*, sect. 1.3, in: F. P. Schäfer (Ed.), *Dye Lasers*, 2nd ed., Topics in Applied Physics, vol. 1, Springer, New York (1977).

[31] W. E. Lamb, W. P. Schleich, M. O. Scully, and C. H. Townes, *Laser physics: Quantum controversy in action*, Rev. Mod. Phys. **71**, S263–S273 (1999).

[32] A. E. Siegman, *Lasers*, University Science Books, Mill Valley (1986), sect. 13.3 and 13.4.

[33] C. C. Davis, *Lasers and Electro-Optics: Fundamentals and Engineering*, Cambridge University Press, Cambridge (1996), pp. 171–173.

[34] Y. Yamamoto and R. E. Slusher, *Optical processes in microcavities*, Phys. Today **46** (6), 66–73 (1993).
[35] Y. Yamamoto, S. Machida, and G. Björk, *Microcavity laser with enhanced spontaneous emission*, Phys. Rev. A **44**, 657–668 (1991).
[36] P. W. Milonni and J. H. Eberly, *Lasers*, John Wiley & Sons, New York (1988), sect. 10.5.
[37] O. Svelto, *Principles of Lasers*, 2nd ed., Plenum, New York (1982), eq. (2.83).
[38] A. E. Siegman, *op. cit.* [32], sect. 13.8.
[39] L. W. Casperson, *Threshold characteristics of mirrorless lasers*, J. Appl. Phys. **48**, 256–262 (1977).
[40] W. T. Silfvast, *Laser fundamentals*, Cambridge University Press, Cambridge (1996), pp. 212–213 and figure 7-9.
[41] M. D. Rosen *et al.*, *Exploding foil technique for achieving a soft x-ray laser*, Phys. Rev. Lett. **54**, 106–109 (1985); D. L. Matthews *et al.*, *Demonstration of a soft x-ray amplifier*, Phys. Rev. Lett. **54**, 110–113 (1985).
[42] K. H. Drexhage, *Structure and properties of laser dyes*, pp. 145–152, in: F. P. Schäfer (Ed.), *op. cit.* [30].
[43] J. M. Drake, R. I. Morse, R. N. Steppel and D. Young, *Kiton Red S and Rhodamine B. The spectroscopy and laser performance of red laser dyes*, Chem. Phys. Lett. **35**, 181–188 (1975).
[44] Sachtleben Chemie GmbH, Hombitan RCL 66 Titandioxid, 89+% TiO_2-rutile, surface coated with alumina/silica, average particle size 220 nm.
[45] D. S. Wiersma, *Light in strongly scattering and amplifying media*, Ph. D. thesis, Universiteit van Amsterdam (1995), p. 79 and table 5.1. Available on the web [150].
[46] G. van Soest, M. Tomita, and A. Lagendijk, *Amplifying volume in scattering media*, Opt. Lett. **24**, 306–308 (1999).
[47] K. Totsuka, G. van Soest, T. Ito, A. Lagendijk, and M. Tomita, *Amplification and diffusion of spontaneous emission in strongly scattering medium*, J. Appl. Phys. **87**, 7623–7628 (2000).
[48] V. S. Letokhov, *Generation of light by a scattering medium with negative resonance absorption*, Sov. Phys. JETP **26**, 835–840 (1968).
[49] G. van Soest, F. J. Poelwijk, R. Sprik, and A. Lagendijk, *Dynamics of a random laser above threshold*, Phys. Rev. Lett. **86**, 1522–1525 (2001).
[50] Cavity lasers in which the modes are mixed more carefully were built by tuning the feedback off resonance or making one mirror scattering, see e.g. R. V. Ambartsumyan, N. G. Basov, P. G. Kryukov, and V. S. Letokhov, *Non-resonant feedback in lasers*, Progr. Quantum Electr. **1**, 109–185 (1970); P. C. de Oliveira, J. A. McGreevy, and N. M. Lawandy, *Speckle-mirror laser*, Opt. Lett **22**, 700–702 (1997).
[51] J. P. Woerdman, J. Dingjan, and M. P. van Exter, *Cavity approach towards a coherent random laser*, pp. 435–446, in: C. M. Soukoulis (Ed.), *Photonic crystals and light localization in the 21st century*, NATO Science Series C, vol. 563, Kluwer, Dordrecht (2001).
[52] H. Cao, Y. G. Zhao, S. T. Ho, E. W. Seelig, Q. H. Wang, and R. P. H. Chang, *Random laser action in semiconductor powder*, Phys. Rev. Lett. **82**, 2278–2281 (1999).

[53] H. Cao, J. Y. Xu, S.-H. Chang, and S. T. Ho, *Transition from amplified spontaneous emission to laser action in strongly scattering media*, Phys. Rev. E **61**, 1985–1989 (2000).
[54] W. T. Silfvast, *op. cit.* [40], p. 217.
[55] C. C. Davis, *op. cit.* [33], p. 1.
[56] N. M. Lawandy, R. M. Balachandran, A. S. L. Gomes, and E. Sauvain, *Laser action in strongly scattering media*, Nature **368**, 436–438 (1994).
[57] M. A. Noginov, H. J. Caufield, N. E. Noginova, and P. Venkateswarlu, *Line narrowing in the dye solution with scattering centers*, Opt. Comm. **118**, 430–437 (1995).
[58] M. Siddique, R. R. Alfano, G. A. Berger, M. Kempe, and A. Z. Genack, *Time-resolved studies of stimulated emission from colloidal dye solutions*, Opt. Lett. **21**, 450–452 (1996).
[59] F. J. Poelwijk, *Interference in Random Lasers*, Master's thesis, Universiteit van Amsterdam (2000), pp. 15–19. Available on the web [150].
[60] G. A. Berger, M. Kempe, and A. Z. Genack, *Dynamics of stimulated emisson from random media*, Phys. Rev. E **56**, 6118–6122 (1997).
[61] D. S. Wiersma, M. P. van Albada, and A. Lagendijk, *Random laser?*, Nature **373**, 203–204 (1995).
[62] R. M. Balachandran, N. M. Lawandy, and J. A. Moon, *Theory of laser action in scattering gain media*, Opt. Lett. **22**, 319–321 (1997).
[63] C. C. Davis, *op. cit.* [33], sect. 12.3.
[64] B. B. Snavely, *Continuous-Wave Dye Lasers*, sect. 2.1.1, in: F. P. Schäfer (Ed.), *op. cit.* [30].
[65] C. W. J. Beenakker, J. C. J. Paasschens, and P. W. Brouwer, *Probability of reflection by a random laser*, Phys. Rev. Lett. **76**, 1368–1371 (1996).
[66] A. A. Burkov and A. Yu. Zyuzin, *Correlations in transmission of light through a disordered amplifying medium*, Phys. Rev. B, **55**, 5736–5741 (1997).
[67] P. Pradhan and N. Kumar, *Localization of light in coherently amplifying random media*, Phys. Rev. B **50**, 9644–9647 (1994).
[68] X. Jiang and C. M. Soukoulis, *Transmission and reflection studies of periodic and random systems with gain*, Phys. Rev. B **59**, 6159–6166 (1999).
[69] M. Patra and C. W. J. Beenakker, *Excess noise for coherent radiation propagating through amplifying random media*, Phys. Rev. A **60**, 4059–4066 (1999).
[70] A. Yu. Zyuzin, *Weak localization in backscattering from an amplifying medium*, Europhys. Lett. **26**, 517–520 (1994).
[71] D. S. Wiersma and A. Lagendijk, *Light diffusion with gain and random lasers*, Phys. Rev. E **54**, 4256–4265 (1996).
[72] M. P. van Exter, G. Nienhuis, and J. P. Woerdman, *Two simple expressions for the spontaneous emission factor* β, Phys. Rev. A **54**, 3553–3558 (1996).
[73] A. E. Siegman, *op. cit.* [32], pp. 502–504, especially eq. (32).
[74] A. E. Siegman, *op. cit.* [32], pp. 958–964.
[75] B. van der Pol, *On "relaxation oscillations"*, Philos. Mag. **2**, 978–992 (1926).
[76] M. Abramowitz and I. A. Stegun, *Handbook of mathematical functions*, Dover Publishing, New York (1965), 25.3.23 on p. 884.

[77] K. E. Atkinson, *An introduction to numerical analysis*, 2nd ed., John Wiley & Sons, New York (1989), sect. 6.9.
[78] W. H. Press, S. A. Teukolsky, W. T. Vetterling, and B. P. Flannery, *Numerical recipes in FORTRAN: the art of scientific computing*, 2nd ed., Cambridge University Press (1992), p. 727.
[79] IMSL routine DMOLCH, IMSL Math/Library Users Manual (IMSL Inc., 2500 City-West Boulevard, Houston TX77042).
[80] A. E. Siegman, *op. cit.* [32], fig. 12.5.
[81] W. L. Sha, C.-H. Liu, F. Liu, and R. R. Alfano, *Competition between two lasing modes of Sulforhodamine 640 in highly scattering media*, Opt. Lett. **21**, 1277–1279 (1996).
[82] R. M. Balachandran, A. E. Perkins, and N. M. Lawandy, *Injection locking of photonic paint*, Opt. Lett. **21**, 650–652 (1996).
[83] D. S. Wiersma, M. P. van Albada, and A. Lagendijk, *Coherent backscattering of light from amplifying random media*, Phys. Rev. Lett. **75**, 1739–1742 (1995).
[84] A. Yu. Zyuzin, *Interference intensification of wave scattering by an amplifying disordered medium*, JETP Lett. **61**, 990–992 (1995).
[85] R. M. Balachandran and N. M. Lawandy, *Understanding bichromatic emission from scattering gain media*, Opt. Lett. **21**, 1603–1605 (1996).
[86] S. John and G. Pang, *Theory of lasing in a multiple scattering medium*, Phys. Rev. A **54**, 3642–3652 (1996).
[87] X. Jiang and C. M. Soukoulis, *Time dependent theory for random lasers*, Phys. Rev. Lett. **85**, 70–73 (2000).
[88] E. Abrahams, P. W. Anderson, D. C. Licciardello, and T. V. Ramakrishnan, *Scaling theory of localization: absence of diffusion in two dimensions*, Phys. Rev. Lett. **42**, 673–676 (1979).
[89] A. Z. Genack, *Fluctuations, correlation and average transport of electromagnetic radiation in random media*, in: P. Sheng (Ed.), *Scattering and localization of classical waves in random media*, World Scientific Series on Directions in Condensed Matter Physics, vol. 8, World Scientific, Singapore (1990).
[90] J. W. Goodman, *Statistical properties of laser speckle patterns*, sect. 2.1, 2.2 (on intensity statistics) and 2.5 (on speckle spot size) in: J. C. Dainty (Ed.), *Laser speckle and related phenomena*, 2nd ed., Topics in Applied Physics, vol. 9, Springer, Berlin (1984).
[91] D. S. Wiersma and A. Lagendijk, *Interference effects in multiple light scattering with gain*, Physica A **241**, 82–88 (1997).
[92] C. Gouedard, D. Husson, C. Sauteret, F. Auzel, and A. Migus, *Generation of spatially incoherent short pulses in laser-pumped neodymium stoichiometric crystals and powders*, J. Opt. Soc. Am. B **10**, 2358–2363 (1993).
[93] M. A. Noginov, S. U. Egarievwe, N. Noginova, H. J. Caulfield, and J. C. Wang, *Interferometric studies of coherence in a powder laser*, Opt. Mat. **12**, 127–134 (1999).
[94] A. A. Burkov and A. Yu. Zyuzin, *Correlation function of speckle in reflection from photonic paint*, JETP Lett. **63**, 878–881 (1996).
[95] V. Freilikher, M. Pustilnik, and I. Yurkevich, *Statistical properties of the reflectance*

and transmittance of an amplifying random medium, Phys. Rev. B **56**, 5974–5977 (1997).

[96] A. Yu. Zyuzin, *Transmission fluctuations and spectral rigidity of lasing states in a random amplifying medium*, Phys. Rev. E **51**, 5274–5278 (1995).

[97] G. Parry, *Speckle patterns in partially coherent light*, sect. 3.1 and 3.2 in: J. C. Dainty (Ed.), *op. cit.* [90].

[98] J. F. de Boer, *Optical fluctuations on the transmission and reflection of mesoscopic systems*, Ph.D. thesis, Universiteit van Amsterdam (1995), sect. 3.3.2 and 3.4.2. Available on the web [150].

[99] K. M. Watson, *Multiple scattering of electromagnetic waves in an underdense plasma*, J. Math. Phys. **10**, 688–702 (1969); Y. Kuga and A. Ishimaru, *Retroreflection from a dense distribution of spherical particles*, J. Opt. Soc. Am. A **8**, 831–835 (1984); M. P. van Albada and A. Lagendijk, *Observation of weak localization of light in a random medium*, Phys. Rev. Lett. **55**, 2692–2695 (1985); P. E. Wolf and G. Maret, *Weak localization and coherent backscattering of photons in disordered media*, Phys. Rev. Lett. **55**, 2696–2699 (1985).

[100] P. C. de Oliveira, A. E. Perkins, and N. M. Lawandy, *Coherent backscattering from high-gain scattering media*, Opt. Lett. **21**, 1685–1687 (1996).

[101] W. Deng, D. S. Wiersma, and Z. Q. Zhang, *Coherent backscattering of light from random media with inhomogeneous gain coefficient*, Phys. Rev. B **56**, 178–181 (1997).

[102] A. Z. Genack and J. M. Drake, *Scattering for super-radiation*, Nature **368**, 400–401 (1994).

[103] D. J. Pine, D. A. Weitz, P. M. Chaikin, and E. Herbolzheimer, *Diffusing wave spectroscopy*, Phys. Rev. Lett. **60**, 1134–1137 (1988).

[104] M. B. van der Mark, *op. cit.* [22], pp. 56–57.

[105] H. Cao *et al.*, *Ultraviolet lasing in resonators formed by scattering in semiconductor polycrystalline films*, Appl. Phys. Lett. **73**, 3656–3658 (1998).

[106] H. Cao, J. Y. Xu, E. W. Seelig, and R. P. H. Chang, *Microlaser made of disordered media*, Appl. Phys. Lett. **76**, 2997–2999 (2000).

[107] H. Cao *et al.*, *Spatial confinement of light in active random media*, Phys. Rev. Lett. **84**, 5584–5587 (2000).

[108] H. Cao, Y. Ling, J. Y. Xu, C. Q. Cao, and P. Kumar, *Photon statistics of random lasers with resonant feedback*, Phys. Rev. Lett. **86**, 4524–4527 (2001).

[109] Y. Sun, J. B. Ketterson, and G. K. L. Wong, *Excitonic gain and stimulated ultraviolet emission in nanocrystalline zinc-oxide powder*, Appl. Phys. Lett. **77**, 2322–2324 (2000).

[110] A. Mitra and R. K. Thareja, *Photoluminescence and ultraviolet laser emission from nanocrystalline ZnO thin films*, J. Appl. Phys. **89**, 2025–2028 (2001).

[111] H. Cao, Y. G. Zhao, H. C. Ong, and R. P. H. Chang, *Far-field characteristics of random lasers*, Phys. Rev. B **59**, 15107–15111 (1999).

[112] H. Cao, Y. G. Zhao, X. Liu, E. W. Seelig, and R. P. H. Chang, *Effect of external feedback on lasing in random media*, Appl. Phys. Lett. **75**, 1213–1215 (1999).

[113] S. Cho, J. Ma, Y. Kim, Y. Sun, G. K. L. Wong, and J. B. Ketterson, *Photoluminescence and ultraviolet lasing of polycrystalline ZnO thin films prepared by the*

oxidation of the metallic Zn, Appl. Phys. Lett. **75**, 2761–2763 (1999).

[114] S. V. Frolov, Z. V. Vardeny, K. Yoshino, A. Zakhidov, and R. Baughman, *Stimulated emission in high-gain organic media*, Phys. Rev. B **59**, R5284–R5287 (1999).

[115] M. N. Shkunov, M. C. DeLong, M. E. Raikh, Z. V. Vardeny, A. A. Zakhidov, and R. H. Baughman, *Photonic versus random lasing in opal photonic single crystals*, Synth. Met. **116**, 485–491 (2001).

[116] D. S. Wiersma, M. P. van Albada, and A. Lagendijk, *Experimental evidence for recurrent multiple scattering of light in disordered media*, Phys. Rev. Lett. **74**, 4193–4196 (1995).

[117] H. J. Egelhaaf and D. Oelkrug, *Luminescence and nonradiative deactivation of excited states involving oxygen defect centers in polycrystalline ZnO*, J. Cryst. Growth **161**, 190–194 (1996).

[118] C. F. Klingshirn, *Linear and nonlinear optics of wide-gap II-VI semiconductors*, Phys. Stat. Sol. B **202**, 857–871 (1997).

[119] C. F. Klingshirn, *Semiconductor optics*, Springer, Berlin (1997), ch. 15 and 21.

[120] J. Gómez Rivas, R. Sprik, and A. Lagendijk, *Optical transmission through very strong scattering media*, Ann. Phys. (Leipzig) **8**, Spec. Issue, 77–80 (1999).

[121] For a review, see: P. V. Kamat, *Photochemistry on nonreactive and reactive (semiconductor) surfaces*, Chem. Rev. **93**, 267–300 (1993).

[122] M. Kaveh, *Localization of photons in disordered systems*, Philos. Mag. B **56**, 693–703 (1987).

[123] M. A. Lax, *Multiple scattering of waves*, Rev. Mod. Phys. **23**, 287–310 (1951).

[124] E. N. Economou and C. M. Soukoulis, *Connection of localization with the problem of the bound state in a potential well*, Phys. Rev. B **28**, 1093–1094 (1983); E. N. Economou, C. M. Soukoulis, and A. D. Zdetsis, *Localized states in disordered systems as bound states in potential wells*, Phys. Rev. B **30**, 1686–1694 (1984).

[125] R. Lang and K. Kobayashi, *External optical feedback effects on semiconductor injection laser properties*, IEEE J. Quantum El. **16**, 347–355 (1980).

[126] Z. K. Tang *et al.*, *Room-temperature ultraviolet laser emission from self-assembled ZnO microcrystallite thin films*, Appl. Phys. Lett. **72**, 3270–3273 (1998); M. Kawasaki *et al.*, *Excitonic ultraviolet laser emission at room temperature from naturally made cavity in ZnO nanocrystal thin films*, Mat. Sci. Eng. B **56**, 239–245 (1998).

[127] P. L. Washington, H. C. Ong, J. Y. Dai, and R. P. H. Chang, *Determination of the optical constants of zinc oxide thin films by spectroscopic ellipsometry*, Appl. Phys. Lett. **72**, 3261–3263 (1998).

[128] M. J. Weber (Ed.), *CRC Handbook of laser science and technology, vol. III. Optical materials: part 1*, CRC Press, Boca Raton, Florida (1986), table 1.1.17.128, p. 197.

[129] H. M. van Driel, *Kinetics of high-density plasmas generated in Si by 1.06- and 0.53-μm picosecond laser pulses*, Phys. Rev. B **35**, 8166–8176 (1987); L. Huang, J. P. Callan, E. N. Glezer, and E. Mazur, *GaAs under ultrafast excitation: response of the dielectric function*, Phys. Rev. Lett. **80**, 185–188 (1998).

[130] D. S. Wiersma, M. P. van Albada, and A. Lagendijk, *An accurate technique to record the angular distribution of backscattered light*, Rev. Sci. Instrum. **66**, 5473–5476 (1995).

[131] H. Cao *et al.*, *Random lasers with coherent feedback*, p. 393 and fig. 4, in: C. M. Soukoulis (Ed.), *op. cit.* [51].
[132] Aldrich Zinc Oxide, powder, $< 1\ \mu$m, 99.9% ZnO. On SEM photos most particles are seen to be rod-like, with aspect ratios ≈ 2, and sizes < 100 nm.
[133] Nanophase NanoTek®1701 Zinc Oxide, 99+% ZnO, average particle size: 24–71 nm; morphology: elongated; crystal phase: zincite (hexagonal).
[134] D. S. Wiersma, *op. cit.* [45], table 3.1.
[135] K. Kemnitz, N. Tamai, I. Yamazaki, N. Nakashima, and K. Yoshihara, *Fluorescence decays and spectral properties of Rhodamine B in submono-, mono-, and multilayer systems*, J. Phys. Chem. **90**, 5094–5101 (1986).
[136] E. Cohen and M. D. Sturge, *Fluorescence line narrowing, localized exciton states, and spectral diffusion in the mixed semiconductor CdS_xSe_{1-x}*, Phys. Rev. B **25**, 3828–3840 (1982).
[137] F. A. Majumder, S. Shevel, V. G. Lyssenko, H. E. Swoboda, and C. Klingshirn, *Luminescence and gain spectroscopy of disordered $CdS_{1-x}Se_x$ under high excitation*, Z. Phys. B **66**, 409–418 (1987).
[138] S. Hughes, A. Knorr, S. W. Koch, R. Binder, R. Indik, and J. V. Moloney, *The influence of electron-hole scattering on the gain spectra of highly excited semiconductors*, Solid State Comm. **100**, 555–559 (1996); I. Galbraith and S. W. Koch, *A comparison of lasing mechanisms in ZnSe and GaAs*, J. Cryst. Growth **159**, 667–671 (1996); M. F. Pereira, Jr. and K. Henneberger, *Gain mechanisms and lasing in II–VI compounds*, Phys. Stat. Sol. B **202**, 751–762 (1997).
[139] A. Diessel *et al.*, *Bleaching of excitonic absorption in II–VI laser diodes under lasing conditions*, J. Cryst. Growth **159**, 661–666 (1996).
[140] A. Yamamoto, T. Kido, T. Goto, Y. Chen, T. Yao, and A. Kasuya, *Dynamics of photoexcited carriers in ZnO epitaxial thin films*, Appl. Phys. Lett. **75**, 469–471 (1999).
[141] M. Kira, F. Jahnke, and S. W. Koch, *Microscopic theory of excitonic signatures in semiconductor photoluminescence*, Phys. Rev. Lett. **81**, 3263–3266 (1998); A. Girndt, S. W. Koch, and W. W. Chow, *Microscopic theory of laser gain in semiconductor quantum wells*, Appl. Phys. A **66**, 1–12 (1998).
[142] H. C. Ong, A. S. K. Li, and G. T. Du, *Depth profiling of ZnO thin films by cathodoluminescence*, Appl. Phys. Lett. **78**, 2667–2669 (2001).
[143] P. Y. Yu and M. Cardona, *Fundamentals of semiconductors: physics and materials properties*, Springer, Berlin (1996), pp. 344–349.
[144] C. Klingshirn and H. Haug, *Optical properties of highly excited direct gap semiconductors*, Phys. Rep. **70**, 315–398 (1981).
[145] *Kodak Laser Dyes*, Eastman Kodak Company, Rochester (1987).
[146] U. Brackmann, *Lambdachrome Laser Dyes*, Lambda Physik GmbH, Göttingen, Germany (1995).
[147] A. Ishimaru, *op. cit.* [15], eq. (8-6).
[148] R. Loudon, *op. cit.* [3], p. 17.
[149] P. W. Milonni and J. H. Eberly, *op. cit.* [36], p. 223.
[150] http://www.science.uva.nl/research/scm/#theses

S. Summary

In this thesis we report on our investigations of random lasers. The title of this work, Experiments on random lasers*, expresses the key role for experiments in this research, but implicitly includes theory, too. We summarize the scientific results.*

Random lasers are strongly scattering media with optical gain. These systems have many features in common with more conventional lasers based on an optical gain medium enclosed in a cavity with two mirrors to enhance stimulated emission. An example is the observation of a threshold for lasing action and frequency narrowing in random lasers. Evidently, the optical properties of random lasers are quite different from conventional lasers: the propagation of pump and fluorescence light is diffusive, and—in absence of well-defined cavity modes—there is no "preferred direction" in feedback and loss processes. The ambiguity as to what exactly constitutes the loss in a random laser, how optical feedback works if it is non-directional, and the theoretical prediction of a intensity divergence, have led to a continuing debate about what happens at, and above, the laser threshold.

There are essentially two approaches to random lasers: one from the viewpoint of laser physics, and one from the viewpoint of multiple scattering of light. The former perspective regards the system as a peculiar laser, and provokes questions into the laserlike behavior: why is there a threshold, what are its properties and what determines them? The latter perspective addresses the random laser as a multiply scattering system with an extra asset: gain. This is particularly interesting if one recalls that absorption is detrimental to many effects in light transport that depend on the survival of long light paths. Minute amounts of absorption can be detected by enhanced backscattering. Gain, however, can be understood up to a certain level as negative absorption, and so could bring out interesting phenomena.

In chapter 1 we introduce the concepts we use in building our picture of random lasers. It draws strongly on elements from both multiple scattering and from laser physics. We start by outlining the basics of classical light–matter interaction, emphasizing the connection between scattering and absorption/gain by treating them on the same footing whenever possible, and present light diffusion in that framework. This

is followed by a brief tutorial in laser physics, based on semiclassical rate equations, including amplified spontaneous emission and laser dye properties. We conclude the chapter with a presentation of random lasers, in our work usually consisting of a suspension of colloidal titania (TiO_2) scatterers in a solution of Sulforhodamine B laser dye in methanol.

One of the primary questions stemming from the "laser perspective" is how the multiple-scattering characteristics influence the threshold in a random laser. In chapter 2 we first present the phenomenology of the laser threshold. Subsequently we describe our experiments investigating the effect of the size of the amplifying volume on the threshold, and so studying the efficiency of diffusive feedback. We demonstrate a strong dependence of the threshold pump fluence on the beam diameter. This effect is due to multiple scattering: it is not observed in the absence of scatterers. Light is amplified less strongly if the amplifying region of the sample has a small diameter, in the order of 5ℓ, giving rise to a threshold that is up to 70 times higher than if the gain volume is large. The experimental data are accurately reproduced by a Monte Carlo random walk simulation.

In the "standard" theory of random lasers, developed from a multiple-scattering perspective, one introduces gain in a scattering medium by a fixed negative absorption coefficient. This has the serious drawback of producing a diverging intensity at the point where the amount of generated light becomes too large to be transported. This explosion has been identified with the laser threshold. In chapter 3 we demonstrate that in a realistic system this explosion does not exist. To the standard theory we add the crucial ingredient of population dynamics, producing gain saturation and a relaxation oscillation by which the threshold crossing is accompanied. Above the laser threshold the population inversion is fixed at a level where the (local) gain exactly compensates the (local) loss, like in an ordinary laser the modal gain equals the modal loss. We introduce β for a random laser, the fraction of spontaneous emission contributing to the laser process. We obtain the random laser threshold from a transport formalism, taking into account the local gain in a population rate equation. The theoretical results presented in this chapter further connect to experimental observations in explaining the proportionality of the laser output with the pump above threshold.

The validity of the model of chapter 3 is established by a quantitative comparison with measurements in chapter 4. Two classic experiments from the physics of multiple light scattering, speckle statistics and enhanced backscattering, are presented in this chapter. Extending the experiment in chapter 2, where a measurement was performed on amplified fluorescence, we now use an externally applied probe beam with known and controlled characteristics. First we discuss speckle in a random laser. In contrast with speckle in passive systems, measurements of the intensity

statistics and the speckle spot size in a random laser do provide information on light transport. The typical Rayleigh statistics of speckle allows a discrimination between fluorescence and amplified probe light, and so lets us determine the amount of amplification that an applied probe experiences near the maximum of the gain, where spectral separation is not possible.

The angular speckle spot size is a measure of the transverse dimension of the diffuse source. We show that this apparent source size increases if the medium is amplifying, due to a larger weight that long light paths get in the ensemble: the speckle spots get smaller. The prediction of chapter 3, that the gain should be invariant well above threshold, is confirmed by the pump-independent spot size in this regime. The average path length is found to be more than 2 times longer than in the passive material.

In the second half of chapter 4 we review our enhanced backscattering experiments. The cone narrows by as much as a factor 3 under the influence of gain upon increasing the pump from zero to above threshold. The long paths, constituting the top of the cone are amplified more strongly and this results in a narrower backscatter cone. Far above threshold the cone shape is approximately constant, reflecting the pump-invariance of the saturated gain. The measured cone shapes can be reproduced well with the data of the model presented in chapter 3, provided we carefully take the dynamics of the problem into account. The typical transport time scales involved in the formation of the backscatter cone are entangled with the time constant of the intrinsic dynamics of a random laser crossing the threshold.

In recent literature, there has been a series of publications reporting on the observation of narrow frequency structure in the fluorescent emission of random lasers. Their occurrence was interpreted as a manifestation of light localization, supposedly resulting in a "coherent random laser" operating in random ring cavities formed by scattering. Chapter 5 concerns our efforts to observe and explain these "narrow peaks". We first present a critical review of literature data, with an assessment of the physical qualities of such a hypothetical random ring cavity. Our own measurements on ZnO powders show that they do not nearly scatter sufficiently strongly to be localizing. Furthermore we observe a very peculiar nonlinearity in the dependence of the emission spectrum and intensity on pump energy and pulse rate. The characteristics of the emission depend strongly on the particular powders, possibly differing in many properties but not in the scattering parameters. Based on these results we conclude that an explanation for the narrow peaks in terms of an optically active electronic excitation in the semiconductor is a more likely candidate than one dependent on scattering. A repetition of the experiment with a dye-based random laser does not yield conclusive results.

S. Samenvatting

Een van de leuke kanten van werken met licht is dat je kunt zien wat je doet. Op de kaft van dit proefschrift staan verschillende voorwerpen met twee gemeenschappelijke eigenschappen: ze zijn ondoorzichtig en roze. Dat zijn ook eigenschappen van de materialen waarmee de meeste experimenten die in dit proefschrift worden beschreven, gedaan zijn. Een voorbeeld van zo'n materiaal is de vloeistof in het flesje op de achterkant, middelste foto. We hebben onderzoek gedaan naar de manier waarop licht vooruit komt in zo'n systeem. Eerst zal worden uitgelegd wat die kleur en ondoorzichtigheid betekenen voor het licht, en wat een random laser is. Verderop gaan we in op de wetenschappelijke resultaten van het onderzoek.

Een voorwerp is doorzichtig als het aan twee voorwaarden voldoet: licht moet er doorheen kunnen reizen, en het moet dat in een eenduidige richting doen. De eerste voorwaarde wil zeggen dat het licht niet wordt geabsorbeerd door het materiaal waarvan het voorwerp gemaakt is. Er komt dus evenveel licht uit als er in ging. De absorptie van licht is meestal verschillend voor verschillende kleuren licht. De kleur van een fietsreflector wordt veroorzaakt doordat groen en blauw licht worden geabsorbeerd uit het opvallende witte licht, waarna geel en vooral rood overblijven. Het resultaat is dat we het plastic van de reflector waarnemen als rood. Een materiaal dat groen licht absorbeert is dus niet goed doorzichtig voor die kleur, maar kan wel transparant zijn voor andere kleuren.

De tweede voorwaarde voor transparantie van een voorwerp betekent dat het voorwerp het licht niet teveel verstrooit. Verstrooiende dingen zien er meestal wit uit. Wolken zijn een voorbeeld: het licht beweegt zich vooral door lucht, maar komt onderweg kleine waterdruppeltjes tegen. Water heeft andere eigenschappen voor lichtvoortplanting (samengevat in de brekingsindex) dan lucht, daarom spiegelt een wateroppervlak en wordt licht afgebogen (een vis onder water lijkt ondieper te zwemmen dan hij doet). De waterdruppels in een wolk zijn zo klein, met zo'n krom oppervlak, dat dat spiegelen en afbuigen in meerdere of mindere mate in alle richtingen gebeurt. Dat heet verstrooiing. De lichtstraal die op de waterdruppel viel heeft zich alle kanten op verspreid. Hoe groter het verschil in brekingsindex

tussen verstrooier en omgeving, hoe sterker de verstrooiing. Als het licht vaak verstrooid wordt op de weg door de wolk, dan is het niet meer duidelijk waar het aan de bovenkant de wolk in gegaan is. Dit heet veelvoudige verstrooiing en de wolk is dan ondoorzichtig: we kunnen de zon niet zien. Het licht in de wolk is diffuus. Andere veelvoudig verstrooiende dingen zijn melk of verf.

Het blijkt in de praktijk handiger om licht in zo'n geval niet als een golf, maar als een verzameling deeltjes te beschrijven. Over de individuele deeltjes zeggen we niets, microscopisch bekeken blijft licht een golf. We zijn vooral geïnteresseerd in hoeveel van die lichtdeeltjes ergens zijn, de dichtheid. Die blijken we goed te kunnen beschrijven als diffusie, een erg algemeen transportverschijnsel. Een voorbeeld van diffusie is de verspreiding van een inktdruppel in een glas water: als de druppel in het glas valt is er ter plaatse veel inkt en elders niets, maar met het verstrijken van de tijd verspreidt de kleur zich door het hele glas, zij het verdund.

We werken met een mengsel van een verstrooiend wit poeder (titaandioxide, hetzelfde pigment dat tandpasta wit maakt) in een rode kleurstof. Het resultaat is een roze suspensie. De moleculen in de kleurstof absorberen groen licht, vandaar de kleur, en raken daardoor in een aangeslagen toestand. Het groene licht heet de "pomp". De moleculen hebben de energie uit de pomp in zich opgeslagen, ten koste van het groene licht. Nu kan de kleurstof rood licht versterken: rood licht dat een aangeslagen kleurstofmolecuul tegenkomt kan van dat molecuul als het ware een extra lichtdeeltje meekrijgen waardoor die rode lichtbundel de energie van het molecuul overneemt. De kleurstof is dan "roder dan rood": de kleur ontstaat niet alleen doordat groen licht wordt geabsorbeerd, maar ook door versterking van opvallend rood licht. Een versterkend, verstrooiend materiaal heet een "random laser".

Lasers maken gebruik van versterking. Normaal gesproken bestaat een laser uit een versterkend medium, bijvoorbeeld zo'n kleurstof, en een zogenaamde "trilholte", gevormd door spiegels. De lichtgolf wordt tussen de spiegels heen en weer gekaatst, en wordt ondertussen versterkt door de kleurstof. Een van de spiegels is niet perfect reflecterend om de laserbundel uit de trilholte te laten ontsnappen. Als de versterking groot genoeg is (door voldoende te pompen) om het lek door de spiegel te compenseren is de laser "aan". De overgang tussen uit en aan heet de laserdrempel.

Er is veel onderzoek gedaan aan lichtvoortplanting in verstrooiende media en nog veel meer aan lasers, zowel voor toepassingen als uit "nieuwsgierigheid". Ons onderzoek is gedaan uit nieuwsgierigheid. Er zijn twee gezichtspunten op random lasers te onderscheiden: één vanuit het veld van veelvoudige verstrooiing, en één vanuit de laserfysica. Er is een duidelijke analogie tussen random en gewone lasers. Gezien vanuit het laser-oogpunt dient zich de vraag aan wat de achtergrond is van deze analogie, waarom twee systemen met zo sterk verschillende optische eigenschappen zich soms zo vergelijkbaar gedragen. Aan de andere kant,

voor veelvoudige verstrooiing van licht is absorptie bijna altijd een probleem. Veel boeiende verschijnselen gerelateerd aan lichttransport verdwijnen in absorberende media. In die zin is het interessant om lichttransport te onderzoeken in versterkende ("anti-absorberende") verstrooiende media: random lasers.

Waar in de gewone laser de spiegels de functie hadden om het licht vaak het versterkende medium te laten passeren, wordt deze rol in een wanordelijk systeem vervuld door veelvoudige verstrooiing. Een bochtig pad tussen twee punten is langer dan een recht pad. Zo bevindt licht zich langer in een veelvoudig verstrooiend dan in een transparant versterkend medium en kan zo dus meer versterkt worden. Hoe meer verstrooiing, hoe langer het licht binnen blijft, dus hoe beter de versterking werkt. Als een gevolg hiervan gedraagt een random laser zich in sommige opzichten als een normale laser. Er is bijvoorbeeld een drempel, en ook zie je dat licht met de kleur die het meest versterkt wordt het "wint" van andere kleuren: net als in een gewone laser wordt die kleur het meest uitgezonden, ten koste van de andere.

De verschillen met een gewone laser zijn minstens even groot als de gelijkenissen. Om die verschillen duidelijk te maken moeten we iets dieper ingaan op wat het betekent dat licht zich gedraagt als golf. Een golf op een wateroppervlak is een serie toppen en dalen die zich langs dat oppervlak voortbewegen, gekarakteriseerd door een golflengte en een snelheid. Twee golven interfereren: als de toppen van beide precies samenvallen dan is de golfhoogte plaatselijk tweemaal zo groot (constructieve interferentie), terwijl de golven elkaar helemaal kunnen uitdoven—het resultaat is een glad wateroppervlak—als de toppen van de een in de dalen van de ander terechtkomen (destructieve interferentie). De golflengte van licht zien wij als kleur.

Versterking van licht is coherent: de golf die wordt uitgezonden door het kleurstofmolecuul loopt precies in de pas met de invallende lichtgolf (de toppen en dalen vallen precies samen) en heeft dezelfde richting. Doordat tussen de spiegels van de lasertrilholte precies een geheel aantal golflengtes past, voegt elk versterkingsproces licht toe dat precies gelijk loopt met de rest. Zo kan boven de laserdrempel door constructieve interferentie een zeer sterk lichtveld opgebouwd worden in de laser. In een random laser is dit natuurlijk niet het geval. Er zijn geen spiegels en dus lopen de toppen van de versterkte lichtgolven niet gelijk, maar allemaal door elkaar.

Het eerste rode licht, dat het versterkingsproces in een random laser start, noemen we de kiem van het proces. Hij kan van buiten komen door dat we het materiaal beschijnen met een flits rood licht, maar kan ook ontstaan doordat een kleurstofmolecuul hem "spontaan" uitzendt (fluorescentie). Een medium zonder versterking vormt een weinig vruchtbare bodem voor de kiem en de kleine hoeveelheid licht wordt verdund als de inkt in het water, diffusief verspreid door het hele glas. Maar als hij voldoende versterkt wordt, dan ontstaat onderweg steeds meer licht en groeit de kiem uit tot een krachtige lichtpuls. "Voldoende" wil zeggen dat het verlies van

licht naar buiten (waaraan we meten) wordt gecompenseerd door de versterking: het systeem is boven de drempel.

We pompen de random laser door de kleurstof aan te slaan met een groene lichtpuls. Dat groene licht wordt geabsorbeerd in een laag bij het oppervlak van het materiaal. Voor grotere diepte is er geen groen licht over; het wordt ook deels naar buiten verstrooid. In die gepompte laag kan rood licht versterkt worden. Licht dat dieper het systeem in diffundeert kan later weer terugkomen in de voorste laag, waar het ontstaan is.

Dit zijn de belangrijkste ingrediënten voor de experimenten en theorie die in dit proefschrift worden beschreven. In hoofdstuk 2 variëren we de afmeting van het gepompte gebied. Als het gepompte gebied klein is ten opzichte van de typische afstand waarover licht zich verspreidt, dan heeft het rode licht dat terugkeert in de voorste laag na een uitstapje diep het systeem in, een grote kans het versterkende gebied te missen. Het wordt dan minder versterkt en zodoende wordt de drempel pas bereikt bij een (veel) grotere energie van de groene pomppuls.

Wat er precies gebeurt bij de drempelovergang onderzoeken we theoretisch in hoofdstuk 3. Lange tijd is een theoretisch model voor random lasers gebruikt, dat een soort explosie voorspelt: de hoeveelheid rood licht groeit naar oneindig. Men noemde deze explosie de laserdrempel. Uit vergelijking met experimenten bleek al snel dat dit model geen goede beschrijving van de werkelijkheid vormt. We passen dit diffusiemodel op een aantal punten aan, waardoor de explosie kan worden voorkomen. Ten eerste houden we rekening met verzadiging: als een kleurstofmolecuul vervalt (doordat het licht versterkt of uitzendt), betekent dat dat de lokale versterking een beetje lager is. Er kan één molecuul minder meedoen met de versterking, totdat het weer is aangeslagen door de pomp. Boven de laserdrempel ontstaat zo een evenwicht tussen pomp-absorptie en verval door versterking. De grootte van de versterking in evenwicht is precies voldoende om het lokale lek van rood licht aan te vullen (en hangt dus niet af van de pompenergie). Ten tweede blijkt deze verzadiging maar langzaam op gang te komen en zo kan de versterking "doorschieten" voorbij de evenwichtswaarde. Dat heeft een felle puls rood licht tot gevolg, die (door het versterkingsproces) de hoeveelheid aangeslagen moleculen vermindert tot beneden de evenwichtswaarde. Er wordt minder rood licht uitgezonden, en zo kan de pomp weer meer moleculen aanslaan. Deze cyclus voltrekt zich een aantal keren tot het evenwicht is ingesteld. Hij werkt als een soort veiligheidsklep die de versterking telkens even verlaagt als er teveel rood licht ontstaat. Dynamica is dus belangrijk in de theorie, anders kan deze slingerbeweging niet worden beschreven en krijgen we alsnog de explosie. Ten derde hebben we een methode bedacht om in rekening te brengen dat van de spontaan uitgezonden kiemen slechts de 10% met de goede kleur kan worden versterkt.

Deze drie aanvullingen zijn direct ontleend aan de laserfysica, zij het dat ze zorgvuldig geïnterpreteerd moeten worden, om de evidente verschillen tussen gewone en random lasers geen geweld aan te doen. Met dat voorbehoud blijkt de theorie nu erg goed te werken, en we gebruiken hem om in hoofdstuk 4 verstrooiingsexperimenten te verklaren. We gebruiken nu als rode lichtbron een externe puls, omdat de eigenschappen daarvan veel beter en gemakkelijker te controleren zijn dan van de fluorescentie. We laten die puls verstrooid worden door de random laser, die tegelijk belicht wordt met de groene pomppuls, en meten aan het rode licht dat uit het medium komt. Met twee klassieke interferentie-experimenten uit de veelvoudige lichtverstrooiing tonen we aan dat boven de laserdrempel de versterking inderdaad praktisch onafhankelijk is van de sterkte van de pomppuls. Ook zien we effecten die we toeschrijven aan de dynamische "veiligheidsklep". We merkten hierboven al op dat versterking afhangt van de lengte van het lichtpad: lange paden worden "bevoordeeld". Uit onze experimenten blijkt hoeveel: afhankelijk van materiaalparameters vinden we dat de gemiddelde padlengte in een random laser meer dan twee keer zo lang is, vergeleken met het niet-versterkende systeem.

Met deze experimenten en de bijbehorende theorie hebben we laten zien dat de laser-eigenschappen van een random laser, zoals de hoogte van de drempel en de manier waarop die wordt overgestoken, direct zijn af te leiden uit een beschrijving van het systeem in termen van veelvoudige verstrooiing. De twee perspectieven op random lasers blijken te kunnen worden samengevoegd tot één consistent plaatje.

Een tikje vreemde eend in de bijt is hoofdstuk 5. In dit hoofdstuk worden de experimenten beschreven die we hebben gedaan aan de zogenaamde "smalle pieken". Dit fenomeen werd in de recente literatuur gepresenteerd als een bewijs dat golven in een random laser bij heel sterke verstrooiing weer met elkaar in de pas zouden gaan lopen als in een gewone laser. We hebben laten zien dat de systemen waarin deze smalle pieken zijn gerapporteerd niet voldoende sterk verstrooien om deze coherentie van belang te laten zijn, als hij al bestaat in wanordelijke media. We meten een zeer ongebruikelijk karakter van de intensiteit en de spectrale vorm van de pieken als functie van de pompsterkte. Dit resultaat maakt een verklaring voor dit verschijnsel in termen van electronische materiaaleigenschappen waarschijnlijker.

Zo'n coherente random laser is wel een interessant systeem, dat waarschijnlijk inderdaad zeer sterke verstrooiing nodig heeft om te bestaan. Het is niet alleen interessant om te kijken hoe zo'n materiaal zich gedraagt en in welke opzichten het anders is dan een "gewone" random laser, maar ook om de analogie met een normale laser verder te onderzoeken. In onze resultaten gaat de vergelijking een eind op, mits de juiste concepten in trilholte-lasers en random lasers worden geïdentificeerd als elkaars equivalent. Op die manier verscherpt random-laseronderzoek niet alleen het inzicht in deze verstrooiende media maar ook het begrip van lasers.

D. Dankwoord

Iedereen die direct of indirect, doelgericht of onbewust heeft bijgedragen aan het werk dat in dit boek beschreven is ben ik zeer erkentelijk. Wetenschap bedrijf je niet alleen. Ook al zit je avonden in je eentje te meten, ideeën worden gevormd onder de continue invloed van je omgeving. Daarmee bedoel ik niet alleen invloed van collega's die slimme vragen stellen, maar ook van anderen waarvan ik gewoon blij ben dat ze er zijn. Een aantal van hen wil ik hier met name noemen.

Allereerst dank ik mijn promotor Ad Lagendijk, die alles aan de kant zet om wetenschap te kunnen doen, voor het gestelde vertrouwen, zowel wat betreft de wetenschappelijke als de sociale kanten van het onderzoek. Ook zijn aanstekelijk enthousiasme voor en heldere kijk op de natuurkunde waardeer ik zeer. Rudolf Sprik dank ik voor de hulp bij het rekenwerk, zonder hem was ik in hoofdstuk 3 en 4 van dit proefschrift niet zo ver gekomen. Ook heeft hij het talent om alle mogelijke beren op de weg te signaleren als je een idee voor een experiment hebt. Als die allemaal zijn afgeschoten kan er zeker niets meer mis gaan. Willem Vos en Gerard Wegdam dank ik voor de niet aflatende stroom van ideetjes waarvan ik er veel te weinig gebruikt heb. Zorro, you are what you is, bedankt voor alles. Gerard, ik hoop dat je je betrokkenheid niet hoeft te bekopen met een lange periode als instituutsdirecteur.

I am very grateful to Makoto Tomita for his patience and lessons in setting up experiments. The beam diameter experiment and the following collaboration gave me a good start in random lasers. Mijn afstudeerstudent Frank J. Poelwijk dank ik voor zijn optimisme en zijn oog voor detail in experimenten. Frank, ik bewaar mooie herinneringen aan onze discussies, zowel over random lasers als over filosofie, moderne muziek en wie weet wat nog meer. Het was inderdaad een goede tijd.

Waar zouden we zijn zonder Wim Koops? Ik bedank hem niet alleen voor de technische, maar ook voor de morele ondersteuning: zijn interesse in de mens achter de wetenschapper, zijn schaatsverhalen en zijn trots als opa.

Zonder de techniek draait er natuurlijk niets in een experimenteel lab. Bedankt Johan van de Ridder (ook voor je onverwoestbare humeur), Flip de Leeuw en Joost Overtoom (ook voor de labborrels—zo hoor je nog eens wat), Johan Soede, Jan Dekker, Jan Mulder en Bert Zwart, voor alle snelle klusjes "even tussendoor". Dank

aan Ina Zwart, Ineke Baaij, Roos Visser en Mariet Bos voor de vlotte administratieve en secretariële ondersteuning. Als er haast is bij de financiën weet Dick Jensen het altijd te regelen. Derk Bouhuijs en Marc Brugman tilden de computersupport naar een hoger plan.

Frederik van den Broek en Huib Bakker van Amolf sloten zich voor een dag aan bij de zoektocht naar de smalle pieken. Niets gezien, maar wel bedankt voor de hulp en het gebruik van de laser. The attempt with Nandini Bhattacharya's setup was a little more successful, and I thank her for her help and for tolerating my stuff in the lab for a week. Wat het probleem ook is, Cor Snoek heeft de oplossing te leen, bouwjaar ca. 1965, maar werkt geheid en je krijgt er mooie verhalen bij.

The curiosity of Diederik Wiersma, Bart van Tiggelen, Jos Dingjan and Costas Soukoulis gave rise to inspiring discussions and ideas on random lasers and localization. I am indebted to Claude Weisbuch for illuminating the tricky subject of II–VI luminescence. Dank aan Ben van Linden van den Heuvell voor zijn belangstelling. Hans Pothuizen, bedankt voor de aanmoediging en je kritische blik.

In de groep Golven in Complexe Media is altijd beweging. Dat is inspirerend en leuk. Bedankt Jaime, poldercharro en partner in wanorde, voor wederzijdse bemoeienis, vrijmibo's en AC/DC, Patrick voor de rake vragen, Martijn die zéker werkt in theorie, Yuri, Juan para los intercambios de idiomas y toda la música, ElectrontransFemius tegen wil en dank, Manu, kamergenoot op de valreep Boris, Lydia voor de roze spullen, Denis, Tom, Bert, Rik, Mark, Frank voor de lol, de rust en de wilde plannen, Mischa voor zijn ongeduld en de vele uitjes, Dirk! (… ja?), Judith voor haar eigenwijsheid, Pedro, de Canadezen Hendrik en Henk, Michiel voor de inzichten van buiten, Arnout, Dau, Dennis, Anouk, Meritt, Pepijn en Allard.

Aan de lotgenoten buiten de groep, zoals Erik Paul, Bas, Michel, Jeroen, Heidi, Lunterense kamergenoot Dirk en β-stuffel Ronald, dank voor hetzelfde schuitje.

Susanne, bestaat er zoiets als een copromovendus? Zonder jou had mijn tijd in Amsterdam er heel anders uitgezien, ik ben erg blij dat je er was. Roelof, dank voor de lange avonden (met nachtnet toe) en de gesprekken over leven en werk, zin en onzin. Marij, bedankt voor je steun, vriendschap en de leuke tijd, Kirsten voor je betrokkenheid, Miranda voor de hulp bij het grafisch ontwerp van dit boek, Rick, Jos en Raymond voor het kabaal, de lol en de rare instrumenten, Thomas voor zijn enthousiasme en de muziek.

De family, Joost, Floor, Francien en Erik, pap en mam, dank voor de steun en aanmoediging en de goede zorgen. Francien, ook bedankt voor de frustitelefoontjes. Tot slot, lieve Suze, je vertrouwen en je praktische instelling in situaties waarin ik het overzicht verloor, zijn ontzettend waardevol geweest in dat toch wel zware laatste jaar. Kom, we gaan de wereld in!

Gijs